Dynamics for open quantum systems : a discrete quantum level strongly coupled to a continuum with a band structure

Etienne Jussiau

Communauté
UNIVERSITÉ Grenoble Alpes

THÈSE

Pour obtenir le grade de

DOCTEUR DE LA COMMUNAUTÉ UNIVERSITÉ GRENOBLE ALPES

Spécialité : physique théorique

Arrêté ministériel : 25 mai 2016

Présentée par

Étienne Jussiau

Thèse dirigée par **Timothy Ziman**, directeur de recherche, CNRS, Institut Laue-Langevin
et codirigée par **Robert S. Whitney**, chargé de recherche, CNRS, Laboratoire de Physique et Modélisation des Milieux Condensés

préparée au sein du **Laboratoire de Physique et Modélisation des Milieux Condensés**
dans **l'École Doctorale de Physique de Grenoble**

Dynamique des systèmes quantiques ouverts

Un niveau quantique discret fortement couplé à un continuum avec une structure de bandes

Dynamics for open quantum systems

A discrete quantum level strongly coupled to a continuum with a band structure

Thèse soutenue publiquement le **18 septembre 2019**,
devant le jury composé de :

Monsieur Dietmar Weinmann
Directeur de recherche, CNRS, Institut de Physique et Chimie des Matériaux de Strasbourg, rapporteur et président du jury

Madame Inès Safi
Chargée de recherche, CNRS, Laboratoire de Physique des Solides, rapporteure

Madame Mireille Lavagna
Directrice de recherche, CNRS, Institut Nanosciences et Cryogénie, Photonique, Électronique et Ingénierie Quantiques, examinatrice

Monsieur Christoph Groth
Ingénieur de recherche, CEA, Institut Nanosciences et Cryogénie, Photonique, Électronique et Ingénierie Quantiques, examinateur

Monsieur Gernot Schaller
Professeur invité, Institut für Theoretische Physik, Technische Universität Berlin, examinateur

A discrete quantum level strongly coupled to a continuum with a band structure

– Rich physics in a simple model –

« L'oracle de Delphes a déclaré que de tous les Grecs, j'étais le plus sage. C'est sans nul doute parce que de tous les Grecs, je suis le seul à savoir que je ne sais rien. »
– Socrate

Remerciements

En premier lieu, je tiens à exprimer ma gratitude aux membres de mon jury de thèse : Gernot Schaller qui a fait le voyage de Berlin à Grenoble, Mireille Lavagna et Christoph Groth qui ont aussi participé à mon comité de suivi de thèse, et enfin Inès Safi et Dietmar Weinmann qui ont généreusement accepté de passer du temps à relire et corriger mon manuscrit de thèse.

Mon aventure au LPMMC a débuté au printemps 2016 par un stage de quatre mois. C'est à cette époque que le squat de la bibliothèque commença faute de place dans les bureaux officiels. Ce qui ne devait être qu'une occupation temporaire dura finalement plus de trois longues années. Je remercie naturellement les membres du personnel du LPMMC, chercheurs, informaticiens et gestionnaires ; notamment Habiba, dont la porte toujours ouverte et l'oreille attentive furent une formidable échappatoire à la thèse et ses tourments. Merci pour ces heures passées à refaire le monde. Bien évidemment, ce travail n'aurait pas été possible sans l'aide de Rob, mon directeur de thèse, qui m'a guidé et soutenu par monts et par vaux, toujours avec bonne humeur. Merci de m'avoir accompagné dans cette première confrontation à la réalité de la recherche et surtout de m'avoir enseigné l'honnêteté et l'humilité indispensables à une pratique scientifique de qualité mais qui m'apparaissent pourtant trop peu valorisées dans le monde de la recherche. Je remercie également Tim qui a accepté la charge de directeur de thèse officiel et qui a toujours tenu à suivre l'évolution de mon travail.

J'ai une pensée toute particulière pour mes camarades d'infortune, jeunes chercheurs précarisés, doctorants et postdoctorants. Le dévoiement continu de la recherche scientifique avec la compétition exacerbée de tous contre tous laisse peu d'espoir en un avenir radieux. Puissions-nous toujours rester solidaires face à ce système qui répose exclusivement sur la concurrence des travailleurs précaires entre eux. Nous avons un monde à gagner. Mais nous avons partagé bien plus qu'un futur incertain, et je souhaite remercier ici tous ceux qui m'ont un tant soit peu accompagné pendant ces trois ans. En premier lieu, mes premiers cobureaux quand la bibliothèque, au pic de sa fréquentation à l'été 2016, accueillait sept stagiaires : Tiphaine, Guillaume, Magali et Bharathi qui sont rapidement partis ; mais aussi mon cher ami Évrard-Ouicem, dont l'exil forcé outre-Rhin, que j'espère salutaire, a laissé un grand vide, et l'inénarrable Nico, le seul qui sera resté avec moi pour la

thèse, qui apportait sa bonhomie communicative à chacune de ses apparitions. Pour leur accueil, je remercie également les anciens du laboratoire Katharina, Natalia, Guillaume, et plus particulièrement Eiji, qui a pris les jeunes sous son aile et nous a fait profiter de son expérience. Je réfléchis encore à ses conseils avisés et à sa vision de la recherche que je pense partager de plus en plus. Merci aussi à ceux qui sont arrivés ensuite et avec qui j'ai partagé la plus grande partie de ma thèse, Aleks, El Pato, alias JPG, fier représentant d'un État souverain huit longues secondes, Davide et Piero, fers de lance de l'invasion italienne sous la houlette de Don Settino. Je pense que notre génération peut s'enorgueillir d'avoir insufflé un esprit neuf au LPMMC. Notre départ signe la fin du squat de la bibliothèque, une parenthèse se ferme dans la vie du laboratoire. Merci de même à la nouvelle génération, Anastasiia, Ale, Jonny, titre de séjour en poche, Olmo, Amit et Giovanni, à qui il incombe désormais de sauvegarder cet esprit de solidarité et de camaraderie. Je tiens enfin à remercier ceux qui ont croisé ma route plus brièvement pendant cette thèse, Arithra, Josh, Masahiro, Tommaso et sûrement bien d'autres que j'oublie ici.

Je ne peux pas terminer sans un mot pour mes proches. En premier lieu, les amitiés que les longues distances n'ont pas entamées. Bien sûr, ma famille, passée et présente, qui m'a transmis le goût des sciences, m'a toujours poussé à donner le meilleur de moi-même et que j'espère avoir rendue fière. Enfin, je n'ai pas de mot assez fort pour exprimer ma gratitude et mon amour à Laetitia. Sans son abnégation et son soutien sans faille, je n'aurais rien accompli. Nous sommes sur le même bateau depuis plus de sept ans alors que nous nous apprêtons à traverser l'océan pour explorer le Nouveau Monde, et rien ne pourrait me combler plus que de vivre ensemble cette nouvelle aventure.

Résumé en français

Suivant les progrès technologiques de la révolution industrielle, la thermodynamique classique a été développée au XIX^{e} siècle dans le but de comprendre la conversion de la chaleur en travail intervenant dans les machines thermiques nouvellement élaborées. Les travaux de Boltzmann apportèrent une autre révolution conceptuelle avec la physique statistique. Il démontra l'origine microscopique des lois de la thermodynamique, celles-ci ne décrivant en fait que le comportement macroscopique de systèmes pour lesquels la thermalisation locale est plus rapide que toutes les autres échelles de temps. Cependant, conséquemment à l'intérêt grandissant pour les nanotechnologies, il est aujourd'hui possible de manipuler des systèmes microscopiques pour lesquels la thermalisation est plus lente que les échelles de temps associés aux flux d'électrons. Une avancée technologique majeure dans ce domaine provient de l'utilisation de boîtes quantiques, des dispositifs nanométriques permettant de confiner les électrons sur des distances si petites qu'ils se répartissent sur des niveaux d'énergie discrets. Il est alors évidemment indispensable de prendre en compte les effets quantiques pour l'étude de ce type de systèmes, c'est-à-dire de concevoir des outils théoriques alliant thermodynamique et mécanique quantique.

Les problèmes de thermodynamique quantique sont souvent abordés dans le cadre de la théorie des systèmes quantiques ouverts. L'idée générale de ce formalisme est d'étudier la dynamique d'un « petit » système quantique lorsqu'il est couplé à un autre système supposé bien plus « gros » et représentant l'environnement. On démontre alors que l'évolution temporelle du petit système peut être décrite par une équation maîtresse dans la limite où il est faiblement couplé à l'environnement. Cependant, on pourrait penser de prime abord qu'une machine pourra délivrer une puissance plus importante dans un contexte de fort couplage.

Pour les problèmes de transport électronique, le formalisme de Landauer-Büttiker permet de décrire le régime de fort couplage. Dans ce cadre, les électrons sont supposés ne subir que des processus de diffusion élastique dans le système central. Toutes les propriétés thermoélectriques de la machine peuvent alors être caractérisées grâce aux propriétés de transmission du diffuseur. Cependant, ce formalisme souffre aussi d'une importante limitation, la structure de bandes des réservoirs étant ignorée.

Ici nous avons choisi d'adopter un point de vue différent pour aborder le régime de fort couplage en étudiant un modèle exactement résoluble. Nous analysons donc le modèle de Fano-Anderson décrivant un niveau discret couplé à un continuum. Nous nous intéressons particulièrement à l'influence de la densité d'états des réservoirs. On démontre en effet que, sous certaines conditions, des états liés discrets apparaissent dans les bandes interdites des réservoirs. Ces états jouent un rôle prépondérant sur la dynamique du niveau discret à temps longs : leur contribution dépend de la

préparation initiale du système et peut donner lieu à des oscillations permanentes de l'occupation du niveau discret.

Nous commençons par expliciter la solution exacte du modèle en nous concentrant particulièrement sur son comportement à temps longs. Nous analysons ensuite deux cas particuliers. En premier lieu, nous nous intéressons aux propriétés de transport d'une boîte quantique à un niveau couplée à un semi-conducteur présentant une unique bande interdite. Un état lié apparaît dans cette bande lorsque le couplage au réservoir dépasse une valeur critique ce qui affecte fortement les propriétés de transport du système. Nous étudions ensuite le cas de réservoirs décrit par un modèle de liaisons fortes dont la densité d'états ne comporte qu'une bande finie d'énergie. Nous montrons qu'un niveau discret couplé à un tel réservoir se comporte comme un système à plusieurs niveaux, sa densité d'états locale et sa fonction de transmission présentant de multiples résonances.

Summary in English

Following the technological advances of the Industrial Revolution, classical thermodynamics was developed in the 19th century in order to understand the conversion of heat into work in newly designed machines. The works of Boltzmann brought another conceptual revolution with statistical mechanics. He demonstrated the microscopical origin of the laws of thermodynamics which actually only describe the macroscopic behaviour of systems in which local thermalization is faster than all other timescales. However, following the growing interest for nanotechnologies, it is now possible to manipulate microscopic systems in which thermalization is slower than the timescales for electron flow. A major technological advance in this field stems from the use of quantum dots, nanoscale devices which confine electrons on such small scales that they spread on discrete energy levels. It is then essential to take into account quantum effects for the study of this type of systems, that is to say to design theoretical tools combining thermodynamics and quantum mechanics.

Problems of quantum thermodynamics are often tackled in the framework of the theory of open quantum systems. The general idea of this formalism is to study the dynamics of a "small" quantum system when it is coupled to another much bigger representing the environment. One can then show that the time evolution of the small system can be described by a master equation in the limit where it is weakly coupled to the environment. However, it intuitively seems that the power output of the machine would be higher in the context of strong coupling.

For problems of electronic transport, the Landauer-Büttiker formalism allows to describe the strong coupling regime. In this framework, electrons are assumed to solely undergo elastic scattering processes in the central system. All the thermoelectric properties of the machine can then be characterized thanks to the transmission properties of the scatterer. However, this formalism has an important limitation; it ignores the band structure of the reservoirs.

Here we have chosen to adopt a different viewpoint to tackle the strong coupling regime by studying an exactly solvable model. We therefore analyze the Fano-Anderson model describing a discrete level coupled to a continuum. We are particularly interested by the influence of the reservoirs' band structure. One can indeed show that, under certain conditions, discrete bound states appear in the band gaps of the reservoirs. These states play an important role on the dynamics of the discrete level at long times: their contribution depends on the initial preparation of the system and gives rise to persistent oscillations of the occupation of the discrete level.

We start by deriving the exact solution of the model especially focusing on its long-time behaviour. We then analyze two special cases. First, we study the transport properties of a single-level quantum dot coupled to a semiconductor with a

single band gap. A bound state appears in this gap when the coupling to the reservoir exceeds a critical value. We show that this greatly affects the transport properties of the device. We then study the case of reservoirs described by a tight-binding model whose density of states consists of a single finite-range energy band. We show that a discrete level coupled to such a reservoir behaves like a multi-level system as its local density of states and transmission function exhibits multiple resonances.

Contents

1 Introduction **14**
- 1.1 Thermodynamics and thermoelectric effects . . . 14
- 1.2 Bound states . . . 17
- 1.3 Thermoelectric transport in the linear response regime . . . 20
  - 1.3.1 Currents and transport coefficients . . . 20
  - 1.3.2 Power and efficiency in the linear response regime . . . 22
- 1.4 Strong coupling . . . 25
- 1.5 The Fano-Anderson model . . . 25

2 Theories of open quantum systems **29**
- 2.1 Scattering theory and the Landauer-Büttiker formalism . . . 29
  - 2.1.1 The Landauer-Büttiker formula . . . 29
  - 2.1.2 Linear response regime . . . 32
- 2.2 Quantum master equations . . . 34
  - 2.2.1 The Lindblad master equation . . . 34
  - 2.2.2 The Bloch-Redfield and Pauli master equations . . . 37

3 Solution of the Fano-Anderson model **43**
- 3.1 Formal solution of the model . . . 43
  - 3.1.1 Heisenberg equations and Laplace transform . . . 43
  - 3.1.2 The continuum limit . . . 45
  - 3.1.3 The inverse Laplace transform . . . 46
  - 3.1.4 Bound states and local density of states by exact diagonalization 49
- 3.2 Physical quantities . . . 53
  - 3.2.1 Occupation of the discrete level . . . 53
  - 3.2.2 Currents . . . 55
  - 3.2.3 Correlations in the discrete level occupation . . . 56
    - 3.2.3.1 Fermions . . . 56
    - 3.2.3.2 General case . . . 57

4 Long-time limit **58**
4.1 The Riemann-Lebesgue lemma . . . 58
4.2 Occupation of the discrete level . . . 59
4.3 Currents . . . 62
4.4 Continuity equation . . . 64
4.5 Long-time correlations in the discrete level occupation . . . 66
4.5.1 Fermions . . . 66
4.5.2 General case . . . 67
4.6 The wide-band limit: an example without bound states . . . 68
4.7 Comparison with approximate schemes . . . 69
4.7.1 Master equation approach . . . 69
4.7.2 Scattering theory . . . 71

5 Mimicking the adiabatic turning on of level-reservoir coupling **73**
5.1 General description of the procedure . . . 73
5.2 Adiabatic occupation . . . 75
5.3 Adiabatic currents . . . 76
5.4 Adiabatic correlations in the discrete level occupation . . . 77

6 Electron transport close to the band edge of a semiconductor **78**
6.1 General results . . . 78
6.1.1 The spectrum . . . 78
6.1.2 Steady-state occupation . . . 80
6.1.3 Current and transmission . . . 81
6.2 Scaling close to the critical point . . . 85
6.2.1 Bound state energy . . . 85
6.2.2 Overlap of the bound state with the dot level . . . 87
6.2.3 Transmission function . . . 89
6.3 Transport properties . . . 92

7 Multiple perfectly transmitting states for tight-binding models **97**
7.1 Spectral density for tight-binding models . . . 97
7.1.1 Density of states for tight-binding models . . . 97
7.1.2 One-dimensional chain . . . 98
7.1.3 Two-dimensional square lattice . . . 102
7.2 Nonlinear Lamb shifts . . . 102
7.2.1 One-dimensional chain . . . 103
7.2.2 Two-dimensional square lattice . . . 104
7.3 Experimental considerations . . . 106
7.3.1 Thermoelectric experiments . . . 106

7.3.1.1 Transmission measured using low-temperature conductance . . . 106
7.3.1.2 Probing the local density of states through scanning tunneling spectroscopy . . . 107
7.3.2 Microwave tight-binding experiments . . . 108
7.4 Theoretical results . . . 109
7.4.1 Resonances and transmission properties . . . 109
7.4.2 Local density of states . . . 116

Concluding remarks **120**

References **124**

Summary chapter by chapter

Chapter 1 – Introduction

This chapter presents the relevant physics for the transport properties of the Fano-Anderson model which will be the main subject of this thesis. The general transport properties of thermoelectric devices are described, with an emphasis on the linear response regime. The effects of strong coupling between a quantum system and its environment are then discussed through the example of bound states. This chapter concludes by introducing the Fano-Anderson model itself.

Chapter 2 – Theories of open quantum systems

In this chapter, we review standard theoretical frameworks used to study quantum thermodynamical problems: the Landauer-Büttiker formalism and the master equation formalism. The Landauer-Büttiker formalism focuses on the description of steady-state transport properties. In this framework, one considers transport between reservoirs of free electrons connected to each other through a small disordered region. Electrons incoming to this central system undergo elastic scattering events which redistribute them among reservoir modes. It is the transmission properties of the scatterer which then give rise to thermoelectric effects. This framework is particularly useful in the linear response regime as all the transport coefficients of the device can be deduced from the scattering properties of the central region. This type of problems can also be addressed within the framework of quantum master equations. It is shown that when a "small" quantum system is weakly coupled to macroscopic reservoirs, all memory of the past states of the system is lost through dissipative effects in the reservoirs. Its dynamics can then be described by a Markovian equation in which transition rates between the states of the system account for the influence of the reservoirs.

Chapter 3 – Solution of the Fano-Anderson model

This chapter reviews an exact solution of the Fano-Anderson model for reservoirs with a band structure. The Heisenberg equations of motion for annihilation operators are solved using a Laplace transform. There is a connection between non-analyticities in Laplace space and the spectrum of the Fano-Anderson Hamiltonian. In particular, the poles of the Laplace transform correspond to bound states, that is eigenmodes of the Hamiltonian whose energy is in a band gap. These bound states have an important influence on the dynamics of the system. This solution of the Heisenberg equations of motion is used to deduce the time-dependence for important physical quantities: occupation of the discrete level, particle currents out of reservoirs and time correlations of the discrete level occupation.

Chapter 4 – Long-time limit

In this chapter, we derive the long-time limit of the formal time-dependent solution of the model. Using the Riemann-Lebesgue lemma, we obtain analytical formulae in this limit. Our results show that three different regimes are possible depending on the number of bound states. In cases without bound states, the system decays to a steady state which is independent of the initial preparation. In cases with one bound state, the system decays to a steady state which depends on the initial preparation. In cases with two bound states or more, the system decays to a limit cycle as the occupation and currents exhibit persistent oscillations which depends on the initial preparation. Considering conservation laws, we then show how the non-oscillatory components of the occupation and currents can be dramatically simplified. In particular, this enables us to define a transmission function for the discrete level as in the Landauer-Büttiker formalism. Finally, we analyze some simplified frameworks, the wide-band limit and the results provided by the master equation and Landauer-Büttiker formalisms. We show that these schemes ignore much of the interesting physics arising from the band structure of the reservoirs.

Chapter 5 – Mimicking the adiabatic turning on of level-reservoir coupling

The methods developed in the previous chapters are suited to the case of a quench, a situation in which we consider the discrete level and reservoirs to be uncoupled before the coupling is suddenly turned on. This is not always possible in realistic set-ups, so we describe a procedure that mimics the adiabatic turning on of the level-reservoir coupling. Adding a vanishingly small constant to the spectral density, we ensure that all states thermalize in the long-time limit. This suppresses all memory of the initial preparation, and thus long-time oscillations of the occupation and currents, even in the presence of bound states. However, we show that the existence of bound states still gives rise to infinite-lifetime correlations in the discrete level occupation.

Chapter 6 – Electron transport close to the band edge of a semiconductor

In this chapter, we consider a single-level quantum dot coupled to two semiconducting electron reservoirs with the same band structure. The dot level is assumed to be close to a band edge in the reservoirs whose spectral density is then phenomenologially described by a power law. In this situation, we show that a bound state exists only if the coupling exceeds a critical value. We analyze the effects of the appearance of this bound state on the properties of system. We particularly

focus on transport properties and show that the band-edge transmission exhibits singular behaviour at the critical point. This affects the transport coefficients of the dot: the electrical and thermal conductances are maximal when the coupling is close to its critical value while the Seebeck coefficient abruptly drops at this point. Finally, we show that the critical point defines a sweet spot if the dot operates as a heat engine: One can get much larger power output without a significant decrease in efficiency close to this point.

Chapter 7 – Multiple perfectly transmitting states for tight-binding models

In this chapter, we study various set-ups where the discrete level is coupled to reservoirs described by a tight-binding Hamiltonian exhibiting narrow bands. We consider three different situations: coupling to the extremity of a one-dimensional chain, coupling to the middle of such chain and coupling to the middle of a two-dimensional square lattice. Each of these cases give rise to a different spectral density with its own features. We are mainly interested in the effects of the strongly nonlinear Lamb shifts arising in such situations. We analyze resonances which correspond to perfectly transmitting states when occurring in the band. Counter-intuitively, we show that a single discrete level can give rise to multiple perfectly transmitting states yielding a transmission function resembling that of a multi-level system. We also show that perfectly transmitting states can appear even when the discrete level is outside the reservoirs' energy bands. Finally, we try study the connection between this rich physics and the features of the local density of states.

Chapter 1

Introduction

1.1 Thermodynamics and thermoelectric effects

The slowly gained control over the conversion of heat into work in the 19th century led to the great technological progress of the Industrial Revolution. This period of immense political turmoil not only shaped the future social structure of our societies, but it was also a time of major scientific endeavours. It was indeed crucial to theoretically understand how a system can transform heat, a fundamentally disordered and incoherent source of energy, into macroscopic work proving to be useful in the human world. This led to the development of thermodynamics which is still nowadays a cornerstone of theoretical physics.

Even though it was developed starting from down-to-earth considerations, thermodynamics turned out to unravel some of the very foundations of physics. An example of this is the work of Sadi Carnot [1] who showed that the efficiency of an engine in contact with two heat sources cannot exceed a universal upper bound known as the Carnot efficiency,

$$\eta_{\text{Carnot}} = 1 - \frac{T_{\text{C}}}{T_{\text{H}}} \tag{1.1}$$

where T_{H} and T_{C} are the temperatures of the hot and cold heat sources respectively. Furthermore, this efficiency can only be reached for reversible transformations, that is idealized, infinitely slow, processes for which the working substance is at equilibrium at all times. This would later lead to the introduction of the concept of entropy which is basically a measure of the irreversibility of a transformation and is well-known to indicate the direction in which time flows as the second law of thermodynamics states that the entropy of an isolated system can never decrease.

The later work of Boltzmann [2, 3] brought another conceptual revolution with statistical mechanics. He unveiled the microscopic origin of the laws of thermodynamics which then appear as emerging from the underlying statistics of

microscopic particles. This also gave a new interpretation of entropy as a measure of the lack of information about the microscopic disorder of a system, enshrined in the celebrated Boltzmann formula,

$$S = k_{\mathrm{B}} \ln \Omega \tag{1.2}$$

where S is the entropy, k_{B} denotes the Boltzmann constant and Ω represents the number of microscopic configurations of the system giving rise to the same macroscopic state. Boltzmann's ideas were groundbreaking as they highlighted the tight relationship between thermodynamics and information, and showed that the laws of thermodynamics were to be understood as the average behaviour of a macroscopic system which can still be prone to fluctuations. These however vanish in the so-called thermodynamic limit where one considers that the system has infinite volume and contains an infinite number of particles.

Classical thermodynamics have been developed in order to study macroscopic systems for which local thermalization is faster than any other time scale. Nevertheless, it is believed that the next revolution in technology will come from the control and manipulation of nanometric systems which are small enough that the typical time it takes for electrons to go through the device is shorter than the thermalization time. Advances in nanotechnologies have notable implications in biology, especially for medical use, in chemistry for the development of nanomaterials, and of course in physics and engineering, with very promising applications of nanoelectronics in energetics and informatics. With the increasing emergency of developing sustainable forms of energy, the design of thermoelectric nanoscale devices appears as a promising opportuntity. It has also been demonstrated that the advent of nanotechnology in photovoltaics can lead to an increase of the efficiency of solar cells [4,5]. More generally, it is quite widely believed that small efficient machines will play a crucial role in the future of energetics due to the increased control over the parameters of a device at the nanoscale.

For some years now it has been possible to experimentally manipulate microscopic systems for which classical transport theories fail. Various such devices have been realized fulfilling different purposes, for example study of thermoelectric transport through molecular or single-atom junctions [6–10], quantum dots [11, 12], or capacitively coupled mesoscopic conductors [13], refrigeration of a small metallic island using quantum dots [14], rectification of thermal current [15, 16], fabrication of a single electron source [17, 18].

In this thesis, we will be mainly interested in thermoelectric effects in nanometric systems. Thermoelectricity occurs when a relation exists between the heat and electric currents in a material. These effects, although known for centuries, have only regained interest for fundamental physics since the 1990s. Thermoelectric effects are thought to be especially promising for applications in refrigeration, thermometry or power generation. One of the main advantage of thermoelectrics

is their reliability and durability as they do not contain any moving part. They are thus used in sensitive contexts such as space exploration, with the notable example of the thermoelectric generators of the Voyager probes and the Curiosity rover, or transport of biological material, where it is imperative to have reliable refrigerators at disposal. Furthermore, the design of nanoscale thermoelectrics gives rise to new promising applications as they prove to be way more efficient than their macroscopic equivalents. The efficiency of a thermoelectric is often measured using the dimensionless figure of merit ZT, the maximum efficiency than can be achieved by a thermoelectric device being given by [19]

$$\eta_{\max} = \frac{\sqrt{ZT+1}-1}{\sqrt{ZT+1}+1}\eta_{\text{Carnot}} \tag{1.3}$$

The bigger ZT, the more efficient the thermoelectric, with the limits $ZT = 0$ and $ZT \to \infty$ corresponding respectively to vanishing efficiency and Carnot efficiency. It is believed that a thermoelectric device has to reach $ZT \sim 3$ for large-scale commercial use to be considered. It has been demonstrated experimentally [20, 21] that nanostructure-based thermoelectrics exhibit values of ZT way larger, up to $ZT \sim 2.5$, than that of standard thermoelectric devices, usually $ZT \sim 1$. Another interesting application for nanoscale thermoelectrics is the refrigeration of micron-sized structures. The use of thermoelectrics has led to significative experimental progress in the refrigeration of electron gases [22, 23]. Indeed, thermoelectric devices cool electrons contrary to standard cryogenics that focus on cooling phonons inside the structure. This opens up new opportunities for the study of quantum effects in cold electrons gases.

Many of the experimental works cited above make use of quantum dots. These are nanoscale semiconductor particles that confine electrons, or holes, in all three directions of space. The typical size of the region in which electrons on a quantum dot are trapped is of the order of their de Broglie wavelength which is typically larger than a few tenths of nanometres for semiconductors. Thus, the wave-like nature of electrons can no longer be ignored in that situation. Dot electrons then have quantified energy and they can be in a coherent superposition of states. Furthermore, decoherence effects can be neglected in systems of such small size because electrons spend such a short time traversing the device that they maintain the coherence of their wavefunction during this time [19, 24]. This gives rise to interference and correlation effects that would not exist in classical systems. We then understand that quantum dots constitute a perfect tool to study quantum machines where coherent dynamics on a few discrete energy levels may induce heat to work conversion.

Independently of purely quantum effects, one should also consider the relaxation time, which is the typical time for an out-of-equilibrium electron to relax back to a local equilibrium state. This relaxation process is due to the numerous collisions, with other electrons or phonons, undergone by electrons in solids. We will consider

here nanoscale devices such that the time spent by electrons in the device is shorter than their relaxation time; this is especially true at low temperature [19, 25]. Thus, one cannot consider that electrons in the thermoelectric have reached thermal equilibrium which is a critical assumption in non-equilibrium thermodynamics [26]. This is because non-equilibrium thermodynamics assumes that thermodynamic quantities such as temperature and chemical potential can be defined locally for each point in space and vary smoothly along the system. As this is typically not satisfied for the nanoscale devices studied here, we have to define quantities globally for the whole thermoelectric device.

1.2 Bound states

A cornerstone of quantum mechanics is the quantization of the energy of a particle in an attractive potential. The wavefunction corresponding to such energy states is known to be localized at the minima of the confining potential; these states are then referred to as *bound states* [27, 28]. However, due to the wave-like nature of quantum mechanics, one would expect that a quantum particle cannot be trapped in a local minimum of the potential forever; it will eventually tunnel to a region of lower potential. Yet, we will show that this does not always happen, a particle can remain partly trapped even though it should be able to tunnel out.

A well-known example of bound states in condensed matter physics is the Kondo effect [29] in which conduction electrons pair up with a magnetic impurity to form a composite non-magnetic object. As a result, electrons which are normally free are now bound to the impurity. However, this effect is rather complicated, and we will focus on examples of bound states in a simpler model (the Fano-Anderson model) for which an exact solution provides a full quantitative description.

We will typically consider situations of the type of figure 1.1 where a discrete quantum level is tunnel-coupled to a continuum of quantum states. If the discrete level has an energy lower than any other state in the continuum (figure 1.1a), a particle in this state will remain trapped forever as it does not have enough energy to escape to the continuum. Tunnel coupling will hybridize the discrete state with the continuum but we expect the value of the wavefunction in the continuum to be exponentially small. One could call this a *trivial bound state*.

On the contrary, if the discrete level has an energy within the continuum, there is no energetic reason for a particle in this state not to leave it. In the case of thick tunneling barriers (figure 1.1b), the decay of the particle to the continuum is typically exponentially long, but its wavefunction has a vanishingly small overlap with the discrete level once it has tunnelled out. However, when tunnel coupling is stronger, typically of the order of the excess energy in the discrete state (figure 1.1c), one observes strong hybridization between the continuum and the discrete level such

(a) **Trivial bound state:**
the particle cannot fully escape the discrete level because it has too little energy

(b) **No bound state:**
the particle will fully escape the discrete level

(c) **Non-trivial bound state:**
the particle cannot fully escape the discrete level even though it has enough energy

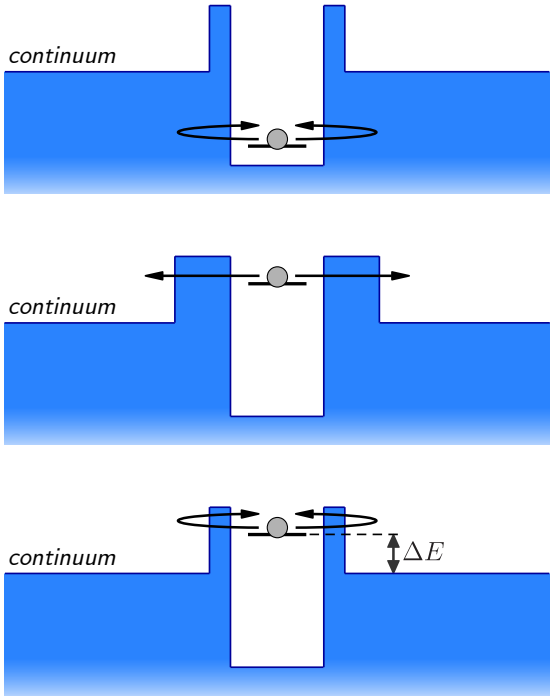

Figure 1.1 – A particle (black dot) evolving in a potential landscape (blue surface) which gives rise to a discrete state (red line) coupled to a continuum. In (a), the energy of the discrete level is lower than all energies in the continuum. The particle does not have enough energy to escape to the continuum and thus never leaves the discrete level (trivial bound state). In (b), the discrete level is weakly coupled to the continuum of states due to the thick tunnel barriers. In the long-time limit, the particle will have fully tunneled out of the discrete level (no bound state). In (c), the discrete level is strongly coupled: the width of the tunneling barrier is of the order of the excess energy ΔE in the discrete state. Even though the particle has enough energy to enter the continuum, it remains partly trapped in the discrete level due to the hybridization between this level and the continuum (non-trivial bound state).

that the particle never fully escape to the continuum. Here, the overlap of the particle's wavefunction with the discrete level initially drops but remains finite at long times. We refer to such situation as a *non-trivial bound state* as the particle gets partly trapped in the discrete level, even though it has the energy to escape.

Figure 1.2 shows the decay of a particle in a discrete state which is coupled to a continuum depending on the position of the discrete level with respect to the continuum [30–34]. If its energy is below the lowest energy in the continuum, there is a high probability that the particle remains trapped in the discrete level forever due to a trivial bound state. However, we see that a little hybridization between

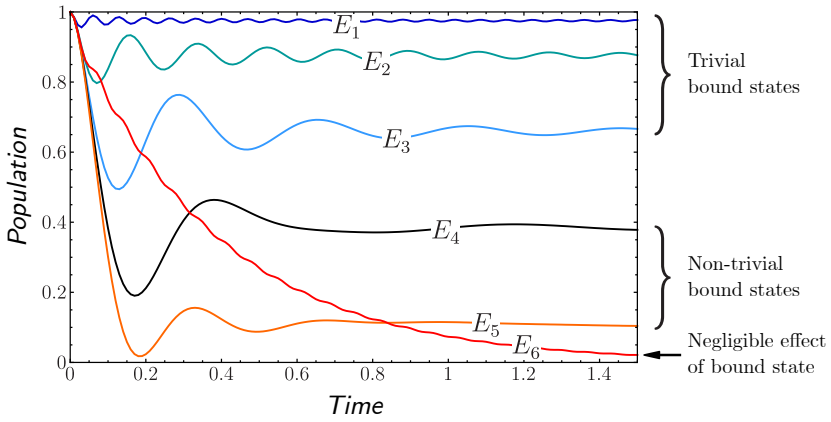

Figure 1.2 – Time evolution of the occupation of a discrete level coupled to a continuum of states [32,34]. From top to bottom, the different curves correspond to raising the energy of the discrete state with respect to the continuum. E_1, E_2 and E_3 correspond to the case of a trivial bound state where it is energetically favourable for the particle to remain in the discrete level. E_4 and E_5 correspond to the case of a non-trivial bound state where the particle never fully leaves the discrete level due to strong hybridization with the continuum. Finally, E_6 corresponds to the case where the discrete level is deep in the continuum such that the discrete level is almost completely empty at long times.

the discrete state and the continuum states causes the population of the discrete level to oscillate slightly. This hybridization is much stronger in cases where the discrete level is close to the edge of the continuum. The population of the discrete level initially drops but then stabilizes. The probability for finding the particle in the discrete level at long times is not negligible even though it is energetically favourable to tunnel out. This corresponds to the case of a non-trivial bound state. Finally, if the discrete level is deep in the continuum, we observe that the population of the level decays exponentially. The discrete level is basically empty in the long-time limit.

A technical remark is necessary here: The Hamiltonian considered to obtain figure 1.2 describes a two-level atom coupled to a photonic continuum and it is not strictly identical to the Fano-Anderson Hamiltonian studied in this thesis which is given in equation (1.16) below. However, the two-level atom reduces to the Fano-Anderson model when the analysis is restricted to the subspace generated by single excitations of the atom or the photonic field. Typically, one considers the initial situation where an excited atom is coupled to an electromagnetic field whose modes are all empty [30–34], such that the only process occurring here is the spontaneous emission of a photon by the atom. This is equivalent to the bosonic Fano-Anderson Hamiltonian at zero temperature.

Trivial bound states will not be considered further in this thesis, thus whenever a reference is made to a bound state, one should keep in mind that it is of the non-trivial type.

1.3 Thermoelectric transport in the linear response regime

1.3.1 Currents and transport coefficients

To study the thermoelectric properties of a device, we consider the typical situation depicted in figure 1.3 where the system of interest is sandwiched between two reservoirs of electrons kept at different temperatures and chemical potentials. This induces a current of electrons and heat across the thermoelectric device. When a thermal bias is introduced, thermally excited electrons in the hot reservoir (reservoir L) can be found in energy states above the chemical potential, and can then flow to the cold reservoir (reservoir R), even if $\mu_{\mathrm{R}} > \mu_{\mathrm{L}}$. However, the temperature bias also allows electrons in reservoir R with energy lower than the chemical to occupy the states left empty by thermally excited electrons in reservoir L. Hence, the direction of the net electric current is not obvious in this situation. Whether current flows one way or the other depends on the energy filtering properties of the system connecting the reservoirs [19]. That is, by preventing electrons at certain energies from going through the system, it is possible to favour a particular direction for the electric current. For example, blocking electrons whose energy is below μ_{R} will give rise to a net current from L to R, that is againt the chemical potential bias. This phenomenon is related to the Seebeck effect which describes the appearance of the voltage gradient between two regions kept at different temperatures in the absence of a net flow of charge. The opposite phenomenon where a heat flow proportional to a displacement of charge appears is known as the Peltier effect and is typically used for refrigeration.

Once a steady state is reached, the device is traversed by constant electric and energy currents. We respectively denote by I_α and U_α the electric and energy current out of reservoir α. Due to particle and energy conservation, these currents are conserved,

$$I_{\mathrm{L}} + I_{\mathrm{R}} = 0 \tag{1.4a}$$

$$U_{\mathrm{L}} + U_{\mathrm{R}} = 0 \tag{1.4b}$$

We then define $I = I_{\mathrm{L}} = -I_{\mathrm{R}}$ and $U = U_{\mathrm{L}} = -U_{\mathrm{R}}$.

The first law of thermodynamics tells us that energy can take two forms: heat and work. In order to study the thermodynamic behaviour of a system, it is then necessary to distinguish these two contributions to the total energy. In

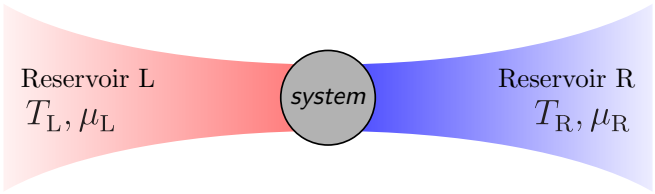

Figure 1.3 – Schematic drawing of a typical thermoelectric device. A system is connected to two electron reservoirs, L and R, with different temperatures and chemical potentials.

thermoelectric devices, work corresponds to the generation of electric power. This means that one can obtain the heat current out of reservoir α by substracting the electric power generated in this reservoir from the total energy current out of the reservoir [19]. This yields $Q_\alpha = U_\alpha - V_\alpha I_\alpha$, where V_α is the electric potential of reservoir α. The electric and chemical potentials are related through $\mu_\alpha = -eV_\alpha$, where $e > 0$ is the elementary charge. In general, heat currents are not conserved.

We will consider here the so-called linear response regime where currents only depend linearly on the temperature and voltage biases [19, 26]. This assumption is justified if the variations of temperature and chemical potential with respect to the average values T and μ are small. More specifically, we require $|\Delta T| \ll T$ and $|\Delta\mu| \ll k_\mathrm{B}T$, where $\Delta T = T_\mathrm{L} - T_\mathrm{R}$ and $\Delta\mu = \mu_\mathrm{L} - \mu_\mathrm{R}$. One then phenomenologically introduces transport coefficients accounting for the amplitude of the system's response to non-equilibrium. These coefficients describe the well-known thermoelectric effects discussed above. The electric and heat currents across the device are then respectively given by [19, 26]

$$I = G\Delta V + GS\Delta T \tag{1.5a}$$
$$Q = G\Pi\Delta V + (C + GS\Pi)\Delta T \tag{1.5b}$$

where G is the electrical conductance, S is the Seebeck coefficient, C is the thermal conductance and Π is the Peltier coefficient. We will assume here that $\Pi = TS$, which is true as long as no external magnetic field is applied [19], although it holds even in the presence of a magnetic field for the simple systems studied in this thesis.

As already stated, the heat current is not conserved along the device in principle. We should then consider the heat current incoming from the left lead and the right lead separately. However, we have $Q_\mathrm{L} + Q_\mathrm{R} = -I\Delta V$ which is of second order in terms of the small biases ΔV and ΔT and can thus be ignored in the linear response regime. A negligible error is incurred if we instead consider the following

heat current

$$Q = U - VI \simeq Q_{\mathrm{L}} \simeq -Q_{\mathrm{R}} \tag{1.6}$$

The currents defined in equation (1.5) above correspond to two different forms of energy conversion: A difference in temperature can induce an electric current against the potential bias, and conversely, a voltage bias can induce a heat flow from the cold reservoir to the hot one. The former situation corresponds to the case where the thermoelectric is used as a heat engine to generate electric power, while the latter case describes the thermoelectric used as a refrigerator powered by electric work.

1.3.2 Power and efficiency in the linear response regime

The simple formulae given in equation (1.5) allow for a description of the thermodynamic behaviour of the machine in terms of transport coefficients. We will focus here on the case where the device works as an engine, absorbing heat from the reservoirs to deliver electrical power. A cornerstone of thermodynamics is the fact that the efficiency of a heat engine cannot exceed the Carnot efficiency (1.1) which only depends on the temperature of the reservoirs. In the analysis of the thermodynamics of the engine, it is then relevant to consider the case where temperatures are fixed whereas the voltage bias can be varied to optimize the behaviour of the device.

First, it is necessary to ensure that the machine is working like an engine, that is that it delivers a positive power output. The electric power generated in the reservoirs is defined as

$$P = Q_{\mathrm{L}} + Q_{\mathrm{R}} = -I\Delta V = -G\Delta V(\Delta V + S\Delta T) > 0 \tag{1.7}$$

where we have used the linear response formulae (1.5). We then find that, for the machine to work like an engine, the voltage bias has to satisfy

$$-1 < \frac{\Delta V}{S\Delta T} < 0 \tag{1.8}$$

The generated power cancels on both edges of the voltage window defined above but it reaches a maximum at $\Delta V = -S\Delta T/2$. At this point, the generated power reads

$$P_{\max} = \frac{1}{4} GS^2(\Delta T)^2 \tag{1.9}$$

The maximum power output is then entirely determined by the quantity GS^2 which is then often referred to as the power factor [19].

The efficiency of the engine is defined as the ratio between the power output and the positive heat current supplied to the machine. The hot reservoir (reservoir L)

will provide heat as a resource whereas the cold reservoir (reservoir R) acts as a heat sink for the excess heat that has not been converted into work. The efficiency then reads

$$\eta = \frac{P}{Q_{\mathrm{L}}} = -\frac{I\Delta V}{Q} = -\frac{G\Delta V(\Delta V + S\Delta T)}{G\Pi\Delta V + (C + GS\Pi)\Delta T} \tag{1.10}$$

At maximum power, we find

$$\eta(P_{\max}) = \frac{ZT}{2ZT+4}\eta_{\mathrm{Carnot}} \tag{1.11}$$

where we have introduced the dimensionless figure of merit [19]

$$ZT = \frac{GS^2T}{C} \tag{1.12}$$

The evolution of $\eta(P_{\max})$ with ZT is shown in figure 1.4 (red curve).

Alternatively, if we are interested in first optimizing the efficiency of the thermoelectric, we find that the bias voltage maximizing the efficiency while ensuring positive power output is given by

$$\Delta V = -\frac{S\Delta T}{ZT}(ZT + 1 - \sqrt{ZT+1}) \tag{1.13}$$

This yields the maximum efficiency, represented by the blue curve in figure 1.4,

$$\eta_{\max} = \frac{\sqrt{ZT+1}-1}{\sqrt{ZT+1}+1}\eta_{\mathrm{Carnot}} \tag{1.14}$$

The corresponding power output is then

$$P(\eta_{\max}) = \frac{4\sqrt{ZT+1}}{ZT+2\sqrt{ZT+1}+2}P_{\max} \tag{1.15}$$

Figure 1.5 depicts $P(\eta_{\max})$ as a function of ZT.

$\eta_{\max}$ and $\eta(P_{\max})$ monotonously increase with ZT, with $\eta_{\max} = \eta(P_{\max}) = 0$ for $ZT = 0$, and $\eta_{\max} = 2\eta(P_{\max}) = \eta_{\mathrm{Carnot}}$ for $ZT \to \infty$. On the contrary, $P(\eta_{\max})$ vanishes for $ZT \to \infty$; this could be expected as this limit corresponds to the Carnot efficiency and thus to an infinitely slow transformation which cannot deliver any power output. We then realize that the figure of merit ZT is a measure of the potential efficiency of the thermoelectric, similarly to the power factor GS^2 which describes the maximum power that it can deliver. All in all, the figure of merit and the power factor constitute powerful tools to describe the quality of a thermoelectric. Thanks to them, we understand that designing a good thermoelectric would require, within the realms of possibility, high electrical conductance and Seebeck coefficient alongside small thermal conductance.

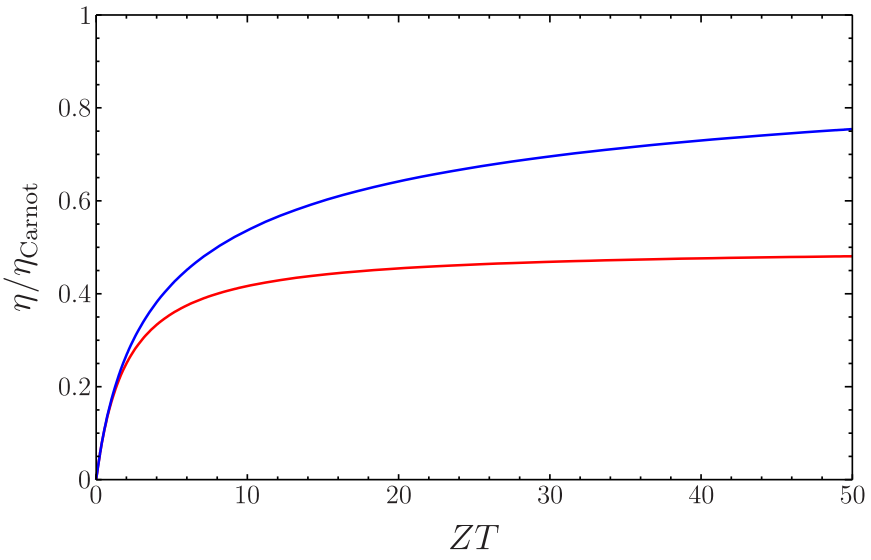

Figure 1.4 – Thermoelectric efficiency as a function of the figure of merit ZT. The blue line represents the maximum efficiency $\eta_{\max}$ and the red line is the efficiency at maximum power $\eta(P_{\max})$. In the limit of large ZT, $\eta_{\max}$ approaches the Carnot efficiency η_{Carnot} while $\eta(P_{\max})$ tends to $\eta_{\mathrm{Carnot}}/2$.

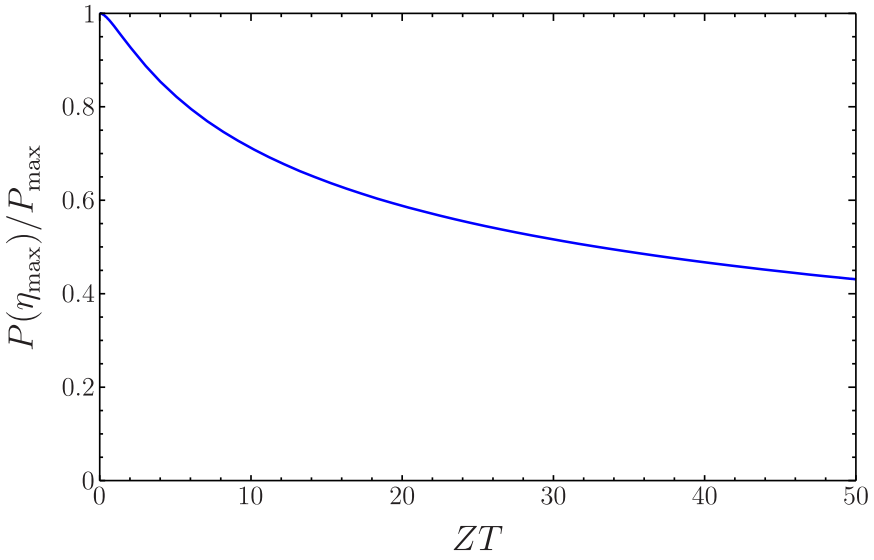

Figure 1.5 – Power at maximum efficiency $P(\eta_{\max})$ as a function of the figure of merit ZT. $P(\eta_{\max})$ is plotted in units of the maximum power $P_{\max}$. For $ZT \to \infty$, the maximum efficiency tends to the Carnot efficiency. This corresponds to an infinitely slow process which does not deliver any power output. Hence, $P(\eta_{\max})$ vanishes in the limit of large ZT.

1.4 Strong coupling

At the handwaving level we expect that strong coupling between a device and its environment will lead to stronger currents going through the device. This thus seems to be the interesting regime to design a thermal machine as one would expect stronger currents to improve the power output of a heat engine or the cooling power of a refrigerator. Tackling the strong coupling regime is however challenging in both classical and quantum mechanics. The main issue comes from the difficulty to distinguish the system from its environment when they are strongly coupled as the border between them fades away. This can lead to counter-intuitive effects, such as the non-trivial bound states discussed in section 1.2. It is thus necessary to adopt a broader point of view where the coupling of a system to its environment is not considered only through the reduced dynamics of the system.

We will show in section 2.2 that the assumption of weak coupling in open quantum systems amounts to neglect memory effects in the environment. The time evolution of the system can then be described by a Markovian master equation as all memory of its past states has been lost. In this framework, coupling is treated as a perturbation and the degrees of freedom of the environment are traced out, leaving a dissipative term in the system dynamics.

Quantum thermodynamics in the strong coupling regime have recently given rise to intense activity where various theoretical schemes have been proposed to tackle this kind of problems [35–39].

This thesis focuses on a simple model (the Fano-Anderson model) which has an exact solution, giving one full access to its dynamics at arbitrary coupling. This makes it an ideal test-bed on which to explore strong-coupling physics.

1.5 The Fano-Anderson model

In chapter 2 we will present two formalisms that can be used to analyze transport and thermoelectric effects in quantum systems; the Landauer-Büttiker formalism and the master equation formalism. However, both suffer from important limitations. In the Landauer-Büttiker formalism, the transport properties are determined from the quantum system's scattering matrix but the derivation of this matrix is not implemented for a reservoir with a band structure. This makes it impossible to trust Landauer-Büttiker theory in some situations, for example close to the band edge of semiconducting reservoirs. Conversely, it is possible to study nanoscale interacting systems using the master equation formalism which solely requires to diagonalize a few-level Hamiltonian. However, one then has to suppose that the scatterer is weakly coupled to the reservoirs.

We then understand that it is necessary to implement new theoretical tools to give a more precise account of open quantum systems in the strong coupling

regime. A widely used method is the Keldysh non-equilibrium Green's function formalism [40, 41]. This approach is based on the projection of the Heisenberg equations for field operators on the Keldysh contour which consists of two branches, one going forward in time while the other goes backwards. This technique has first been introduced during the 1970s [42] but has mostly regained interest many years later with the work of Meir and Wingreen [43] who derived a formal generalization of the Landauer formula expressed in terms of the exact Green function of the device. Within this framework, coupling between the central system and the reservoirs can be treated to all orders and the band structure of the reservoirs can be taken into account. However, most works assume that the coupling between the central region and the reservoirs is adiabatically turned on and thus completely ignore the influence of initial preparation. This is for example known to yield an incomplete description of systems whose spectrum contains isolated energy levels [44, 45].

In this work, we adopt a different point of view and try to approach the general properties of open quantum systems considering an exactly solvable model. We will extensively analyze its solution in order to see how its properties may differ from what approximate theoretical schemes would predict. We consequently study the situation depicted in figure 1.6 where a single discrete quantum level is coupled to various reservoirs of non-interacting particles. The corresponding Hamiltonian is

$$\hat{H} = \hbar\omega_{\mathrm{d}}\hat{d}^{\dagger}\hat{d} + \hbar\sum_{\alpha,k}\omega_{\alpha k}\hat{c}^{\dagger}_{\alpha k}\hat{c}_{\alpha k} + \hbar\sum_{\alpha,k}\left(g_{\alpha k}\hat{d}^{\dagger}\hat{c}_{\alpha k} + g^{*}_{\alpha k}\hat{c}^{\dagger}_{\alpha k}\hat{d}\right) \tag{1.16}$$

$\hat{d}$ and $\hat{c}_{\alpha k}$ denote field operators for a particle on the discrete level and in mode k of reservoir α respectively; the corresponding energies are ω_{d} and $\omega_{\alpha k}$. Finally, $g_{\alpha k}$ describes the coupling between the discrete level and mode k in reservoir α.

This model was introduced by Fano [46] in 1961 to study the autoionization of an atom. The same year Anderson [47] studied the same Hamiltonian as a simplifying limit of his well-known impurity model introduced to study magnetic impurities in metals. Hamiltonian (1.16) is now widely referred to as the Fano-Anderson Hamiltonian. It differs from Anderson's Hamiltonian because the latter takes into account spin degeneracy and Coulomb interaction. The Anderson impurity model is typically used to describe a single-level quantum dot that can be occupied by two electrons with opposite spins which then repel each other. Such quantum dot can be described by the Fano-Anderson Hamiltonian if a strong magnetic field is applied in order to lift spin degeneracy to the point that the higher energy level is always empty.

The annihilation and creation operators in Hamiltonian (1.16) can be either fermionic or bosonic. The fermionic version of the Fano-Anderson model has been used to analyze transport in systems of noninteracting electrons [44, 45, 48–50]. The bosonic version of the Fano-Anderson model has been widely studied in the context of a photonic continuum with a band structure coupled to an atomic level [32,

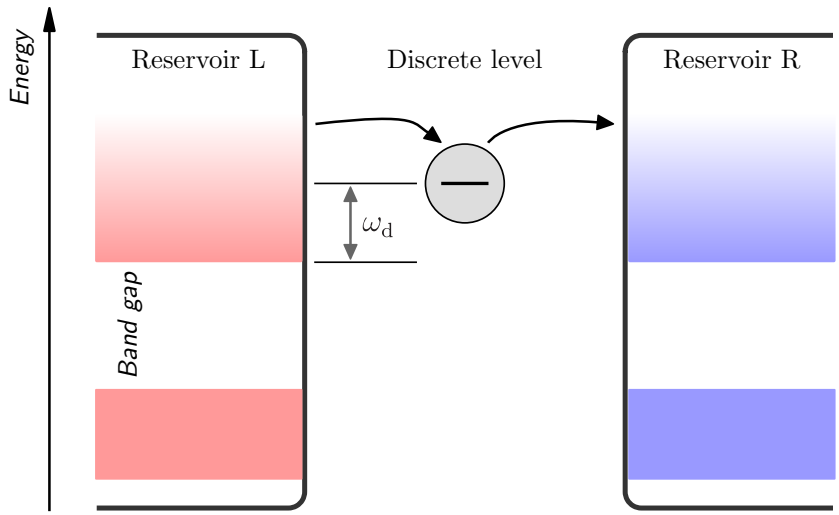

Figure 1.6 – Schematic representation of the Fano-Anderson model: a discrete level is coupled to various reservoirs with which it can exchange particles. In this thesis, we consider reservoirs which exhibit a band structure.

33] or a nanocavity [34, 51–54], or for the analysis of the transport properties of nanophotonic devices [51] and Bose-Einstein condensates [55]. More generally, as the Fano-Anderson model is exactly solvable, it is widely used as a benchmark for the dynamics of open quantum systems [56, 57].

In the Fano-Anderson Hamiltonian (1.16), particles in the reservoirs are considered to be free. This corresponds to different situations depending on the nature of the particles involved. In cold atom gases for example, one typically considers contact interactions between hard-core bosons. These can then be neglected if the density of particles is low. On the contrary, interactions between electrons can be neglected in the limit of high density [58]. This is a counter-intuitive consequence of the long range of Coulomb interaction which thus still plays an important role for low densities. However, due to the screening effects taking place if the density of electrons is high, these can then be considered as free particles provided renormalization of their mass. Finally, the case of photons is trivial because they do not intereract with each other.

A crucial feature of the Fano-Anderson model is that it can exhibit infinite-lifetime bound states in the band gaps of the reservoirs. The existence of such state is strongly linked to the band structure of the reservoirs. It was first highlighted in the context of a superconducting band edge [59] where it is known to give rise to Landau-Zener-Stueckelberg physics [60]. It has been intensively studied in photonics since then [30–34, 51, 57]. For an atomic level coupled to a photonic continuum, it is known to prevent full decay of the atomic state as it gets partially trapped in this

bound state. Such effect have been recently observed for a nitrogen-vacancy centre coupled to a waveguide [61]. It has also been shown that the existence of more than two bound states leads to persistent oscillations of the state of the system at long times [44, 45].

Chapter 2

Theories of open quantum systems

In this chapter, we review standard theoretical frameworks used to study quantum thermodynamical problems: the Landauer-Büttiker formalism and the master equation formalism. The Landauer-Büttiker formalism focuses on the description of steady-state transport properties. In this framework, one considers transport between reservoirs of free electrons connected to each other through a small disordered region. Electrons incoming to this central system undergo elastic scattering events which redistribute them among reservoir modes. It is the transmission properties of the scatterer which then give rise to thermoelectric effects. This framework is particularly useful in the linear response regime as all the transport coefficients of the device can be deduced from the scattering properties of the central region. This type of problems can also be addressed within the framework of quantum master equations. It is shown that when a "small" quantum system is weakly coupled to macroscopic reservoirs, all memory of the past states of the system is lost through dissipative effects in the reservoirs. Its dynamics can then be described by a Markovian equation in which transition rates between the states of the system account for the influence of the reservoirs.

2.1 Scattering theory and the Landauer-Büttiker formalism

2.1.1 The Landauer-Büttiker formula

Starting as early as 1957, Landauer [62, 63] carried out foundational works studying transport through a small region connected to two terminals. His results were generalized to the case of multi-terminal geometries by Büttiker [64, 65] in the late 1980s, and this technique is now widely referred to as the Landauer-Büttiker formalism. This formalism is based on the idea that a transport problem consists

of a small scattering region coupled to idealized reservoirs of free electrons. It is moreover assumed that all the scattering events ocurring in the central region are elastic such that electrons do not lose energy in the scatterer. Thermalization thus only takes place in the reservoirs. The scattering region is connected to the reservoirs by perfectly conducting leads and electrons at a given energy in the leads may be found in different propagation states. One can for example imagine that these different channels correspond to different spin states [66]. However, they are more often introduced as transverse modes due to spatial confinement when one considers the case where the leads are electron waveguides [19, 24, 66]. Through elastic collisions in the disordered scattering region, the various incoming electron modes will be mixed and then transmitted possibly to a different channel.

Hence, the central region is characterized by a scattering matrix $\mathcal{S}$, where $\mathcal{S}_{\alpha' k', \alpha k}(\omega)$ relates the amplitude of an incoming wavefunction with energy $\hbar\omega$ in mode k of lead α to the amplitude of the corresponding outgoing electron wave in mode k' of lead α'. The corresponding transmission probability is then given by [19, 24, 66]

$$\mathcal{T}_{\alpha' k', \alpha k}(\omega) = \left| \mathcal{S}_{\alpha' k', \alpha k}(\omega) \right|^2 \tag{2.1}$$

The total transmission from reservoir α to reservoir α' is obtained by summing over all quantum occupied channels

$$\mathcal{T}_{\alpha' \alpha}(\omega) = \sum_{k,k'} \mathcal{T}_{\alpha' k', \alpha k}(\omega) \tag{2.2}$$

The Landauer approach states that the currents flowing through the scattering region can be written simply in terms of the above transmission probabilities. The total current outgoing from reservoir α to the scatterer can be seen at the sum of two contributions. First, we have the positive contribution of electrons that leave reservoir α and then head to another reservoir α'. The corresponding transmission probability is $\mathcal{T}_{\alpha' \alpha}(\omega)$. Conversely, we have to count negatively electrons incoming from reservoir α' to reservoir α. The corresponding transmission probability is $\mathcal{T}_{\alpha \alpha'}(\omega)$. Furthermore, the number of electrons in each reservoir-mode at energy ω has to be taken into account. It is given by the Fermi factor

$$n_\alpha(\omega) = \left(\mathrm{e}^{\beta_\alpha(\hbar\omega - \mu_\alpha)} + 1 \right)^{-1} \tag{2.3}$$

where β_α and μ_α respectively are the inverse temperature and chemical potential of reservoir α. The electric current from reservoir α to the scatterer is then given by [66]

$$I_\alpha = -\frac{e}{2\pi} \sum_{\alpha'} \int \mathrm{d}\omega \left(\mathcal{T}_{\alpha' \alpha}(\omega) n_\alpha(\omega) - \mathcal{T}_{\alpha \alpha'}(\omega) n_{\alpha'}(\omega) \right) \tag{2.4}$$

Remarkably, all factors (like the reservoirs' density of states or the Fermi velocity) cancel in the derivation of the relation leaving only the factor $(2\pi)^{-1}$.

Denoting by M_α the number of transmission channels in lead α, we have [19]

$$\sum_{\alpha'} \mathcal{T}_{\alpha'\alpha}(\omega) = \sum_{\alpha'} \mathcal{T}_{\alpha\alpha'}(\omega) = M_\alpha \tag{2.5}$$

Using this relation in the formula for the electric current yields the Landauer-Büttiker formula

$$I_\alpha = -\frac{e}{2\pi} \sum_{\alpha'} \int \mathrm{d}\omega\, \mathcal{T}_{\alpha\alpha'}(\omega)(n_\alpha(\omega) - n_{\alpha'}(\omega)) \tag{2.6}$$

Similarly, the energy current reads

$$U_\alpha = \frac{\hbar}{2\pi} \sum_{\alpha'} \int \mathrm{d}\omega\, \omega \mathcal{T}_{\alpha\alpha'}(\omega)(n_\alpha(\omega) - n_{\alpha'}(\omega)) \tag{2.7}$$

Equations (2.6) and (2.7) guarantee particle and energy conservation as that the total currents vanish,

$$\sum_\alpha I_\alpha = 0 \tag{2.8a}$$

$$\sum_\alpha U_\alpha = 0 \tag{2.8b}$$

As in section 1.3, we define the heat current out of reservoir α as $Q_\alpha = U_\alpha - V_\alpha I_\alpha$, where we recall that $V_\alpha = -\mu_\alpha/e$. Using the expressions (2.6) and (2.7) of the electric and energy currents, we find

$$Q_\alpha = \frac{1}{2\pi} \sum_{\alpha'} \int \mathrm{d}\omega\, (\hbar\omega - \mu_\alpha) \mathcal{T}_{\alpha\alpha'}(\omega)(n_\alpha(\omega) - n_{\alpha'}(\omega)) \tag{2.9}$$

The above formula provides a new interpretation of heat as the energy induced by the distribution of particles over the energy levels of the Hamiltonian [19, 67]. The heat carried by an electron at energy ω in reservoir α is then defined as $\hbar\omega - \mu_\alpha$. This basically measures the difference between the ground state of the many-body system (zero temperature) and the thermally broadened distribution of electrons [19]. This spread is typically due to thermal fluctuations on which there is no experimental control. On the contrary, work is typically defined as the energy generated by a change of the energy levels themselves. One could indeed argue that this can be controlled externally, through time-dependent parameters in the Hamiltonian for example.

We then understand that, in order to describe the transport properties of the device, it is only necessary to calculate its scattering matrix. The latter is often accounted for phenomenologically rather than a complicated microscopic description of the scattering events taking place in the central region. Besides its simplicity, this

formalism is also very interesting since no assumption has been made on the coupling between the scatterer and the reservoirs, the regime of strong coupling is then in principle accessible in this framework. Nevertheless, scattering theory cannot be applied to any situation. Indeed, currents are calculated counting electrons going through the device one by one. The scattering of an electron is then assumed to be independent of the dynamics of all the other electrons crossing the device at the same time, possible correlations due to electron-electron interactions are completely overlooked. This assumption may seem quite far-fetched in nanostructures as the small size of the system could induce strong Coulomb repulsion between electrons. Nevertheless, scattering theory still provides satisfactory results for a wide-range of nanoscale devices [19].

2.1.2 Linear response regime

As explained in section 1.3, thermoelectric transport is often described in the linear response regime. We thus consider here the Landauer-Büttiker formalism in the situation where the device is assumed to be very close to equilibrium [19, 24, 66], that is, thermodynamic quantities differ very slightly from one reservoir to another. The temperature and chemical potential of reservoir α are then written in terms of deviations from average values T and μ, $T_\alpha = T + \delta T_\alpha$ and $\mu_\alpha = \mu + \delta\mu_\alpha$. In the linear response regime, the deviations δT_α and $\delta\mu_\alpha$ are assumed to be small. The Fermi factor for reservoir α can then be expanded as follows

$$n_\alpha(\omega) \simeq n(\omega) + \Phi(\omega)\left(\delta\mu_\alpha + (\hbar\omega - \mu)\frac{\delta T_\alpha}{T}\right) \tag{2.10}$$

where $n(\omega)$ is the Fermi factor at temperature T and chemical potential μ and $\Phi(\omega)$ is proportional to the derivative of the Fermi factor

$$\Phi(\omega) = -\frac{1}{\hbar}\frac{\partial n}{\partial \omega} = \frac{\beta}{4\cosh^2(\beta(\hbar\omega - \mu)/2)} \tag{2.11}$$

The average temperature T defines the relevant energy scale for expression (2.10) to be valid: The expansion holds if $\delta\mu_\alpha \ll k_\mathrm{B}T$ and $\delta T_\alpha \ll T$.

For simplicity, we focus here on the two-terminal case where the scatterer is only coupled to two leads L and R as in section 1.3. Using equations (2.6) and (2.8a), we then find the following the following electric current

$$I = I_\mathrm{L} = -I_\mathrm{R} = -\frac{e}{2\pi}\int \mathrm{d}\omega\, \mathcal{T}(\omega)(n_\mathrm{L}(\omega) - n_\mathrm{R}(\omega)) \tag{2.12}$$

where $\mathcal{T}(\omega) = \mathcal{T}_\mathrm{LR}(\omega) = \mathcal{T}_\mathrm{RL}(\omega)$. Using the expansion (2.10), the Fermi factor difference in the above equation can be simplified and we can write the electric

current in terms of the small voltage and temperature biases $\Delta V = V_{\mathrm{L}} - V_{\mathrm{R}}$ and $\Delta T = T_{\mathrm{L}} - T_{\mathrm{R}}$,

$$I = e^2 \iota_0 \Delta V - \frac{e\iota_1}{T} \Delta T \tag{2.13}$$

with

$$\iota_n = \frac{1}{2\pi} \int \mathrm{d}\omega \, (\hbar\omega - \mu)^n \mathcal{T}(\omega) \Phi(\omega) \tag{2.14}$$

The expression (2.13) for the electric current takes the same form as the general linear response expression (1.5a). Comparing the coefficients in equations (2.13) and (1.5a), we see that the Landauer-Büttiker formalism provides a simple relation between transport coefficients and the microscopic scattering properties of the device. Here we find that the electrical conductance G and the Seebeck coefficient S are given by [19]

$$G = e^2 \iota_0 \tag{2.15a}$$

$$S = -\frac{\iota_1}{eT\iota_0} \tag{2.15b}$$

The same treatment can be carried out for the heat current. According to equations (2.7) and (2.8b), we have the energy current

$$U = U_{\mathrm{L}} = -U_{\mathrm{R}} = \frac{\hbar}{2\pi} \int \mathrm{d}\omega \, \omega \mathcal{T}(\omega) (n_{\mathrm{L}}(\omega) - n_{\mathrm{R}}(\omega)) \tag{2.16}$$

We then deduce the heat currents

$$Q_{\mathrm{L}} = U - V_{\mathrm{L}} I \tag{2.17a}$$

$$Q_{\mathrm{R}} = -U + V_{\mathrm{R}} I \tag{2.17b}$$

Even though heat currents are not conserved across the device in general, we have shown in section 1.3 that the difference between Q_{L} and Q_{R} is of second order in terms of the small biases ΔV and ΔT. As such, we write $Q = U - VI \simeq Q_{\mathrm{L}} \simeq -Q_{\mathrm{R}}$. Using equation (2.10), we then find

$$Q = -e\iota_1 \Delta V + \frac{\iota_2}{T} \Delta T \tag{2.18}$$

Comparing this expression with the general linear response expression (1.5b), we find that the thermal conductance C and the Peltier coefficient Π are given by [19]

$$C = \frac{1}{T} \left(\iota_2 - \frac{\iota_1^2}{\iota_0} \right) \tag{2.19a}$$

$$\Pi = -\frac{\iota_1}{e\iota_0} = TS \tag{2.19b}$$

The expressions (2.15) and (2.19) of transport coefficients in terms of the integrals ι_n also provide a description of the thermodynamic properties of the device through the power factor GS^2 and the figure of merit ZT,

$$GS^2 = \frac{\iota_1^2}{T^2 \iota_0} \tag{2.20a}$$

$$ZT = \frac{GS^2 T}{C} = \frac{GS\Pi}{C} = \frac{\iota_1^2}{\iota_0 \iota_2 - \iota_1^2} \tag{2.20b}$$

The linear response formalism can be straightforwardly adapted to the multi-terminal case. Transport coefficients then become matrices which elements $G_{\alpha\alpha'}$, $C_{\alpha\alpha'}$, $S_{\alpha\alpha'}$ and $\Pi_{\alpha\alpha'}$ describe transport properties between lead α and lead α'.

2.2 Quantum master equations

The Landauer-Büttiker formalism focuses on the steady-state transport properties of a "small" quantum system coupled to macroscopic electron reservoirs. However, it does not describe the transient dynamics of the central system as this requires a precise microscopic description of the scattering events occurring in this region. The dynamics of an open quantum system can be addressed within the framework of quantum master equations. This dynamics is a combination of the intrinsic unitary time evolution of the system and the dissipative dynamics induced by the reservoirs. If we suppose that the reservoir consists of a thermodynamically big amount of particles, it is natural to assume that it loses memory of its past dynamics on very short time scales. One can for example imagine that particles in the reservoir have their degrees of freedom repeatedly reset due to frequent collisions. We thus assume the reduced dynamics of the system to be Markovian, that is that it is independent of the past states of the system.

2.2.1 The Lindblad master equation

The dynamics of the system is studied considering its reduced density matrix $\hat{p}$. It is obtained from the total density matrix $\hat{\varrho}$ by tracing out the reservoir degrees of freedom,

$$\hat{p} = \mathrm{Tr}_{\mathrm{res}}\, \hat{\varrho} \tag{2.21}$$

Moreover, we assume here factorized initial conditions, that is that the initial density matrix is given by

$$\hat{\varrho}_0 = \hat{p}_0 \otimes \hat{\varrho}_{\mathrm{res}} \tag{2.22}$$

where $\hat{p}_0$ is the initial system density matrix and $\hat{\varrho}_{\text{res}}$ represents the initial state of the reservoir, which is usually chosen to be some reference state like the canonical distribution. The time evolution of the system density matrix can then be described with a dynamical map,

$$\hat{p}(t) = V(t)[\hat{p}_0] \tag{2.23}$$

where the dynamical map $V(t)$ is a super-operator acting on the space of density matrices. The assumption of a Markovian time evolution constrains the dynamical map, namely, a Markov-type evolution must satisfy the semigroup property [26, 68]

$$V(t+t') = V(t)V(t') \tag{2.24}$$

As such, the time evolution of the system can then be expressed as follows

$$\frac{\mathrm{d}\hat{p}}{\mathrm{d}t} = \lim_{\delta t \to 0} \frac{1}{\delta t}(V(t+\delta t)[\hat{p}_0] - V(t)[\hat{p}_0]) = \lim_{\delta t \to 0} \frac{1}{\delta t}(V(\delta t)[\hat{p}(t)] - \hat{p}(t)) \tag{2.25}$$

In order to find an expression for the dynamical map $V(t)$, we analyze the dynamics of the set-up made up of the combined system and reservoir. It is provided by the Schrödinger equation such that the total density matrix at time t is given by

$$\hat{\varrho}(t) = \hat{U}(t)\hat{\varrho}_0\hat{U}(t)^\dagger \tag{2.26}$$

where $\hat{U}(t)$ is the (unitary) time evolution operator for the set-up. The reduced density matrix of the system is obtained taking the partial trace over the reservoir's degrees of freedom and we then find a first way of expressing the dynamical map,

$$V(t)[\hat{p}_0] = \hat{p}(t) = \mathrm{Tr}_{\text{res}}\left(\hat{U}(t)\hat{\varrho}_0\hat{U}(t)^\dagger\right) = \mathrm{Tr}_{\text{res}}\left(\hat{U}(t)\hat{p}_0 \otimes \hat{\varrho}_{\text{res}}\hat{U}(t)^\dagger\right) \tag{2.27}$$

To perform the partial tracial, it is convenient to work in the eigenbasis of the reservoir density matrix. It can indeed always be written as follows

$$\hat{\varrho}_{\text{res}} = \sum_M P_M \, |M\rangle\langle M| \tag{2.28}$$

where the states $|M\rangle$ form an orthonormal basis of the reservoir Hilbert space $\mathbb{H}_{\text{res}}$ and the positive numbers P_M satisfy $\sum_M P_M = 1$. We then have

$$V(t)[\hat{p}] = \sum_{M,N} \hat{W}_{MN}(t)\hat{p}\hat{W}_{MN}(t)^\dagger \tag{2.29}$$

where $\hat{W}_{MN}$ are operators acting on the system Hilbert space $\mathbb{H}_{\text{sys}}$ given by

$$\hat{W}_{MN}(t) = \sqrt{P_N}\,\langle M|\hat{U}(t)|N\rangle \tag{2.30}$$

It is straightforward to show that $\sum_{M,N} \hat{W}_{MN}(t)^\dagger\hat{W}_{MN}(t) = 1$. This ensures that the time evolution preserves the trace of the density matrix, namely $\mathrm{Tr}\,\hat{p}(t) = 1$.

For simplicity, we will only consider here the case where the dimension d of $\mathbb{H}_{\text{sys}}$ is finite. The operators $\hat{W}_{MN}(t)$ can then be written as follows

$$\hat{W}_{MN}(t) = \sum_{j=1}^{d^2} w^j_{MN}(t)\hat{A}_j \tag{2.31}$$

Here the $\hat{A}_j$ are a basis of orthonormal operators on $\mathbb{H}_{\text{sys}}$, that is

$$\text{Tr}\left(\hat{A}^\dagger_j \hat{A}_k\right) = \delta_{jk} \tag{2.32}$$

Without loss of generality we choose: $\hat{A}_{d^2} = 1/\sqrt{d}$, such that all the other basis operators are traceless. We consequently obtain

$$V(t)[\hat{p}] = \sum_{j=1}^{d^2}\sum_{k=1}^{d^2} v_{jk}(t)\hat{A}_j\hat{p}\hat{A}^\dagger_k \tag{2.33}$$

with $v_{jk}(t) = \sum_{M,N} w^j_{MN}(t)w^k_{MN}(t)^*$. Taking the limit of short times and after some algebra, one finds that the system density matrix satisfies a linear first-order differential equation

$$\frac{\mathrm{d}\hat{p}}{\mathrm{d}t} = -\frac{\mathrm{i}}{\hbar}[\hat{H},\hat{p}] + \sum_{j=1}^{d^2-1}\sum_{k=1}^{d^2-1} a_{jk}\left(\hat{A}_j\hat{p}\hat{A}^\dagger_k - \frac{1}{2}\{\hat{A}^\dagger_k\hat{A}_j,\hat{p}\}\right) \tag{2.34}$$

where we have defined

$$a_{jk} = \lim_{\delta t\to 0}\frac{v_{jk}(\delta t)}{\delta t} \tag{2.35}$$

and

$$\hat{H} = \frac{\hbar}{2\mathrm{i}\sqrt{d}}\sum_{j=1}^{d^2-1}\left(a^*_{jd^2}\hat{A}^\dagger_j - a_{jd^2}\hat{A}_j\right) \tag{2.36}$$

It is worth noting that the sums in equation (2.34) range from 1 to d^2-1, this is due to our particular choice of basis operators $\hat{A}_j$. Furthermore, although it may seem tempting to identify $\hat{H}$ to a Hamiltonian, it is neither the Hamiltonian of the reduced system nor the one describing the combined system and reservoir. $\hat{H}$ accounts for the Hermitian part of the dynamics of the system and typically consists of the Hamiltonian of the system alone with a contribution of the reservoir yielding a Lamb shift of the system energy levels.

On the other hand, the second term in the right-hand side of equation (2.34) describes the dissipative effects due to the coupling of the system to the reservoir, this term is hence often called the dissipator. The matrix (a_{jk}) is Hermitian and

positive [68], it is therefore diagonalizable and its eigenvalues γ_j are positive. The dissipator can then be written in a diagonal form, such that

$$\frac{\mathrm{d}\hat{p}}{\mathrm{d}t} = -\frac{\mathrm{i}}{\hbar}[\hat{H}, \hat{p}] + \sum_{j=1}^{d^2-1} \gamma_j \left(\hat{L}_j \hat{p} \hat{L}_j^\dagger - \frac{1}{2}\{\hat{L}_j^\dagger \hat{L}_j, \hat{p}\} \right) \tag{2.37}$$

with the operators $\hat{L}_j$ simply being linear combinations of the $\hat{A}_j$.

In 1976, Gorini, Kossakowski and Sudarshan [69] mathematically demonstrated that equation (2.37) defines the most general dynamical map preserving the fundamental properties of the density matrix, namely trace and complete positivity. Some months later, Lindblad [70] provided a generalization of this result to a larger class of systems and equation (2.37) now often bears his name. The Lindblad master equation has foundational implications for the mathematical formulation of quantum mechanics: The Schrödinger equation indeed only describes the dynamics of a strictly closed quantum system, a realistic description of a quantum system has to take into account the unavoidable interaction of a system with its environment. The Lindblad equation accounts for the dissipative effects of the coupling to the environment based on the Markov hypothesis, it thus provides more general description of the dynamics of a quantum system than the Schrödinger equation. Nevertheless, the physical interpretation of the Lindblad master equation might be rather involved: The derivation of equation (2.37) does not clearly stem from the underlying microscopic dynamics and the Hermitian operator $\hat{H}$ as well as the Lindblad operators $\hat{L}_j$ are not uniquely defined [68]. Given a specific microscopic model of an open quantum system, one cannot straightforwardly write the corresponding Lindblad equation. For practical applications, it will be necessary to take a step back and specify some physical hypotheses at the expense of generality.

2.2.2 The Bloch-Redfield and Pauli master equations

We will now detail physically meaningful assumptions necessary to the derivation of a Markovian equation for the dynamics of an open quantum system. No specific assumption needs to be made on the total Hamiltonian of the set-up. It is written $\hat{H} = \hat{H}_{\mathrm{sys}} + \hat{H}_{\mathrm{res}} + \hat{V}$, where we suppose that the system Hamiltonian $\hat{H}_{\mathrm{sys}}$ has been previously diagonalized so it reads

$$\hat{H}_{\mathrm{sys}} = \hbar \sum_j \omega_j \, |j\rangle\langle j| \tag{2.38}$$

The system is coupled to a reservoir with Hamiltonian $\hat{H}_{\mathrm{res}}$ through the interaction Hamiltonian $\hat{V}$. The latter can be written in the general from

$$\hat{V} = \sum_\mu \hat{S}_\mu \otimes \hat{R}_\mu \tag{2.39}$$

where $\hat{S}_\mu$ and $\hat{R}_\mu$ are operators acting on $\mathbb{H}_{\text{sys}}$ and $\mathbb{H}_{\text{res}}$ respectively.

We study the total density matrix $\hat{\varrho}$ in the interaction picture, considering $\hat{V}$ as a perturbation. In the interaction picture, its time evolution is given by

$$\frac{\mathrm{d}\hat{\varrho}^{(\text{int})}}{\mathrm{d}t} = -\frac{\mathrm{i}}{\hbar}[\hat{V}^{(\text{int})}, \hat{\varrho}^{(\text{int})}] \tag{2.40}$$

This can be alternatively written in the integral form

$$\hat{\varrho}^{(\text{int})}(t) = \hat{\varrho}_0 - \frac{\mathrm{i}}{\hbar}\int_0^t \mathrm{d}t' \, [\hat{V}^{(\text{int})}(t'), \hat{\varrho}^{(\text{int})}(t')] \tag{2.41}$$

Iterating this relation and taking the derivative yields the integro-differential evolution equation

$$\frac{\mathrm{d}\hat{\varrho}^{(\text{int})}}{\mathrm{d}t} = -\frac{\mathrm{i}}{\hbar}[\hat{V}^{(\text{int})}(t), \hat{\varrho}_0] - \frac{1}{\hbar^2}\int_0^t \mathrm{d}t' \, [\hat{V}^{(\text{int})}(t), [\hat{V}^{(\text{int})}(t'), \hat{\varrho}^{(\text{int})}(t')]] \tag{2.42}$$

To proceed, we perform the Born approximation [68,71,72]: Considering the fact that the reservoir is much larger than the system and assuming that the coupling between those is somewhat weak, the influence of the system on the reservoir can be neglected. We assume that the combined set-up is prepared in an uncorrelated initial state like equation (2.22), with the initial reservoir state $\hat{\varrho}_{\text{res}}$ being a stationary state of the reservoir: $[\hat{H}_{\text{res}}, \hat{\varrho}_{\text{res}}] = 0$. The Born approximation states that the reservoir state is only negligibly affected by the coupling to the system so that excitations from the stationary state $\hat{\varrho}_{\text{res}}$ can be ignored. The reduced state of the reservoir is then represented by $\hat{\varrho}_{\text{res}}$ at all times and system-reservoir correlations are neglected. The total density matrix then reads

$$\hat{\varrho}^{(\text{int})}(t) = \hat{p}(t) \otimes \hat{\varrho}_{\text{res}} \tag{2.43}$$

Furthermore, one usually states that

$$\mathrm{Tr}_{\text{res}}[\hat{V}^{(\text{int})}(t), \hat{\varrho}_0] = \sum_\mu \langle \hat{R}_\mu \rangle_{\text{res}} \, [\hat{S}_\mu^{(\text{int})}(t), \hat{p}_0] = 0 \tag{2.44}$$

where we have introduced the reservoir expectation value

$$\langle \hat{O} \rangle_{\text{res}} = \mathrm{Tr}_{\text{res}} \left(\hat{\varrho}_{\text{res}} \hat{O}\right) \tag{2.45}$$

The assumption of equation (2.44) often happens to be verified, this is for example the case when the $\hat{R}_\mu$ are creation or annihilation operators and $\hat{\varrho}_{\text{res}}$ represents the canonical distribution for free particles. Plus, it is always possible to slightly redefine $\hat{H}_{\text{sys}}$ and $\hat{V}$ to ensure that equation (2.44) is satisfied [71].

With all these simplifications, we can now take the trace over the reservoir in equation (2.42) to find

$$\frac{\mathrm{d}\hat{p}^{(\mathrm{int})}}{\mathrm{d}t} = -\frac{1}{\hbar^2}\sum_{\mu,\nu}\int_0^t \mathrm{d}t' \Big(G_{\mu\nu}(t-t')[\hat{S}_\mu^{(\mathrm{int})}(t), \hat{S}_\nu^{(\mathrm{int})}(t')\hat{p}^{(\mathrm{int})}(t')] - G_{\nu\mu}(t'-t)[\hat{S}_\mu^{(\mathrm{int})}(t), \hat{p}^{(\mathrm{int})}(t')\hat{S}_\nu^{(\mathrm{int})}(t')]\Big) \tag{2.46}$$

where we define the reservoir correlation functions $G_{\mu\nu}(t-t')$ as

$$G_{\mu\nu}(t-t') = \langle \hat{R}_\mu^{(\mathrm{int})}(t)\hat{R}_\nu^{(\mathrm{int})}(t')\rangle_{\mathrm{res}} = \langle \hat{R}_\mu^{(\mathrm{int})}(t-t')\hat{R}_\nu\rangle_{\mathrm{res}} \tag{2.47}$$

These functions describe the time-correlation between excitations in the reservoir due to the coupling to the system.

No precise hypothesis on the Markovian behaviour of the time evolution has been made so far. However, since the reservoir is assumed to be large, we expect that it quickly dissipates the effects of the interaction with the system. Echoing the Born approximation (2.43), it means that the reservoir barely feels the perturbation due to its coupling with the system and almost immediately returns to its stationary state once driven out of equilibrium. Hence, the reservoir can retain memory of its past states only on the very short time scale necessary to relax to a stationary state. We then introduce the correlation time of the reservoir τ_{corr}. It is the time scale over which the reservoir correlation functions decay: $G_{\mu\nu}(\tau)$ is considered non-zero only for $|\tau| \lesssim \tau_{\mathrm{corr}}$. We deduce that the integrand in equation (2.46) is significant only on the time interval $t - \tau_{\mathrm{corr}} \lesssim t' \leq t$.

In order to justify rigorously the assumption of very short correlation time, it is necessary to compare τ_{corr} to another characteristic time scale of the dynamics of the problem, namely the damping time τ_{damp} which is the time scale over which the state of the system varies appreciably. If $\tau_{\mathrm{corr}} \ll \tau_{\mathrm{damp}}$, then $\hat{p}^{(\mathrm{int})}(t') \simeq \hat{p}^{(\mathrm{int})}(t)$ for $t - \tau_{\mathrm{corr}} \lesssim t' \leq t$. In this situation, the Markov approximation holds [68,71,72]: one can replace $\hat{p}^{(\mathrm{int})}(t')$ by $\hat{p}^{(\mathrm{int})}(t)$ in the integrand of equation (2.46) to obtain

$$\frac{\mathrm{d}\hat{p}^{(\mathrm{int})}}{\mathrm{d}t} = -\frac{1}{\hbar^2}\sum_{\mu,\nu}\int_0^t \mathrm{d}t' \Big(G_{\mu\nu}(t-t')[\hat{S}_\mu^{(\mathrm{int})}(t), \hat{S}_\nu^{(\mathrm{int})}(t')\hat{p}^{(\mathrm{int})}(t)] - G_{\nu\mu}(t'-t)[\hat{S}_\mu^{(\mathrm{int})}(t), \hat{p}^{(\mathrm{int})}(t)\hat{S}_\nu^{(\mathrm{int})}(t')]\Big) \tag{2.48}$$

It is important to note that the Born-Markov approximation implies that we give up on detailing the behaviour of the system on time scales of the order of τ_{corr} [68,71,72]. This corresponds to a coarse-graining of the density matrix, the dynamics described in this framework is actually time averaged over a time scale large with respect to τ_{corr} but short compared to τ_{damp}.

Equation (2.48) describes the dynamics of an open quantum system through a linear first-order differential equation, it is similar to the Lindblad master

equation (2.37) in this respect. However, contrary to the latter, the coefficients in the former are time-dependent, hinting at the fact that equation (2.48) still retains non-Markovian features [68]. To obtain a fully Markovian evolution equation, we make use of the approximation of short correlation time once again. Upon the simple change of variables $\tau = t - t'$, equation (2.48) becomes

$$\frac{\mathrm{d}\hat{p}^{(\mathrm{int})}}{\mathrm{d}t} = -\frac{1}{\hbar^2}\sum_{\mu,\nu}\int_0^t \mathrm{d}\tau \left(G_{\mu\nu}(\tau)[\hat{S}_\mu^{(\mathrm{int})}(t), \hat{S}_\nu^{(\mathrm{int})}(t-\tau)\hat{p}^{(\mathrm{int})}(t)] - G_{\nu\mu}(-\tau)[\hat{S}_\mu^{(\mathrm{int})}(t), \hat{p}^{(\mathrm{int})}(t)\hat{S}_\nu^{(\mathrm{int})}(t-\tau)]\right) \tag{2.49}$$

The upper bound in the above integral can be extended from t to ∞ with negligible error provided that the time t is large compared to τ_{corr} [68, 71, 72]. As already pointed out, it should be the case as an important underlying idea of the Markov approximation is the fact that the dynamics of the system is not accurately described on time scales of the order of τ_{corr}. Thus, we can freely assume that t is much larger than τ_{corr} as any of the evolution equations given here will anyway provide a poor description of the short time behaviour of the system. This yields the Bloch-Redfield master equation [73, 74]

$$\frac{\mathrm{d}\hat{p}^{(\mathrm{int})}}{\mathrm{d}t} = -\frac{1}{\hbar^2}\sum_{\mu,\nu}\int_0^\infty \mathrm{d}\tau \left(G_{\mu\nu}(\tau)[\hat{S}_\mu^{(\mathrm{int})}(t), \hat{S}_\nu^{(\mathrm{int})}(t-\tau)\hat{p}^{(\mathrm{int})}(t)] - G_{\nu\mu}(-\tau)[\hat{S}_\mu^{(\mathrm{int})}(t), \hat{p}^{(\mathrm{int})}(t)\hat{S}_\nu^{(\mathrm{int})}(t-\tau)]\right) \tag{2.50}$$

Examining the matrix elements $p_{jk}^{(\mathrm{int})}(t) = \langle j|\hat{p}^{(\mathrm{int})}(t)|k\rangle$, this can be written in the following from

$$\frac{\mathrm{d}p_{jk}^{(\mathrm{int})}}{\mathrm{d}t} = \sum_{l,m} D_{jklm} p_{lm}^{(\mathrm{int})}(t) \mathrm{e}^{\mathrm{i}(\omega_{jk}-\omega_{lm})t} \tag{2.51}$$

Here we have used to notation $\omega_{jk} = \omega_j - \omega_k$ for the frequency differences. The coefficients D_{jklm} are compact notations for the somewhat complicated quantity

$$\begin{aligned} D_{jklm} = \frac{1}{2\hbar^2}\sum_{\mu,\nu}\Bigg(& \langle m|\hat{S}_\mu|k\rangle \langle j|\hat{S}_\nu|l\rangle \left(F_{\mu\nu}(\omega_{jl}) - \frac{\mathrm{i}}{\pi}\Delta(\omega_{jl})\right) \\ & + \langle m|\hat{S}_\mu|k\rangle \langle j|\hat{S}_\nu|l\rangle \left(F_{\mu\nu}(\omega_{km}) + \frac{\mathrm{i}}{\pi}\Delta(\omega_{km})\right) \\ & - \sum_n \delta_{km} \langle j|\hat{S}_\mu|n\rangle \langle n|\hat{S}_\nu|l\rangle \left(F_{\mu\nu}(\omega_{nl}) - \frac{\mathrm{i}}{\pi}\Delta(\omega_{nl})\right) \\ & - \sum_n \delta_{jl} \langle m|\hat{S}_\mu|n\rangle \langle n|\hat{S}_\nu|k\rangle \left(F_{\mu\nu}(\omega_{nm}) + \frac{\mathrm{i}}{\pi}\Delta(\omega_{nm})\right)\Bigg) \end{aligned} \tag{2.52}$$

where $F_{\mu\nu}(\omega)$ is the Fourier transform of the correlation function

$$F_{\mu\nu}(\omega) = \int_{-\infty}^{\infty} \mathrm{d}\tau\, G_{\mu\nu}(\tau)\mathrm{e}^{-\mathrm{i}\omega\tau} \tag{2.53}$$

and $\Delta_{\mu\nu}(\omega)$ is the following principal value integral

$$\Delta_{\mu\nu}(\omega) = \mathcal{P}\int_{-\infty}^{\infty} \mathrm{d}\omega' \, \frac{F_{\mu\nu}(\omega')}{\omega - \omega'} \tag{2.54}$$

The Bloch-Redfield master equation (2.51) is a purely quantum master equation in the sense that it couples the diagonal and off-diagonal terms of the density matrix. Indeed, a density matrix with only diagonal elements is not fundamentally different from a classical random process. Taking into account the dynamics of quantum coherences (off-diagonal elements) is what makes equation (2.51) really quantum. However, the coupling between diagonal and off-diagonal elements of the density matrix increases the complexity of the problem and, for practical purposes, it will often be necessary to find a way to decouple the dynamics of diagonal and off-diagonal elements of the density matrix. This can be achieved performing a secular approximation [68,71,72] on equation (2.51), that is, we only keep the terms such that $\omega_{jk} - \omega_{lm} = 0$. Denoting by τ_{sys} the typical time scale of the intrinsic evolution of the system, this approximation is justified if $\tau_{\mathrm{sys}} \ll \tau_{\mathrm{damp}}$. Indeed, τ_{sys} is given by the typical value for the inverse of the frequency differences involved, therefore, the non-secular terms in the above equation oscillate very rapidly during the time over which the density matrix varies appreciably and are then neglected. Going back to the Schrödinger picture, this yields

$$\frac{\mathrm{d}p_{jk}}{\mathrm{d}t} = -\mathrm{i}\omega_{jk} p_{jk} + \sum_{\omega_{jk}=\omega_{lm}} D_{jklm} p_{lm} \tag{2.55}$$

where $p_{jk}(t) = \langle j|\hat{p}(t)|k\rangle = p_{jk}^{(\mathrm{int})}(t)\mathrm{e}^{-\mathrm{i}\omega_{jk}t}$.

We first focus on the diagonal elements $p_j(t) = p_{jj}(t)$. If the spectrum of $\hat{H}_{\mathrm{sys}}$ is non-degenerate, one can show that the dynamics of the populations satisfy a classical rate master equation [68, 71, 72], often referred to as the Pauli master equation,

$$\frac{\mathrm{d}p_j}{\mathrm{d}t} = \sum_{k\neq j} \left(\Gamma_{jk} p_k - \Gamma_{kj} p_j\right) \tag{2.56}$$

Here the transition rates are given by

$$\Gamma_{jk} = \frac{1}{\hbar^2} \sum_{\mu,\nu} \langle k|\hat{S}_\mu|j\rangle \, \langle j|\hat{S}_\nu|k\rangle \, F_{\mu\nu}(\omega_{jk}) \tag{2.57}$$

The above expression is the most general one can find in the framework described. Writing the reservoir density matrix as in equation (2.28), it takes the Fermi golden rule form [71, 72]

$$\Gamma_{jk} = \frac{2\pi}{\hbar^2} \sum_{M,N} P_N |\langle j, M|\hat{V}|k, N\rangle|^2 \delta(\omega_{jk} + \Omega_{MN}) \tag{2.58}$$

We move on to the study of the off-diagonal elements of the density matrix. Assuming that the energy levels of the system are irregularly spaced, we find that quantum coherences decay exponentially with time [71, 72]:

$$\frac{\mathrm{d}p_{jk}}{\mathrm{d}t} = -\Big(\kappa_{jk} + \mathrm{i}\omega_{jk} - \mathrm{i}\Big(\Lambda_j - \Lambda_k\Big)\Big)p_{jk} \tag{2.59}$$

The decay rate κ_{jk} is given by

$$\kappa_{jk} = \frac{1}{2}\left(\sum_{l\neq j}\Gamma_{lj} + \sum_{l\neq k}\Gamma_{lk}\right) + \alpha_{jk} \tag{2.60}$$

where α_{jk} is the so-called adiabatic decay rate,

$$\alpha_{jk} = \frac{1}{2\hbar^2}\sum_{\mu,\nu}\Big(\langle j|\hat{S}_\mu|j\rangle\langle j|\hat{S}_\nu|j\rangle + \langle k|\hat{S}_\mu|k\rangle\langle k|\hat{S}_\nu|k\rangle - 2\langle k|\hat{S}_\mu|k\rangle\langle j|\hat{S}_\nu|j\rangle\Big)F_{\mu\nu}(0) \tag{2.61}$$

Finally, Λ_j reads

$$\Lambda_j = \frac{1}{2\pi\hbar^2}\sum_k\sum_{\mu,\nu}\langle j|\hat{S}_\mu|k\rangle\langle k|\hat{S}_\nu|j\rangle\,\Delta_{\mu\nu}(\omega_{kj}) \tag{2.62}$$

It is the Lamb shift corresponding to system state $|j\rangle$, that is, it describes the renormalization of the system's energy levels due to the coupling to the reservoir. Hence, the interaction with the reservoir will not only destroy quantum coherences at long times, but it will also change the frequencies at which these oscillate.

Chapter 3

Solution of the Fano-Anderson model

This chapter reviews an exact solution of the Fano-Anderson model for reservoirs with a band structure. The Heisenberg equations of motion for annihilation operators are solved using a Laplace transform. There is a connection between non-analyticities in Laplace space and the spectrum of the Fano-Anderson Hamiltonian. In particular, the poles of the Laplace transform correspond to bound states, that is eigenmodes of the Hamiltonian whose energy is in a band gap. These bound states have an important influence on the dynamics of the system. This solution of the Heisenberg equations of motion is used to deduce the time-dependence for important physical quantities: occupation of the discrete level, particle currents out of reservoirs and time correlations of the discrete level occupation.

3.1 Formal solution of the model

3.1.1 Heisenberg equations and Laplace transform

The Fano-Anderson model described by Hamiltonian (1.16) has been addressed through various techniques: Heisenberg equations of motion [32–34,44,46,49,50,55], Green's functions [45,47,75–77] or Feynman-Vernon path integrals [48,51–54,56,57]. Here, we solve the model using the first of these options considering the Heisenberg equations of motion for the annihilation operators $\hat{d}$ and $\hat{c}_{\alpha k}$. For convenience, we use the generic notation $\hat{c}_m$ where the index m spans the discrete level and all the reservoirs modes α, k. The evolution equation for $\hat{c}_m$ in the Heisenberg picture is given by

$$\frac{\mathrm{d}\hat{c}_m^{(\mathrm{H})}}{\mathrm{d}t} = -\frac{\mathrm{i}}{\hbar}[\hat{c}_m^{(\mathrm{H})}, \hat{H}] \tag{3.1}$$

Due to the form of Hamiltonian (1.16), it then suffices to compute commutators of the type $[\hat{c}_m, \hat{c}_n^\dagger \hat{c}_p]$. Irrespective of the statistics of the involved particles, we find

$$[\hat{c}_m, \hat{c}_n^\dagger \hat{c}_p] = \delta_{mn} \hat{c}_p \tag{3.2}$$

Hence, both bosons and fermions will obey the same equations of motion, namely

$$\begin{cases} \dfrac{\mathrm{d}\hat{d}^{(\mathrm{H})}}{\mathrm{d}t} = -\mathrm{i}\omega_\mathrm{d} \hat{d}^{(\mathrm{H})} - \mathrm{i} \displaystyle\sum_{\alpha,k} g_{\alpha k} \hat{c}_{\alpha k}^{(\mathrm{H})} \\ \dfrac{\mathrm{d}\hat{c}_{\alpha k}^{(\mathrm{H})}}{\mathrm{d}t} = -\mathrm{i}\omega_{\alpha k} \hat{c}_{\alpha k}^{(\mathrm{H})} - \mathrm{i} g_{\alpha k}^* \hat{d}^{(\mathrm{H})} \end{cases} \tag{3.3}$$

The initial condition is given by the Schrödinger picture annihilation operators

$$\begin{cases} \hat{d}^{(\mathrm{H})}(t=0) = \hat{d} \\ \hat{c}_{\alpha k}^{(\mathrm{H})}(t=0) = \hat{c}_{\alpha k} \end{cases} \tag{3.4}$$

We solve the equations of motion (3.3) using a Laplace transform [32–34, 49, 50, 55]. We thus define [78]

$$\hat{D}(z) = \int_0^\infty \mathrm{d}t\, \mathrm{e}^{-zt} \hat{d}^{(\mathrm{H})}(t) \tag{3.5a}$$

$$\hat{C}_{\alpha k}(z) = \int_0^\infty \mathrm{d}t\, \mathrm{e}^{-zt} \hat{c}_{\alpha k}^{(\mathrm{H})}(t) \tag{3.5b}$$

It is only because the equations of motion (3.3) are linear that we can use this technique. This point is crucial as a product of operators in time domain would become a convolution in Laplace space. In the situation at stake here, the Heisenberg equations (3.3) are transformed into an ordinary system of linear equations

$$\begin{cases} z\hat{D}(z) - \hat{d} = -\mathrm{i}\omega_\mathrm{d} \hat{D}(z) - \mathrm{i} \displaystyle\sum_{\alpha,k} g_{\alpha k} \hat{C}_{\alpha k}(z) \\ z\hat{C}_{\alpha k}(z) - \hat{c}_{\alpha k} = -\mathrm{i}\omega_{\alpha k} \hat{C}_{\alpha k}(z) - \mathrm{i} g_{\alpha k}^* \hat{D}(z) \end{cases} \tag{3.6}$$

where the Schrödinger picture operators $\hat{d}$ and $\hat{c}_{\alpha k}$ correspond to the initial condition (3.4). This system is straightforwardly solved

$$\begin{cases} \hat{D}(z) = \dfrac{1}{\Delta(z)} \left(\hat{d} - \mathrm{i} \displaystyle\sum_{\alpha,k} \frac{g_{\alpha k}}{z + \mathrm{i}\omega_{\alpha k}} \hat{c}_{\alpha k} \right) \\ \hat{C}_{\alpha k}(z) = \dfrac{1}{z + \mathrm{i}\omega_{\alpha k}} (\hat{c}_{\alpha k} - \mathrm{i} g_{\alpha k}^* \hat{D}(z)) \end{cases} \tag{3.7}$$

where we have used the short notation

$$\Delta(z) = z + \mathrm{i}(\omega_\mathrm{d} + \Sigma(z)) \tag{3.8}$$

Here $\Sigma(z)$ is the self-energy defined as follows

$$\Sigma(z) = \sum_{\alpha,k} \frac{|g_{\alpha k}|^2}{\mathrm{i}z - \omega_{\alpha k}} \tag{3.9}$$

The equations of motion being solved in Laplace space, it is now necessary to perform the inverse Laplace transform in order to obtain the solution for the Heisenberg picture field operators in real time. Actually, in order to derive the full solution of the problem, it suffices to compute the inverse Laplace transform of $1/\Delta(z)$ denoted by $\varphi(t)$, the calculation of which will be detailed in section 3.1.3 below. Indeed, we can write the discrete level annihilation operator as follows

$$\hat{d}^{(\mathrm{H})}(t) = \varphi(t)\hat{d} + \sum_{\alpha,k} g_{\alpha k}\psi(t,\omega_{\alpha k})\hat{c}_{\alpha k} \tag{3.10}$$

where the properties of the Laplace transform provide a simple expression for $\psi(t,\omega)$,

$$\psi(t,\omega) = -\mathrm{i}\int_0^t \mathrm{d}t'\,\varphi(t')\mathrm{e}^{-\mathrm{i}\omega(t-t')} \tag{3.11}$$

Similarly, performing the inverse Laplace transform on $\hat{C}_{\alpha k}(z)$ yields

$$\begin{aligned}\hat{c}^{(\mathrm{H})}_{\alpha k}(t) &= \mathrm{e}^{-\mathrm{i}\omega_{\alpha k}t}\hat{c}_{\alpha k} - \mathrm{i}g^*_{\alpha k}\int_0^t \mathrm{d}t'\,\mathrm{e}^{-\mathrm{i}\omega_{\alpha k}(t-t')}\hat{d}^{(\mathrm{H})}(t') \\ &= \mathrm{e}^{-\mathrm{i}\omega_{\alpha k}t}\hat{c}_{\alpha k} + g^*_{\alpha k}\psi(t,\omega_{\alpha k})\hat{d} + g^*_{\alpha k}\sum_{\alpha',k'} g_{\alpha' k'}\chi(t,\omega_{\alpha k},\omega_{\alpha' k'})\hat{c}_{\alpha' k'}\end{aligned} \tag{3.12}$$

Here we have defined

$$\chi(t,\omega,\omega') = -\mathrm{i}\int_0^t \mathrm{d}t'\,\psi(t',\omega')\mathrm{e}^{-\mathrm{i}\omega(t-t')} \tag{3.13}$$

Hence, we see that if one is able to derive an explicit expression for $\varphi(t)$, the subsequent calculations of $\psi(t,\omega)$ and $\chi(t,\omega,\omega')$ will not raise additional difficulties.

3.1.2 The continuum limit

In the following, we will take the thermodynamic limit for the reservoirs assuming that they contain infinitely many modes whose distribution can be described by a continuous density of states. However, our results can be more generally expressed in terms of the so-called spectral density where every state bears a weight corresponding to its coupling amplitude. The spectral density for reservoir α is then given by

$$J_\alpha(\omega) = \sum_k |g_{\alpha k}|^2\delta(\omega - \omega_{\alpha k}) \tag{3.14}$$

For convenience, we also define the total spectral density $J(\omega) = \sum_\alpha J_\alpha(\omega)$.

One often assumes the wide-band limit at this point. In this limit, one considers that the variations in energy induced by the coupling of the discrete level to the reservoirs are very small with respect to the typical scale of variation of the spectral densities (3.14). These are then assumed to be constant. A corollary of this assumption is the fact that any band gap in the reservoirs can be ignored as these are necessarily very far from the energy window of interest in the wide-band limit. Although it is not straightforward to find a general criterion for the validity of the wide-band limit, it is typically justified in the regime of weak coupling. It is also generally valid for metallic reservoirs where the Fermi energy, and hence the distance between the band edge to the Fermi surface, is typically of order 10^5 K which is huge compared to relevant values for the coupling.

Crucially, we *do not* consider this simplifying limit here, we study the general case where spectral densities may be energy-dependent and exhibit band gaps. In the continuum limit, the sums over reservoir states can be rewritten as integrals over energies. For example, the self-energy (3.9) reads

$$\Sigma(z) = \sum_{\alpha,k} \frac{|g_{\alpha k}|^2}{\mathrm{i}z - \omega_{\alpha k}} = \int \mathrm{d}\omega \, \frac{J(\omega)}{\mathrm{i}z - \omega} \tag{3.15}$$

Here it is important to note that the self-energy cannot be properly defined on the whole complex plane; it exhibits branch cuts which correspond to the band structure of the reservoirs. Indeed, the integral defining $\Sigma(z)$ in equation (3.15) diverges if one takes $z = -\mathrm{i}\omega$ with ω such that $J(\omega) \neq 0$. Therefore, we understand that $\Sigma(z)$ is defined on the whole complex plane except for branch cuts on the imaginary axis corresponding to the energy bands of the reservoirs (see figure 3.1). Equation (3.19) below gives the jump of $\Sigma(z)$ across this branch cut.

3.1.3 The inverse Laplace transform

Considering the similarities between the Fourier and Laplace transforms, we understand that the inverse Laplace transform is carried out integrating along a vertical line in the complex plane [78]. This line is often referred to as the Bromwich contour and the real part of this line can be chosen arbitrarily, provided it is greater than the real part of all the non-analyticities of the Laplace transform.

Concerning the calculation of the inverse Laplace transform $\varphi(t)$, we have already pointed out that $\Sigma(z)$ features branch cuts on the imaginary axis and we now have to study the zeroes of $\Delta(z)$ defined in equation (3.8). Taking the real part of $\Delta(z) = 0$, with $x = \mathrm{Re}\, z$ and $y = \mathrm{Im}\, z$, we find

$$x + \mathrm{Re}(\mathrm{i}\Sigma(x + \mathrm{i}y)) = x\left(1 + \int \mathrm{d}\omega \, \frac{J(\omega)}{x^2 + (y+\omega)^2}\right) = 0 \tag{3.16}$$

As $J(\omega)$ is necessarily positive, this equation yields $x = 0$. Hence $z = \mathrm{i}y$, where y has to satisfy $J(-y) = 0$ to ensure that $\Sigma(z)$ is well-defined. We then conclude that all the non-analyticities of $1/\Delta(z)$ are located on the imaginary axis, such that $\varphi(t)$ can be written

$$\varphi(t) = \frac{1}{2\mathrm{i}\pi} \int_{x-\mathrm{i}\infty}^{x+\mathrm{i}\infty} \mathrm{d}z \, \frac{\mathrm{e}^{zt}}{\Delta(z)} \tag{3.17}$$

where x is a strictly positive real number. To actually perform the complex integration, we close the contour on the left by a circle of arbitrarily large radius [78]. One should however note that it is necessary to thouroughly deal with the non-analyticities on the imaginary line (see figure 3.1). Using Jordan's lemma [78], one can show that the only non-vanishing contributions to the contour integral are given by the non-analyticities of $1/\Delta(z)$. First, we have an integral contribution accounting for the jump of the value of $\Delta(z)$ accross the branch cut. Then the zeroes $\Delta(z)$ are taken into account using the residue theorem. $\varphi(t)$ eventually reads

$$\varphi(t) = \frac{1}{2\pi} \int \mathrm{d}\omega \, \mathrm{e}^{-\mathrm{i}\omega t} \lim_{\varepsilon \to 0^+} \left(\frac{1}{\Delta(\varepsilon - \mathrm{i}\omega)} - \frac{1}{\Delta(-\varepsilon - \mathrm{i}\omega)} \right) + \sum_b R_b \tag{3.18}$$

The index b labels the poles $z_b = -\mathrm{i}\omega_b$ of $1/\Delta(z)$, with R_b denoting the corresponding residues.

The limit $\varepsilon \to 0^+$ in the branch cut integral is calculated using the Sokhotski-Plemelj theorem [78]. The self-energy can be simplified as follows

$$\lim_{\varepsilon \to 0^+} \Sigma(\pm\varepsilon - \mathrm{i}\omega) = \lim_{\varepsilon \to 0^+} \int \mathrm{d}\omega' \, \frac{J(\omega')}{\omega - \omega' \pm \mathrm{i}\varepsilon} = \Lambda(\omega) \mp \mathrm{i}\pi J(\omega) \tag{3.19}$$

where $\Lambda(\omega)$ is given by the Cauchy principal value integral

$$\Lambda(\omega) = \fint \mathrm{d}\omega' \, \frac{J(\omega')}{\omega - \omega'} \tag{3.20}$$

Substituting this into equation (3.8), we find

$$\lim_{\varepsilon \to 0^+} \left(\frac{1}{\Delta(\varepsilon - \mathrm{i}\omega)} - \frac{1}{\Delta(-\varepsilon - \mathrm{i}\omega)} \right) = 2\pi S(\omega) \tag{3.21}$$

where we have introduced the short notation

$$S(\omega) = \frac{J(\omega)}{(\omega - \omega_\mathrm{d} - \Lambda(\omega))^2 + \pi^2 J(\omega)^2} \tag{3.22}$$

We now investigate the residues R_b. We recall that the zeroes of $\Delta(z)$ are purely imaginary and we thus write $z_b = -\mathrm{i}\omega_b$, with $J(\omega_b) = 0$. These satisfy

$$\Delta(-\mathrm{i}\omega_b) = 0 \implies \Omega(\omega_b) = 0, \tag{3.23}$$

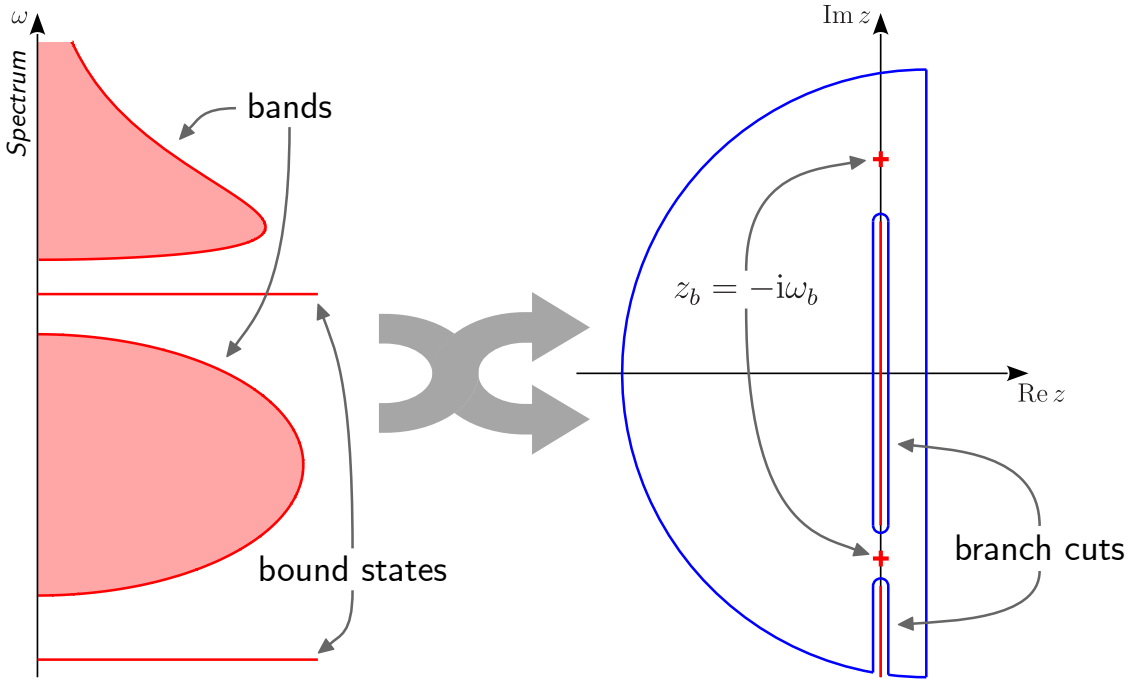

Figure 3.1 – Depiction of the correspondence between the spectrum of the Fano-Anderson Hamiltonian (on the left) and the structure of the Laplace transform in the complex plane (on the right). The non-analyticities of $1/\Delta(z)$ are represented in red in the right plot; the band structure of the reservoirs gives rise to branch cuts in the Laplace transform while the poles of $1/\Delta(z)$ correspond to bound states in band gaps. The integration contour used to perform the inverse Laplace transform is depicted in blue; one has to consider the limit in which the radius of the circle closing the Bromwich from the left goes to infinity.

with $\Omega(\omega) = \omega - \omega_\mathrm{d} - \Lambda(\omega)$. Note that here the definition of $\Lambda(\omega)$ has been extended to ω outside energy bands.[1] For ω in a band gap, it is straightforward to show that $\Omega(\omega)$ is an increasing function of ω:

$$\frac{\mathrm{d}\Omega}{\mathrm{d}\omega} = \frac{\mathrm{d}}{\mathrm{d}\omega}\left(\omega - \int \mathrm{d}\omega' \, \frac{J(\omega')}{\omega - \omega'}\right) = 1 + \int \mathrm{d}\omega' \, \frac{J(\omega')}{(\omega - \omega')^2} > 0 \tag{3.24}$$

We thus deduce that the equation $\Omega(\omega_b) = 0$ has *at most* one solution per band gap, whether or not such solution exists is inferred from the values of $\Omega(\omega)$ at the band edges.

The residue R_b is then calculated taking the Laurent series of $\mathrm{e}^{zt}/\Delta(z)$ at z_b. We find

$$R_b = Z_b \mathrm{e}^{-\mathrm{i}\omega_b t} \tag{3.25}$$

[1] It is not necessary to take the principal value in this case.

with

$$Z_b = \frac{1}{1-\Lambda'(\omega_b)} = \left(1 + \int \mathrm{d}\omega \, \frac{J(\omega)}{(\omega-\omega_b)^2}\right)^{-1} \tag{3.26}$$

Obviously Z_b is meaningless if ω_b does not exist. In such situations we will therefore take $Z_b = 0$.

In conclusion, we can now write $\varphi(t)$ as follows

$$\varphi(t) = \int \mathrm{d}\omega \, S(\omega) \mathrm{e}^{-\mathrm{i}\omega t} + \sum_b Z_b \mathrm{e}^{-\mathrm{i}\omega_b t} \tag{3.27}$$

As previously stated, it is now straightforward to time-integrate $\varphi(t)$ to obtain expressions for $\psi(t,\omega)$ and $\chi(t,\omega,\omega')$. A first integration yields

$$\psi(t,\omega) = \int \mathrm{d}\omega' \, S(\omega') E(t,\omega,\omega') + \sum_b Z_b E(t,\omega,\omega_b) \tag{3.28}$$

where we have defined

$$E(t,\omega,\omega') = \frac{\mathrm{e}^{-\mathrm{i}\omega t} - \mathrm{e}^{-\mathrm{i}\omega' t}}{\omega - \omega'} \tag{3.29}$$

We integrate a second time to obtain

$$\chi(t,\omega,\omega') = \int \mathrm{d}\omega'' \, S(\omega'') \frac{E(t,\omega,\omega') - E(t,\omega,\omega'')}{\omega' - \omega''} + \sum_b Z_b \frac{E(t,\omega,\omega') - E(t,\omega,\omega_b)}{\omega' - \omega_b} \tag{3.30}$$

3.1.4 Bound states and local density of states by exact diagonalization

In this section, we try to investigate the physical significance of the mathematical structure of the model. To do so, we come back to Hamiltonian (1.16) and we now treat the reservoir modes in a discrete way. As this Hamiltonian is quadratic, one can perform a Bogoliubov rotation in order to find the eigenstates of the full Hamiltonian. In this framework, we write the Fano-Anderson Hamiltonian as follows

$$\hat{H} = \hat{c}^\dagger \mathscr{H} \hat{c} \tag{3.31}$$

where $\hat{c}$ represents the column vector consisting of annihilation operators $\hat{d}$ and $\hat{c}_{\alpha k}$,

$$\hat{c} = \begin{pmatrix} \hat{d} \\ \hat{c}_{\alpha_1 k_1} \\ \hat{c}_{\alpha_1 k_2} \\ \vdots \\ \hat{c}_{\alpha_2 k_1} \\ \hat{c}_{\alpha_2 k_2} \\ \vdots \end{pmatrix} \tag{3.32}$$

while the matrix $\mathscr{H}$ is made up of the various coefficients connecting the creation and annihilation operators in the Hamiltonian. In the case of Hamiltonian (1.16), $\mathscr{H}$ takes the simple form of a Hermitian arrowhead matrix [79],

$$\mathscr{H} = \hbar \begin{pmatrix} \omega_{\mathrm{d}} & g_{\alpha_1 k_1} & g_{\alpha_1 k_2} & \cdots & g_{\alpha_2 k_1} & g_{\alpha_2 k_2} & \cdots \\ g^*_{\alpha_1 k_1} & \omega_{\alpha_1 k_1} & & & & & \\ g^*_{\alpha_1 k_2} & & \omega_{\alpha_1 k_2} & & & & \\ \vdots & & & \ddots & & & \\ g^*_{\alpha_2 k_1} & & & & \omega_{\alpha_2 k_1} & & \\ g^*_{\alpha_2 k_2} & & & & & \omega_{\alpha_2 k_2} & \\ \vdots & & & & & & \ddots \end{pmatrix} \tag{3.33}$$

where all blank elements are zero. The idea of a Bogoliubov transformation is to diagonalize the matrix $\mathscr{H}$ to obtain the eigenmodes of the total Hamiltonian. Indeed, $\mathscr{H}$ can be written

$$\mathscr{H} = \mathscr{U}\mathscr{D}\mathscr{U}^\dagger \tag{3.34}$$

where $\mathscr{U}$ is a unitary and $\mathscr{D}$ is a diagonal matrix whose elements are the eigenvalues of $\mathscr{H}$,

$$\mathscr{D} = \hbar \begin{pmatrix} \Omega_{\mathrm{d}} & & & & & & \\ & \Omega_{\alpha_1 k_1} & & & & & \\ & & \Omega_{\alpha_1 k_2} & & & & \\ & & & \ddots & & & \\ & & & & \Omega_{\alpha_2 k_1} & & \\ & & & & & \Omega_{\alpha_2 k_2} & \\ & & & & & & \ddots \end{pmatrix} \tag{3.35}$$

We then rewrite Hamiltonian (1.16) in the compact form

$$\hat{H} = \hat{a}^\dagger \mathscr{D} \hat{a} = \hbar \sum_n \Omega_n \hat{a}^\dagger_n \hat{a}_n \tag{3.36}$$

where the index n spans the discrete level and all the reservoir modes α, k. Moreover, we have introduced the new field operators $\hat{a}_n$ such that

$$\hat{a} = \begin{pmatrix} \hat{a}_{\mathrm{d}} \\ \hat{a}_{\alpha_1 k_1} \\ \hat{a}_{\alpha_1 k_2} \\ \vdots \\ \hat{a}_{\alpha_2 k_1} \\ \hat{a}_{\alpha_2 k_2} \\ \vdots \end{pmatrix} = \mathscr{U}^\dagger \hat{c} \tag{3.37}$$

The eigenvectors of the matrix $\mathcal{H}$ are given by the columns of $\mathcal{U}$. Hence

$$\begin{cases} \omega_{\mathrm{d}}\mathcal{U}_{\mathrm{d}n} + \sum_{\alpha,k} g_{\alpha k}\mathcal{U}_{\alpha k,n} = \Omega_n \mathcal{U}_{\mathrm{d}n} \\ g^*_{\alpha k}\mathcal{U}_{\mathrm{d}n} + \omega_{\alpha k}\mathcal{U}_{\alpha k,n} = \Omega_n \mathcal{U}_{\alpha k,n} \end{cases} \tag{3.38}$$

If $\Omega_n \neq \omega_{\alpha k}$, the second line yields

$$\mathcal{U}_{\alpha k,n} = \frac{g^*_{\alpha k}\mathcal{U}_{\mathrm{d}n}}{\Omega_n - \omega_{\alpha k}} \tag{3.39}$$

Inserting this result back in the first line of the system, we find [79]

$$\Omega_n - \omega_{\mathrm{d}} - \sum_{\alpha,k} \frac{|g_k|^2}{\Omega_n - \omega_{\alpha k}} = 0 \tag{3.40}$$

Taking the continuum limit,[1] we find that Ω_n satisfies equation (3.23). Hence, the isolated poles $z_b = -\mathrm{i}\omega_b$ of the Laplace transform correspond to the eigenmodes of the full Hamiltonian whose energies lie in the band gaps. These modes are mixtures of the discrete level and reservoir degrees of freedom. As they do not decay into the continuum, we will then refer to these states as *bound states* [32, 33, 60]. The spectrum of $\hat{H}$ then consists of a continuous part corresponding to reservoir bands alongside isolated modes in the band gaps (one per band gap at most), this is depicted in figure 3.2. This structure clearly appears in the expression (3.27) of $\varphi(t)$.

Even if the origin of the various contributions to $\varphi(t)$ is now clear, we still have to give a physical meaning to the quantities $S(\omega)$ and Z_b that appear in equation (3.27). So far, we only have only investigated the eigenmodes Ω_n of the system, overlooking the corresponding eigenvectors. These are given by the columns $\mathcal{U}$ and are then normalized to unity, that is

$$\sum_m |\mathcal{U}_{mn}|^2 = |\mathcal{U}_{\mathrm{d}n}|^2 + \sum_{\alpha,k} \left|\mathcal{U}_{\alpha k,n}\right|^2 = 1 \tag{3.41}$$

Using equation (3.39), we finally obtain [79]

$$Z_n = |\mathcal{U}_{\mathrm{d}n}|^2 = \left(1 + \sum_{\alpha,k} \frac{|g_{\alpha k}|^2}{(\Omega_n - \omega_{\alpha k})^2}\right)^{-1} \tag{3.42}$$

Z_n can be interpreted as the overlap between eigenmode n and the original discrete level, it thus describes how the discrete level hybridizes with reservoir modes to give

[1] This does not raise any subtlety as we have stated earlier that Ω_n should be outside the bands.

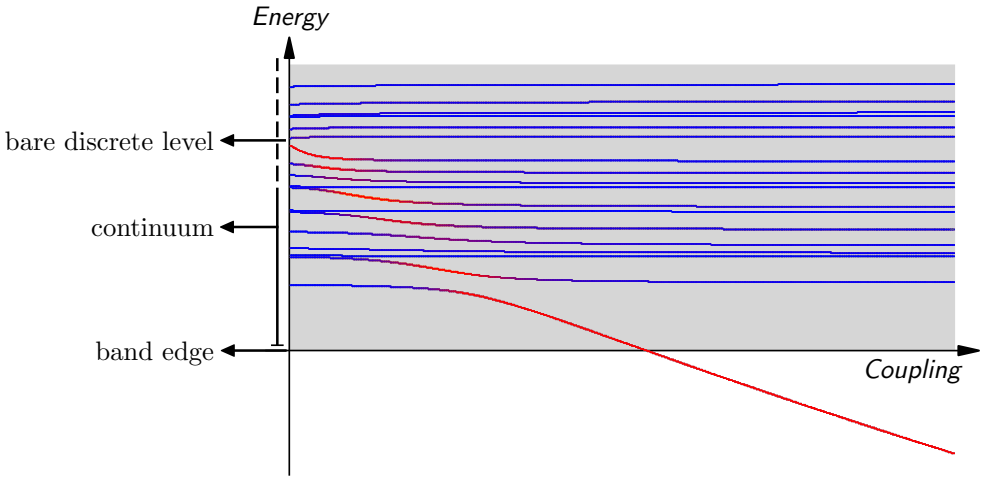

Figure 3.2 – Eigenenergies Ω_n of the Fano-Anderson Hamiltonian as a function of the level-reservoir coupling. At strong coupling, one of these modes is outside the continuum and thus corresponds to a bound state. The colour of the lines corresponds to the value of Z_n, the overlap of the eigenmode with the bare discrete level. Red corresponds to high Z_n and blue corresponds to low Z_n.

rise to new quasiparticle states when the level-reservoir coupling is turned on. Again, we assume that Ω_n is in a band gap and take the continuum limit in equation (3.42). We then find that Z_n corresponds to the quantity Z_b defined in equation (3.26).

Considering the similarities between $S(\omega)$ and Z_b in equation (3.27), we can guess that $S(\omega)$ is the equivalent of Z_b for continuum states, that is $S(\omega)$ corresponds to the density of eigenstates in reservoir bands at energy ω.[1] To justify this rigorously, we try to reproduce the expression for $\varphi(t)$ given in equation (3.27) with the discrete formalism used in this section. This function first appeared in the expression (3.10) for the discrete level annihilation operator in the Heisenberg picture. Here, we start by writing the annihilation operator $\hat{d}$ in terms of the eigenmodes operators $\hat{a}_n$ as these take a very simple form in the Heisenberg picture,

$$\hat{a}_n^{(\mathrm{H})}(t) = \mathrm{e}^{-\mathrm{i}\Omega_n t}\hat{a}_n \tag{3.43}$$

This yields

$$\hat{d}^{(\mathrm{H})}(t) = \sum_n \mathcal{U}_{\mathrm{d}n}\mathrm{e}^{-\mathrm{i}\Omega_n t}\hat{a}_n \tag{3.44}$$

To compare this expression to equation (3.10), we have to go back to the original basis of operators. We have

$$\hat{a}_n = \sum_m \mathcal{U}^*_{mn}\hat{c}_m = \mathcal{U}^*_{\mathrm{d}n}\hat{d} + \sum_{\alpha,k}\mathcal{U}^*_{\alpha k,n}\hat{c}_{\alpha k} \tag{3.45}$$

[1] Note that $S(\omega)$ vanishes if ω lies in a band gap.

We consequently find

$$\hat{d}^{(\mathrm{H})}(t) = \sum_n Z_n \mathrm{e}^{-\mathrm{i}\Omega_n t}\hat{d} + \sum_n \sum_{\alpha,k} \mathcal{U}^*_{\alpha k,n}\mathcal{U}_{\mathrm{d}n}\mathrm{e}^{-\mathrm{i}\Omega_n t}\hat{c}_{\alpha k} \tag{3.46}$$

The first term in the above expression then gives

$$\varphi(t) = \sum_n Z_n \mathrm{e}^{-\mathrm{i}\Omega_n t} \tag{3.47}$$

Hence, we realize that $\varphi(t)$ is the (inverse) Fourier transform of the local density of states $\nu_{\mathrm{d}}(\omega)$ which describes how the discrete level spreads among all the eigenmodes of the full Hamiltonian due to the coupling to the reservoirs. It is indeed given by

$$\nu_{\mathrm{d}}(\omega) = \sum_n Z_n \delta(\omega - \Omega_n) \tag{3.48}$$

Comparing equation (3.47) with expression (3.27), we conclude that, in the continuum limit, the local density of states reads

$$\nu_{\mathrm{d}}(\omega) = S(\omega) + \sum_b Z_b \delta(\omega - \omega_b) \tag{3.49}$$

This confirms that $S(\omega)$ corresponds to the continuous part of the local density of states. It also provides an interpretation for the factor $\Lambda(\omega)$ defined in (3.20) appearing in the expression (3.22) of $S(\omega)$. At the handwaving level, we see that $S(\omega)$ is essentially a skewed Lorentzian whose centre is inferred from $\Lambda(\omega)$. This means that $\Lambda(\omega)$ will essentially describe how the discrete level energy is shifted due to the coupling to the reservoirs. This is why we referred to $\Lambda(\omega)$ as the *Lamb shift* in the following. Similarly, the spectral density $J(\omega)$ accounts for the broadening of the discrete level induced by the coupling to the reservoirs. However, both the Lamb shift and the level-broadening depend on ω in the general case which greatly complicates the picture.

3.2 Physical quantities

3.2.1 Occupation of the discrete level

The exact dynamics of the field operators derived previously provide a full solution of the model. We will now use these results to investigate the time evolution of the physical properties of the system. We first consider the average number of particles in the discrete level also referred to as the occupation of the level. We introduce the number operator

$$\hat{n}(t) = \hat{d}^{(\mathrm{H})}(t)^\dagger \hat{d}^{(\mathrm{H})}(t) \tag{3.50}$$

The occupation is then given by

$$n(t) = \langle \hat{n}(t) \rangle \tag{3.51}$$

where the average value of an operator $\hat{O}$ is defined as

$$\langle \hat{O} \rangle = \mathrm{Tr}(\hat{\varrho}(t=0)\hat{O}) \tag{3.52}$$

In the following, we will only address the case of factorized initial conditions [32–34, 44, 45, 48–57, 77]. This typically corresponds to the case of a quench: The discrete level and reservoirs are uncoupled from one another for $t < 0$, coupling is then instantaneously turned on at $t = 0$ and remains constant afterwards ($t > 0$). Hence, as in equation (2.22), we assume that the initial density matrix is of the form

$$\hat{\varrho}_0 = \hat{\varrho}(t=0) = \hat{p}_0 \bigotimes_\alpha \hat{\varrho}_\alpha \tag{3.53}$$

where $\hat{\varrho}_\alpha$ is the grand canonical density matrix for reservoir α with inverse temperature β_α and chemical potential μ_α, that is

$$\hat{\varrho}_\alpha = \frac{1}{\Xi_\alpha} \exp\left(-\beta_\alpha \sum_k (\hbar\omega_{\alpha k} - \mu_\alpha) \hat{c}^\dagger_{\alpha k} \hat{c}_{\alpha k} \right) \tag{3.54}$$

where Ξ_α is the partition function for reservoir α. Within this framework, the only non-zero expectation values for reservoir field operators are

$$\langle \hat{c}^\dagger_{\alpha k} \hat{c}_{\alpha k} \rangle = n_\alpha(\omega_{\alpha k}) \tag{3.55a}$$

$$\langle \hat{c}_{\alpha k} \hat{c}^\dagger_{\alpha k} \rangle = 1 \pm n_\alpha(\omega_{\alpha k}) \tag{3.55b}$$

where we have denoted by $n_\alpha(\omega)$ the distribution for reservoir α. For bosons, we take the plus sign and $n_\alpha(\omega)$ is the Bose-Einstein distribution. For fermions, we take the minus sign and $n_\alpha(\omega)$ is the Fermi-Dirac distribution.

The occupation of the discrete level then reads

$$\begin{aligned} n(t) = \langle \hat{d}^{(\mathrm{H})}(t)^\dagger \hat{d}^{(\mathrm{H})}(t) \rangle &= n_0 |\varphi(t)|^2 + \sum_{\alpha,k} |g_{\alpha k}|^2 n_\alpha(\omega_{\alpha k}) |\psi(t, \omega_{\alpha k})|^2 \\ &= n_0 |\varphi(t)|^2 + \int \mathrm{d}\omega \, J(\omega) N(\omega) |\psi(t,\omega)|^2 \end{aligned} \tag{3.56}$$

Here n_0 denotes the initial occupation: $n_0 = n(t=0)$, and $N(\omega)$ is the generalized distribution function

$$N(\omega) = \frac{1}{J(\omega)} \sum_\alpha J_\alpha(\omega) n_\alpha(\omega) \tag{3.57}$$

3.2.2 Currents

In the following we will investigate the transport properties of the model. We thus have to study the particle currents through the discrete level. The particle current out of reservoir α is defined as the variation of the number of particles in this reservoir as particles can only tunnel out of the reservoirs through the discrete level. The corresponding current operator thus reads

$$\hat{\jmath}_\alpha(t) = -\sum_k \frac{\mathrm{d}}{\mathrm{d}t}\Big(\hat{c}_{\alpha k}^{(\mathrm{H})}(t)^\dagger \hat{c}_{\alpha k}^{(\mathrm{H})}(t)\Big) \tag{3.58}$$

Using the Heisenberg equations of motion (3.3), one straightforwardly finds

$$\hat{\jmath}_\alpha(t) = -\mathrm{i}\sum_k \Big(g_{\alpha k}\hat{d}^{(\mathrm{H})}(t)^\dagger \hat{c}_{\alpha k}^{(\mathrm{H})}(t) - g_{\alpha k}^* \hat{c}_{\alpha k}^{(\mathrm{H})}(t)^\dagger \hat{d}^{(\mathrm{H})}(t)\Big) \tag{3.59}$$

The particle current out of reservoir α is then given by

$$j_\alpha(t) = \langle \hat{\jmath}_\alpha(t)\rangle = 2\,\mathrm{Im}\left(\sum_k g_{\alpha k}\,\langle \hat{d}^{(\mathrm{H})}(t)^\dagger \hat{c}_{\alpha k}^{(\mathrm{H})}(t)\rangle\right) \tag{3.60}$$

With the expressions of $\hat{d}^{(\mathrm{H})}(t)$ and $\hat{c}_{\alpha k}^{(\mathrm{H})}(t)$ derived previously, we then obtain

$$\begin{aligned} j_\alpha(t) &= 2\,\mathrm{Im}\sum_k |g_{\alpha k}|^2 \Bigg(n_0\varphi(t)^*\psi(t,\omega_{\alpha k}) + n_\alpha(\omega_{\alpha k})\psi(t,\omega_{\alpha k})^* \mathrm{e}^{-\mathrm{i}\omega_{\alpha k}t} \\ &\qquad + \sum_{\alpha',k'} |g_{\alpha' k'}|^2 n_{\alpha'}(\omega_{\alpha' k'})\psi(t,\omega_{\alpha' k'})^* \chi(t,\omega_{\alpha k},\omega_{\alpha' k'})\Bigg) \\ &= 2\,\mathrm{Im}\Bigg(n_0\varphi(t)^* \int \mathrm{d}\omega\, J_\alpha(\omega)\psi(t,\omega) + \int \mathrm{d}\omega\, J_\alpha(\omega) n_\alpha(\omega)\psi(t,\omega)^* \mathrm{e}^{-\mathrm{i}\omega t} \\ &\qquad + \int \mathrm{d}\omega \int \mathrm{d}\omega'\, J_\alpha(\omega) J(\omega') N(\omega')\psi(t,\omega')^* \chi(t,\omega,\omega')\Bigg) \end{aligned} \tag{3.61}$$

Similarly, one defines the energy currents

$$\begin{aligned} u_\alpha(t) &= 2\hbar\,\mathrm{Im}\left(\sum_k g_{\alpha k}\omega_{\alpha k}\,\langle \hat{d}^{(\mathrm{H})}(t)^\dagger \hat{c}_{\alpha k}^{(\mathrm{H})}(t)\rangle\right) \\ &= 2\hbar\,\mathrm{Im}\Bigg(n_0\varphi(t)^* \int \mathrm{d}\omega\, \omega J_\alpha(\omega)\psi(t,\omega) + \int \mathrm{d}\omega\, \omega J_\alpha(\omega) n_\alpha(\omega)\psi(t,\omega)^* \mathrm{e}^{-\mathrm{i}\omega t} \\ &\qquad + \int \mathrm{d}\omega \int \mathrm{d}\omega'\, \omega J_\alpha(\omega) J(\omega') N(\omega')\psi(t,\omega')^* \chi(t,\omega,\omega')\Bigg) \end{aligned} \tag{3.62}$$

3.2.3 Correlations in the discrete level occupation

3.2.3.1 Fermions

In order to achieve a precise understanding of the dynamics of the system, it is necessary to investigate the time correlations of physical quantities. In this work, we will study the correlation function describing the dynamics of the discrete level given by

$$G(t_1,t_2)=\langle\hat{n}(t_1)\hat{n}(t_2)\rangle-\langle\hat{n}(t_1)\rangle\langle\hat{n}(t_2)\rangle \tag{3.63}$$

It reads

$$\begin{aligned}
&G(t_1,t_2)\\
&=|\varphi(t_1)|^2|\varphi(t_2)|^2\Big(\langle\hat{d}^\dagger\hat{d}\hat{d}^\dagger\hat{d}\rangle-\langle\hat{d}^\dagger\hat{d}\rangle\langle\hat{d}^\dagger\hat{d}\rangle\Big)\\
&\quad+|\varphi(t_1)|^2\sum_{\alpha,k}\sum_{\alpha',k'}g^*_{\alpha k}g_{\alpha'k'}\psi(t_2,\omega_{\alpha k})^*\psi(t_2,\omega_{\alpha'k'})\\
&\qquad\qquad\times\Big(\langle\hat{d}^\dagger\hat{d}\hat{c}^\dagger_{\alpha k}\hat{c}_{\alpha'k'}\rangle-\langle\hat{d}^\dagger\hat{d}\rangle\langle\hat{c}^\dagger_{\alpha k}\hat{c}_{\alpha'k'}\rangle\Big)\\
&\quad+\varphi(t_1)^*\varphi(t_2)\sum_{\alpha,k}\sum_{\alpha',k'}g_{\alpha k}g^*_{\alpha'k'}\psi(t_1,\omega_{\alpha k})\psi(t_2,\omega_{\alpha'k'})^*\\
&\qquad\qquad\times\Big(\langle\hat{d}^\dagger\hat{c}_{\alpha k}\hat{c}^\dagger_{\alpha'k'}\hat{d}\rangle-\langle\hat{d}^\dagger\hat{c}_{\alpha k}\rangle\langle\hat{c}^\dagger_{\alpha'k'}\hat{d}\rangle\Big)\\
&\quad+\varphi(t_1)\varphi(t_2)^*\sum_{\alpha,k}\sum_{\alpha',k'}g^*_{\alpha k}g_{\alpha'k'}\psi(t_1,\omega_{\alpha k})^*\psi(t_2,\omega_{\alpha'k'})\\
&\qquad\qquad\times\Big(\langle\hat{c}^\dagger_{\alpha k}\hat{d}\hat{d}^\dagger\hat{c}_{\alpha'k'}\rangle-\langle\hat{c}^\dagger_{\alpha k}\hat{d}\rangle\langle\hat{d}^\dagger\hat{c}_{\alpha'k'}\rangle\Big)\\
&\quad+|\varphi(t_2)|^2\sum_{\alpha,k}\sum_{\alpha',k'}g^*_{\alpha k}g_{\alpha'k'}\psi(t_1,\omega_{\alpha k})^*\psi(t_1,\omega_{\alpha'k'})\\
&\qquad\qquad\times\Big(\langle\hat{c}^\dagger_{\alpha k}\hat{c}_{\alpha'k'}\hat{d}^\dagger\hat{d}\rangle-\langle\hat{c}^\dagger_{\alpha k}\hat{c}_{\alpha'k'}\rangle\langle\hat{d}^\dagger\hat{d}\rangle\Big)\\
&\quad+\sum_{\alpha,k}\sum_{\alpha',k'}\sum_{\beta,l}\sum_{\beta',l'}g^*_{\alpha k}g_{\alpha'k'}g^*_{\beta l}g_{\beta'l'}\psi(t_1,\omega_{\alpha k})^*\psi(t_1,\omega_{\alpha'k'})\psi(t_2,\omega_{\beta l})^*\psi(t_2,\omega_{\beta'l'})\\
&\qquad\qquad\times\Big(\langle\hat{c}^\dagger_{\alpha k}\hat{c}_{\alpha'k'}\hat{c}^\dagger_{\beta l}\hat{c}_{\beta'l'}\rangle-\langle\hat{c}^\dagger_{\alpha k}\hat{c}_{\alpha'k'}\rangle\langle\hat{c}^\dagger_{\beta l}\hat{c}_{\beta'l'}\rangle\Big)
\end{aligned} \tag{3.64}$$

We start by studying the case of fermions because all the expectations values in this expression can be dramatically simplified. We first have

$$\langle\hat{d}^\dagger\hat{d}\hat{d}^\dagger\hat{d}\rangle-\langle\hat{d}^\dagger\hat{d}\rangle\langle\hat{d}^\dagger\hat{d}\rangle=\langle\hat{d}^\dagger\hat{d}\rangle-\langle\hat{d}^\dagger\hat{d}\rangle^2=n_0-n_0^2=n_0(1-n_0) \tag{3.65}$$

As we consider factorized initial conditions (3.53), we then find

$$\langle\hat{d}^\dagger\hat{d}\hat{c}^\dagger_{\alpha k}\hat{c}_{\alpha'k'}\rangle-\langle\hat{d}^\dagger\hat{d}\rangle\langle\hat{c}^\dagger_{\alpha k}\hat{c}_{\alpha'k'}\rangle=\langle\hat{d}^\dagger\hat{d}\rangle\langle\hat{c}^\dagger_{\alpha k}\hat{c}_{\alpha'k'}\rangle-\langle\hat{d}^\dagger\hat{d}\rangle\langle\hat{c}^\dagger_{\alpha k}\hat{c}_{\alpha'k'}\rangle=0 \tag{3.66}$$

Similarly

$$\langle\hat{c}^\dagger_{\alpha k}\hat{c}_{\alpha'k'}\hat{d}^\dagger\hat{d}\rangle-\langle\hat{c}^\dagger_{\alpha k}\hat{c}_{\alpha'k'}\rangle\langle\hat{d}^\dagger\hat{d}\rangle=0 \tag{3.67}$$

Next, we have

$$\langle\hat{d}^\dagger\hat{c}_{\alpha k}\hat{c}^\dagger_{\alpha'k'}\hat{d}\rangle-\langle\hat{d}^\dagger\hat{c}_{\alpha k}\rangle\langle\hat{c}^\dagger_{\alpha'k'}\hat{d}\rangle=\langle\hat{d}^\dagger\hat{d}\rangle\langle\hat{c}_{\alpha k}\hat{c}^\dagger_{\alpha'k'}\rangle=n_0\delta_{\alpha\alpha'}\delta_{kk'}(1-n_\alpha(\omega_{\alpha k})) \tag{3.68}$$

and

$$\langle \hat{c}^\dagger_{\alpha k} \hat{d} \hat{d}^\dagger \hat{c}_{\alpha' k'} \rangle - \langle \hat{c}^\dagger_{\alpha k} \hat{d} \rangle \langle \hat{d}^\dagger \hat{c}_{\alpha' k'} \rangle = (1 - n_0) \delta_{\alpha \alpha'} \delta_{k k'} n_\alpha(\omega_{\alpha k}) \tag{3.69}$$

Eventually, we use Wick's theorem to find

$$\begin{aligned} \langle \hat{c}^\dagger_{\alpha k} \hat{c}_{\alpha' k'} \hat{c}^\dagger_{\beta l} \hat{c}_{\beta' l'} \rangle - \langle \hat{c}^\dagger_{\alpha k} \hat{c}_{\alpha' k'} \rangle \langle \hat{c}^\dagger_{\beta l} \hat{c}_{\beta' l'} \rangle &= \langle \hat{c}^\dagger_{\alpha k} \hat{c}_{\alpha' k'} \rangle \langle \hat{c}^\dagger_{\beta l} \hat{c}_{\beta' l'} \rangle - \langle \hat{c}^\dagger_{\alpha k} \hat{c}^\dagger_{\beta l'} \rangle \langle \hat{c}_{\alpha' k'} \hat{c}_{\beta' l'} \rangle \\ &\quad + \langle \hat{c}^\dagger_{\alpha k} \hat{c}_{\beta' l'} \rangle \langle \hat{c}_{\alpha' k'} \hat{c}^\dagger_{\beta l} \rangle - \langle \hat{c}^\dagger_{\alpha k} \hat{c}_{\alpha' k'} \rangle \langle \hat{c}^\dagger_{\beta l} \hat{c}_{\beta' l'} \rangle \\ &= \langle \hat{c}^\dagger_{\alpha k} \hat{c}_{\beta' l'} \rangle \langle \hat{c}_{\alpha' k'} \hat{c}^\dagger_{\beta l} \rangle \\ &= \delta_{\alpha \beta'} \delta_{k l'} \delta_{\alpha' \beta} \delta_{k' l} n_\alpha(\omega_{\alpha k}) (1 - n_{\alpha'}(\omega_{\alpha' k'})) \end{aligned} \tag{3.70}$$

Through some additional algebra, the correlation function can eventually be factorized as follows

$$\begin{aligned} G(t_1, t_2) &= \left(n_0 \varphi(t_1)^* \varphi(t_2) + \sum_{\alpha, k} |g_{\alpha k}|^2 n_\alpha(\omega_{\alpha k}) \psi(t_1, \omega_{\alpha k})^* \psi(t_2, \omega_{\alpha k}) \right) \\ &\quad \times \left((1 - n_0) \varphi(t_2)^* \varphi(t_1) + \sum_{\alpha, k} |g_{\alpha k}|^2 (1 - n_\alpha(\omega_{\alpha k})) \psi(t_2, \omega_{\alpha k})^* \psi(t_1, \omega_{\alpha k}) \right) \\ &= \left(n_0 \varphi(t_1)^* \varphi(t_2) + \int \mathrm{d}\omega \, J(\omega) N(\omega) \psi(t_1, \omega)^* \psi(t_2, \omega) \right) \\ &\quad \times \left((1 - n_0) \varphi(t_2)^* \varphi(t_1) + \int \mathrm{d}\omega \, J(\omega) (1 - N(\omega)) \psi(t_2, \omega)^* \psi(t_1, \omega) \right) \end{aligned} \tag{3.71}$$

3.2.3.2 General case

The result is more complicated for bosons than for fermions. In the general case (which works for bosons as well as fermions), the correlation function is

$$\begin{aligned} G(t_1, t_2) &= \varphi(t_1)^* \varphi(t_2) \\ &\quad \times \Bigg(G(0,0) \varphi(t_2)^* \varphi(t_1) \\ &\qquad + n_0 \int \mathrm{d}\omega \, J(\omega) (1 \pm N(\omega)) \psi(t_2, \omega)^* \psi(t_1, \omega) \Bigg) \\ &\quad + \Bigg((1 \pm n_0) \varphi(t_2)^* \varphi(t_1) \\ &\qquad + \int \mathrm{d}\omega \, J(\omega) (1 \pm N(\omega)) \psi(t_2, \omega)^* \psi(t_1, \omega) \Bigg) \\ &\qquad \times \int \mathrm{d}\omega \, J(\omega) N(\omega) \psi(t_1, \omega)^* \psi(t_2, \omega) \end{aligned} \tag{3.72}$$

where the plus sign is for bosons and the minus sign is for fermions.

Chapter 4

Long-time limit

In this chapter, we derive the long-time limit of the formal time-dependent solution of the model. Using the Riemann-Lebesgue lemma, we obtain analytical formulae in this limit. Our results show that three different regimes are possible depending on the number of bound states. In cases without bound states, the system decays to a steady state which is independent of the initial preparation. In cases with one bound state, the system decays to a steady state which depend on the initial preparation. In cases with two bound states or more, the system decays to a limit cycle as the occupation and currents exhibit persistent oscillations which depend on the initial preparation. Considering conservation laws, we then show how the non-oscillatory components of the occupation and currents can be dramatically simplified. In particular, this enables us to define a transmission function for the discrete level as in the Landauer-Büttiker formalism. Finally, we analyze some simplified frameworks, the wide-band limit and the results provided by the master equation and Landauer-Büttiker formalisms. We show that these schemes ignore much of the interesting physics arising from the band structure of the reservoirs.

4.1 The Riemann-Lebesgue lemma

Although the expressions derived in the previous section give the most general solution to the problem, it is in general impossible to obtain time-dependent expressions that do not require costly integral computations. We will therefore focus on the study of the state of the system for long times. In order to estimate the quantities of interest in the long-time limit, the main tool we will use is the Riemann-Lebesgue lemma. It states that a function vanishes in the long-time limit if its Fourier transform is integrable [78]. In other words, if $X(\omega)$ is an integrable function, then:

$$\int \mathrm{d}\omega\, X(\omega)\mathrm{e}^{-\mathrm{i}\omega t} \underset{t\to\infty}{\longrightarrow} 0 \tag{4.1}$$

In the following, we will assume that all the functions we are dealing with are integrable so that the Riemann-Lebesgue lemma applies. Even though we do not provide a rigorous proof of this assertion in general, it can usually be demonstrated for any particular choice of density of states but requires going through some tedious algebra. Ultimately, the results derived in the following turn out to be consistent with numerical estimates of the long-time limit.

4.2 Occupation of the discrete level

We start by investigating the long-time limit of the number of particles in the discrete level. As a first step, we estimate $\varphi(t)$ in the long-time limit. The Riemann-Lebesgue lemma[1] straightforwardly yields [33, 57]

$$\varphi(t \to \infty) = \sum_b Z_b \mathrm{e}^{-\mathrm{i}\omega_b t} \tag{4.2}$$

This first result hints at the fact that the long-time state of the site will be highly influenced by the band structure of the reservoirs. For a reservoir without band gaps there are no bound states and $\varphi(t)$ consequently decays in the long-time limit whereas it oscillates forever for a band structure which gives rise to bound states [33, 44, 45, 52–54, 56, 57].

Contrary to $\varphi(t)$, the asymptotics of $\psi(t,\omega)$ is not straightforward due to the factor $E(t,\omega,\omega')$ which introduces a denominator that has to be dealt with carefully. We start by splitting the integral in $\psi(t,\omega)$ into three parts avoiding the non-analyticity at $\omega' = \omega$

$$\int \mathrm{d}\omega'\, S(\omega')E(t,\omega,\omega') = \lim_{\varepsilon\to 0^+} \left(\int_{-\infty}^{\omega-\varepsilon} \mathrm{d}\omega' + \int_{\omega-\varepsilon}^{\omega+\varepsilon} \mathrm{d}\omega' + \int_{\omega+\varepsilon}^{\infty} \mathrm{d}\omega'\right) S(\omega')E(t,\omega,\omega') \tag{4.3}$$

The function $\omega' \mapsto S(\omega')E(t,\omega,\omega')$ being analytic in the vicinity of $\omega' = \omega$, the integral encompassing this point vanishes and we can now write

$$\int \mathrm{d}\omega'\, S(\omega')E(t,\omega,\omega') = \mathrm{e}^{-\mathrm{i}\omega t} \oint \mathrm{d}\omega' \, \frac{S(\omega')}{\omega-\omega'} - \oint \mathrm{d}\omega' \, \frac{S(\omega')\mathrm{e}^{-\mathrm{i}\omega' t}}{\omega-\omega'} \tag{4.4}$$

The time dependence first term in the right-hand side of the above equation is straightforward, we then focus on the second term. To estimate its long-time limit, we consider a complex-plane contour of the type of the one depicted in figure 4.1. The principal value integral is computed by making a vanishingly small detour around the pole at $\omega' = \omega$; the contour is then closed by an arbitrary path γ_- in the lower-half complex plane. Using the residue theorem, we find

$$\oint \mathrm{d}\omega' \, \frac{S(\omega')\mathrm{e}^{-\mathrm{i}\omega' t}}{\omega-\omega'} - \mathrm{i}\pi S(\omega)\mathrm{e}^{-\mathrm{i}\omega t} + \int_{\gamma_-} \mathrm{d}z \, \frac{S(z)\mathrm{e}^{-\mathrm{i}zt}}{\omega - z} = 2\mathrm{i}\pi \sum_m \zeta_m \mathrm{e}^{-\mathrm{i}z_m t} \tag{4.5}$$

[1] $S(\omega)$ is integrable as $\varphi(0) = 1$ and $S(\omega) > 0$.

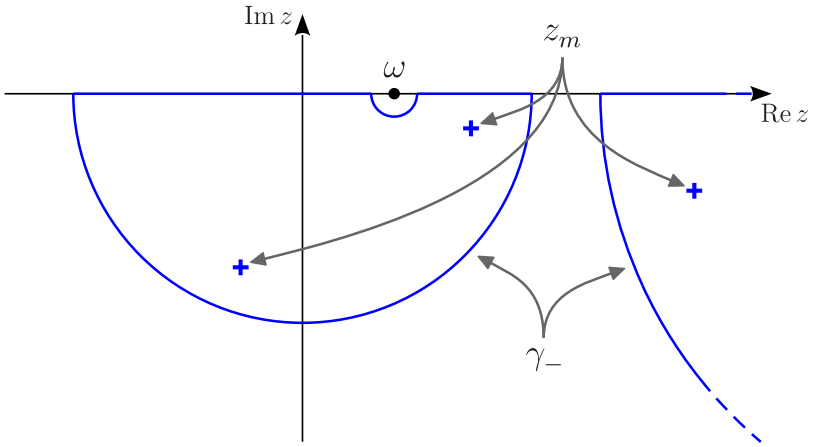

Figure 4.1 – The contour in the complex plane used to obtain equation (4.5). Only the vanishingly small circle around $\omega' = \omega$ contributes to the long-time limit of the real-line integral.

where the second term in the left-hand side is the contribution of the small circle, and m labels the poles z_m of $S(z)$ lying inside the contour. By definition, $\mathrm{Im}\, z_m < 0$, which means that the right-hand side of the above equation vanishes in the long-time limit. The same goes for the integral along γ_- as this path entirely lies in the lower-half plane. We deduce that only the contribution of the small detour around the singularity remains at long times,

$$\fint \mathrm{d}\omega' \, \frac{S(\omega')\mathrm{e}^{-\mathrm{i}\omega' t}}{\omega - \omega'} \underset{t\to\infty}{\simeq} \mathrm{i}\pi S(\omega)\mathrm{e}^{-\mathrm{i}\omega t} \tag{4.6}$$

The long-time limit of $\psi(t,\omega)$ is then given by

$$\begin{aligned} \psi(t\to\infty,\omega) &= (\sigma(\omega) - \mathrm{i}\pi S(\omega))\mathrm{e}^{-\mathrm{i}\omega t} + \sum_b Z_b E(t,\omega,\omega_b) \\ &= \left(\sigma(\omega) + \sum_b \frac{Z_b}{\omega-\omega_b} - \mathrm{i}\pi S(\omega)\right)\mathrm{e}^{-\mathrm{i}\omega t} - \sum_b \frac{Z_b \mathrm{e}^{-\mathrm{i}\omega_b t}}{\omega-\omega_b} \end{aligned} \tag{4.7}$$

with the principal value integral

$$\sigma(\omega) = \fint \mathrm{d}\omega' \, \frac{S(\omega')}{\omega - \omega'} \tag{4.8}$$

We now have all the ingredients to estimate the long-time occupation. Replacing $\varphi(t)$ and $\psi(t,\omega)$ in equation (3.56) by the asymptotic expressions (4.2) and (4.7),

we obtain

$$\begin{aligned} n(t) &= n_0|\varphi(t)|^2 + \int \mathrm{d}\omega\, J(\omega)N(\omega)|\psi(t,\omega)|^2 \\ &\underset{t\to\infty}{\simeq} n_0\left|\sum_b Z_b \mathrm{e}^{-\mathrm{i}\omega_b t}\right|^2 \\ &\quad + \int \mathrm{d}\omega\, J(\omega)N(\omega)\left|\left(\sigma(\omega) + \sum_b \frac{Z_b}{\omega-\omega_b} - \mathrm{i}\pi S(\omega)\right)\mathrm{e}^{-\mathrm{i}\omega t} - \sum_b \frac{Z_b \mathrm{e}^{-\mathrm{i}\omega_b t}}{\omega-\omega_b}\right|^2 \end{aligned} \tag{4.9}$$

This expression still needs simplifications. Using the same kind of arguments as before, we find after many algebraic manipulations

$$\begin{aligned} n(t\to\infty) = &\int \mathrm{d}\omega\, J(\omega)A(\omega)N(\omega) \\ &+ \sum_{b,b'} Z_b Z_{b'} \cos(\omega_{bb'}t)\left(n_0 + \int \mathrm{d}\omega\, \frac{J(\omega)N(\omega)}{(\omega-\omega_b)(\omega-\omega_{b'})}\right) \end{aligned} \tag{4.10}$$

where $\omega_{bb'} = \omega_b - \omega_{b'}$, and $A(\omega)$ is a short notation for the somewhat complicated quantity

$$A(\omega) = \left(\sigma(\omega) + \sum_b \frac{Z_b}{\omega-\omega_b}\right)^2 + \pi^2 S(\omega)^2 \tag{4.11}$$

The long-time occupation is given by the sum of two terms, the second of which vanishes in the case of a reservoir without band gaps. This is a striking example of the strong influence of the reservoir band structure. Indeed, the second term in the right-hand side of equation (4.10) exhibits two interesting features. First, it depends on the initial occupation n_0; the discrete level then retains memory of the state in which it was prepared *forever* if the coupling to the reservoirs gives rise to bound states. Second, this term persistently oscillates at frequencies $\omega_{bb'}$ if there is more than one bound state.

Hence, the behaviour of the occupation at long times depends strikingly on the number of bound states. If there are no bound states, the discrete level decays to a steady state which is independent of the initial occupation. If there is one bound state, the occupation decays to a steady state that depends on the initial occupation. If there are two or more bound states, the occupation decays to a limit cycle, whose properties (magnitude of both the oscillatory and non-oscillatory components) depend on the initial occupation.

We warn the reader not to use equation (4.10) in calculations, because we will derive a simpler version of it below in equation (4.20).

The surprising influence of bound states on the long-time occupation of the discrete level has first been described qualitatively by Dhar and Sen [44], and Stefanucci [45] later obtained an analytical formula of the type of equation (4.20)

below quantitatively accounting for the dependence on initial occupation and persistent oscillations. The effects of bound states in the long-time limit have raised concerns about the physical significance of the non-Markovian features carried by bound states. Dhar and Sen were mainly concerned about the fact that these unsual features remain in an equilibrium set-up with no temperature nor voltage bias. They showed that one can retrieve the usual equilibrium result if an additional equilibration process with a wide-band spectral density is introduced. However, non-equilibrium results obtained with this method depend on the details of the equilibration process. Stefanucci showed that this ambuguity could be solved considering a different preparation process, the so-called partition-free approach which was first proposed by Cini [80]. These questions are explored in more details in chapter 5, whose main topic is the equilibration of bound states with a process similar to that introduced by Dhar and Sen.

4.3 Currents

We now turn to the estimates of long-time currents. This turns out to be much more complicated than the calculations of the long-time density matrix above as the time dependence of the current in expression (3.61) is very involved. We first have to study the function $\chi(t,\omega,\omega')$. Proceeding as before, we obtain the rather complicated expression

$$\begin{aligned}\chi(t\to\infty,\omega,\omega') &= \sigma(\omega')E(t,\omega,\omega') - \mathrm{e}^{-\mathrm{i}\omega t}\oint \mathrm{d}\omega''\,\frac{S(\omega'')}{(\omega-\omega'')(\omega'-\omega'')} \\ &\qquad - \mathrm{i}\pi\frac{S(\omega)\mathrm{e}^{-\mathrm{i}\omega t}-S(\omega')\mathrm{e}^{-\mathrm{i}\omega' t}}{\omega-\omega'} + \sum_b Z_b\frac{E(t,\omega,\omega')-E(t,\omega,\omega_b)}{\omega'-\omega_b} \\ &= \left(\sigma(\omega')+\sum_b\frac{Z_b}{\omega'-\omega_b}\right)E(t,\omega,\omega') - \mathrm{i}\pi\frac{S(\omega)\mathrm{e}^{-\mathrm{i}\omega t}-S(\omega')\mathrm{e}^{-\mathrm{i}\omega' t}}{\omega-\omega'} \\ &\qquad - \mathrm{e}^{-\mathrm{i}\omega t}\int \mathrm{d}\omega''\,\mathscr{P}\frac{S(\omega'')}{(\omega-\omega'')(\omega'-\omega'')} - \sum_b\frac{Z_b}{\omega'-\omega_b}E(t,\omega,\omega_b)\end{aligned} \tag{4.12}$$

We now use the long-time estimates (4.2), (4.7) and (4.12) in the current expression (3.61). After some tedious algebra, we find that the long-time particle

currents read

$$\begin{aligned} j_\alpha(t\to\infty) &= 2\pi \int \mathrm{d}\omega\, J_\alpha(\omega)(S(\omega)n_\alpha(\omega) - J(\omega)A(\omega)N(\omega)) \\ &\quad - \sum_{b,b'} Z_b Z_{b'}(\Lambda_\alpha(\omega_b) - \Lambda_\alpha(\omega_{b'}))\sin(\omega_{bb'}t)\left(n_0 + \int \mathrm{d}\omega\, \frac{J(\omega)N(\omega)}{(\omega-\omega_b)(\omega-\omega_{b'})}\right) \end{aligned} \tag{4.13}$$

where, similarly to $\Lambda(\omega)$ given in equation (3.20), $\Lambda_\alpha(\omega)$ is defined as[1]

$$\Lambda_\alpha(\omega) = \fint \mathrm{d}\omega'\, \frac{J_\alpha(\omega')}{\omega-\omega'} \tag{4.14}$$

Similarly to the long-time occupation in equation (4.10), we see that the long-time currents are given by the sum of two contributions. The first term in the right-hand side of equation (4.13) is constant, independent both of time and initial prepration. In contrast, the second contribution to the long-time currents corresponds to persistent oscillations at frequencies $\omega_{bb'}$ which depend on the initial occupation n_0 and exist only if there are two or more bound states.

As already explained, such phenomena were first described by Dhar and Sen [44] and then Stefanucci [45]. However, Dhar and Sen focused on the occupation of the discrete level and seldom addressed the influence of bound states on currents, while Stefanucci obtained analytical results for both the occupation and currents in the long-time limit.

Persistent oscillations in the occupation and currents are tightly linked through particle conservation. As particles can only exit a reservoir to go on the discrete level and vice versa, any time-dependence in the occupation of this level is necessarily reflected in the currents to guarantee conservation of the total number of particles. This is why we observe oscillations at the same frequencies in the occupation and currents at long times. Conservation laws are considered with more details in the following section.

As the second-term in equation (4.13) oscillates at high frequency, it will not be observed in a standard dc measurement, which only measure the zero-frequency component of the current. We then define the dc current as the non-oscillatory contribution to the long-time current, that is

$$j_\alpha^{(\mathrm{dc})} = 2\pi \int \mathrm{d}\omega\, J_\alpha(\omega)(S(\omega)n_\alpha(\omega) - J(\omega)A(\omega)N(\omega)) \tag{4.15}$$

This dc current is independent of the initial occupation, in contrast to the non-oscillatory component of the long-time occupation.

[1] Note that it is not necessary to take the principal value in the expression for the long-time currents as the bound state energies ω_b lie in band gaps.

Again, the reader should not to use equations (4.13) and (4.15) in calculations, because we will derive simpler versions of them below in equations (4.21) and (4.23).

4.4 Continuity equation

The long-time occupation (4.10) and currents (4.13) derived above remain difficult to study, mainly due to the factor $A(\omega)$ in which basically all the complicated mathematical quantities have been hidden. We will show here that they can be dramatically simplified considering the conservation laws applying to the model. Indeed, using the Heisenberg equations of motion (3.3), it is straightforward to obtain the continuity equation [42, 43]

$$\frac{\mathrm{d}\hat{n}}{\mathrm{d}t} = \sum_{\alpha} \hat{\jmath}_{\alpha} \tag{4.16}$$

This simply describes particle conservation: the variation of the number of particles in the discrete level is only due to exchanges of particles with the reservoirs, that is particle currents. Taking the expectation value on equation (4.16) and using the long-time quantities (4.10) and (4.13), we obtain

$$\begin{aligned} &-\sum_{b,b'} \omega_{bb'} Z_b Z_{b'} \sin(\omega_{bb'} t) \left(n_0 + \int \mathrm{d}\omega \, \frac{J(\omega) N(\omega)}{(\omega - \omega_b)(\omega - \omega_{b'})} \right) \\ &\quad = 2\pi \int \mathrm{d}\omega \, J(\omega)(S(\omega) - J(\omega)A(\omega))N(\omega) \\ &\qquad\qquad - \sum_{b,b'} Z_b Z_{b'} (\Lambda(\omega_b) - \Lambda(\omega_{b'})) \sin(\omega_{bb'} t) \left(n_0 + \int \mathrm{d}\omega \, \frac{J(\omega) N(\omega)}{(\omega - \omega_b)(\omega - \omega_{b'})} \right) \end{aligned} \tag{4.17}$$

From equation (3.23), we find that the bound state energies satisfy $\omega_b = \omega_{\mathrm{d}} + \Lambda(\omega_b)$, such that $\omega_{bb'} = \Lambda(\omega_b) - \Lambda(\omega_{b'})$. The oscillating terms then cancel each other in the above continuity equation which thus reduces to

$$\int \mathrm{d}\omega \, J(\omega)(S(\omega) - J(\omega)A(\omega))N(\omega) = 0 \tag{4.18}$$

This relation holds for any choice of reservoirs, more specifically for all admissible values of temperatures and chemical potentials. Moreover, these degrees of freedom are already factorized in the integrand of equation (4.18): only $N(\omega)$ depends on the thermodynamic properties of the reservoirs. We deduce that the other factor in this integrand must cancel to ensure that equation (4.18) is always satisfied, that is

$$S(\omega) - J(\omega)A(\omega) = 0 \implies A(\omega) = \frac{S(\omega)}{J(\omega)} \tag{4.19}$$

The problematic quantity $A(\omega)$ can then be replaced by a much simpler one in equations (4.10) and (4.13). The long-time occupation is then given by [45]

$$n(t\to\infty) = \int \mathrm{d}\omega\, S(\omega)N(\omega) + \sum_{b,b'} Z_b Z_{b'} \cos(\omega_{bb'}t)\left(n_0 + \int \mathrm{d}\omega\, \frac{J(\omega)N(\omega)}{(\omega-\omega_b)(\omega-\omega_{b'})}\right) \tag{4.20}$$

The long-time currents can be simplified as well [45]

$$\begin{aligned} j_\alpha(t\to\infty) &= \frac{1}{2\pi}\int \mathrm{d}\omega\, \mathcal{T}_{\alpha\alpha'}(\omega)(n_\alpha(\omega)-n_{\alpha'}(\omega)) \\ &\quad - \sum_{b,b'} Z_b Z_{b'}(\Lambda_\alpha(\omega_b)-\Lambda_\alpha(\omega_{b'}))\sin(\omega_{bb'}t)\left(n_0 + \int \mathrm{d}\omega\, \frac{J(\omega)N(\omega)}{(\omega-\omega_b)(\omega-\omega_{b'})}\right) \end{aligned} \tag{4.21}$$

with

$$\mathcal{T}_{\alpha\alpha'}(\omega) = \frac{4\pi^2 J_\alpha(\omega)J_{\alpha'}(\omega)}{(\omega-\omega_\mathrm{d}-\Lambda(\omega))^2+\pi^2 J(\omega)^2} \tag{4.22}$$

Using the continuity equation, the time-independent part of the long-time occupation and currents have been dramatically simplified. As such, the dc currents read

$$j_\alpha^{(\mathrm{dc})} = \frac{1}{2\pi}\int \mathrm{d}\omega\, \mathcal{T}_{\alpha\alpha'}(\omega)(n_\alpha(\omega)-n_{\alpha'}(\omega)) \tag{4.23}$$

These currents thus turn out to obey a relation of the type of the Landauer formula (2.6). In analogy to this framework, we refer to $\mathcal{T}_{\alpha\alpha'}(\omega)$ as the transmission function from reservoir α' to reservoir α; it describes the probability for a particle coming on the discrete level from reservoir α' to be transmitted to reservoir α afterwards.

In the following, we will mostly consider transport between two reservoirs L and R. In this situation, we have a single transmission function

$$\mathcal{T}(\omega) = \frac{4\pi^2 J_\mathrm{L}(\omega)J_\mathrm{R}(\omega)}{(\omega-\omega_\mathrm{d}-\Lambda(\omega))^2+\pi^2 J(\omega)^2} \tag{4.24}$$

We have seen that the equation $\omega-\omega_\mathrm{d}-\Lambda(\omega)=0$ can have at most one solution in a band gap, that is when $J(\omega)=0$, but there is no such limitation on the number of solutions to this equation when $J(\omega)\neq 0$. This is because, contrary to what happens in energy gaps, the variations of the Lamb shift $\Lambda(\omega)$ within a band are not monotonous in general.

We note that the value of the transmission for a fixed energy ω is maximized when ω_d is tuned such that $\omega-\omega_\mathrm{d}-\Lambda(\omega)=0$, and we then find

$$\mathcal{T}(\omega) = 4J_\mathrm{L}(\omega)J_\mathrm{R}(\omega)/J(\omega)^2 \tag{4.25}$$

Of particular interest is the case of symmetric coupling where both reservoirs share the same spectral density, $J_{\mathrm{L}}(\omega) = J_{\mathrm{R}}(\omega) = J(\omega)$, since $\mathcal{T}(\omega) = 1$ if $\omega - \omega_{\mathrm{d}} - \Lambda(\omega) = 0$ in this situation. This means that the discrete level is transparent for a particle incoming at this energy as it cannot be reflected back into the reservoir from which it came, it will necessarily be transmitted to the other reservoir. As such, we will refer to such energy states as perfectly transmitting states. Perfectly transmitting states can be considered as the in-band equivalents of bound states since their energies satisfy the same resonance relation $\omega - \omega_{\mathrm{d}} - \Lambda(\omega) = 0$, with $J(\omega) = 0$ for bound states but $J(\omega) \neq 0$ for perfectly transmitting state. Despite this intimate relation, perfectly transmitting states and bound states have opposite transport properties as bound state do not participate to dc current.

Finally, we find that the long-time energy currents share the global features of the long-time particle currents; the dc energy currents are given by

$$u_{\alpha}^{(\mathrm{dc})} = \frac{\hbar}{2\pi} \int \mathrm{d}\omega \, \omega \mathcal{T}_{\alpha\alpha'}(\omega)(n_{\alpha}(\omega) - n_{\alpha'}(\omega)) \tag{4.26}$$

4.5 Long-time correlations in the discrete level occupation

By long-time correlations, we mean that we consider $G(t_1, t_2)$ with both t_1 and t_2 taken in the long-time limit for a given $\tau = t_1 - t_2$. To perform such calculation, the limits $t_1 \to \infty$ and $t_2 \to \infty$ cannot be taken independently. Instead, we consider

$$G(\tau) = \lim_{t \to \infty} G(t + \tau, t) \tag{4.27}$$

4.5.1 Fermions

As before, we start by studying the case of fermions which give simpler expressions. After some tedious algebra, we find

$$\begin{aligned} G(\tau) = \Bigg(\int \mathrm{d}\omega \, S(\omega) N(\omega) \mathrm{e}^{\mathrm{i}\omega\tau} \\ + \sum_{b,b'} Z_b Z_{b'} \mathrm{e}^{\mathrm{i}\omega_{bb'}t} \mathrm{e}^{\mathrm{i}\omega_b \tau} \left(n_0 + \int \mathrm{d}\omega \, \frac{J(\omega) N(\omega)}{(\omega - \omega_b)(\omega - \omega_{b'})} \right) \Bigg) \\ \times \Bigg(\int \mathrm{d}\omega \, S(\omega)(1 - N(\omega)) \mathrm{e}^{-\mathrm{i}\omega\tau} \\ + \sum_{b,b'} Z_b Z_{b'} \mathrm{e}^{-\mathrm{i}\omega_{bb'}t} \mathrm{e}^{-\mathrm{i}\omega_b \tau} \left(1 - n_0 + \int \mathrm{d}\omega \, \frac{J(\omega)(1 - N(\omega))}{(\omega - \omega_b)(\omega - \omega_{b'})} \right) \Bigg) \end{aligned} \tag{4.28}$$

We see that $G(\tau)$ explicitly depends on Z_b. Therefore, the existence of bound states yields an additional type of correlations in the dynamics of the discrete level. Furthermore, these turn out to be particularly robust as the large-τ limit yields

$$\begin{aligned} G(\tau \to \infty) = \sum_{b,b'} Z_b Z_{b'} \mathrm{e}^{\mathrm{i}\omega_{bb'}t} \mathrm{e}^{\mathrm{i}\omega_b \tau} \left(n_0 + \int \mathrm{d}\omega \, \frac{J(\omega) N(\omega)}{(\omega - \omega_b)(\omega - \omega_{b'})} \right) \\ \times \sum_{b,b'} Z_b Z_{b'} \mathrm{e}^{-\mathrm{i}\omega_{bb'}t} \mathrm{e}^{-\mathrm{i}\omega_b \tau} \left(1 - n_0 + \int \mathrm{d}\omega \, \frac{J(\omega)(1 - N(\omega))}{(\omega - \omega_b)(\omega - \omega_{b'})} \right) \end{aligned} \tag{4.29}$$

The influence of bound states in even more striking here than before as large-τ correlations simply vanish when there are no bound states. In cases with two or more bound states, persistent oscillations are found again.

4.5.2 General case

Again the result is more complicated for bosons than for fermions. In the general case, we find

$$\begin{aligned} & G(\tau) \\ & = \sum_{b,b'} Z_b Z_{b'} \mathrm{e}^{\mathrm{i}\omega_{bb'}t} \mathrm{e}^{\mathrm{i}\omega_b \tau} \\ & \qquad \times \left(n_0 \int \mathrm{d}\omega \, S(\omega)(1 \pm N(\omega)) \mathrm{e}^{-\mathrm{i}\omega\tau} \right. \\ & \qquad\qquad \left. + \sum_{b,b'} Z_b Z_{b'} \mathrm{e}^{-\mathrm{i}\omega_{bb'}t} \mathrm{e}^{-\mathrm{i}\omega_b \tau} \left(G(0,0) + n_0 \int \mathrm{d}\omega \, \frac{J(\omega)(1 \pm N(\omega))}{(\omega - \omega_b)(\omega - \omega_{b'})} \right) \right) \\ & \quad + \left(\int \mathrm{d}\omega \, S(\omega)(1 \pm N(\omega)) \mathrm{e}^{-\mathrm{i}\omega\tau} \right. \\ & \qquad\qquad \left. + \sum_{b,b'} Z_b Z_{b'} \mathrm{e}^{-\mathrm{i}\omega_{bb'}t} \mathrm{e}^{-\mathrm{i}\omega_b \tau} \left(1 \pm n_0 + \int \mathrm{d}\omega \, \frac{J(\omega)(1 \pm N(\omega))}{(\omega - \omega_b)(\omega - \omega_{b'})} \right) \right) \\ & \qquad \times \left(\int \mathrm{d}\omega \, S(\omega) N(\omega) \mathrm{e}^{\mathrm{i}\omega\tau} + \sum_{b,b'} Z_b Z_{b'} \mathrm{e}^{\mathrm{i}\omega_{bb'}t} \mathrm{e}^{\mathrm{i}\omega_b \tau} \int \mathrm{d}\omega \, \frac{J(\omega) N(\omega)}{(\omega - \omega_b)(\omega - \omega_{b'})} \right) \end{aligned} \tag{4.30}$$

where the plus sign is for bosons and the minus sign is for fermions. In the limit where τ also goes to infinity, we have

$$G(\tau\to\infty) = \sum_{a,a',b,b'} Z_a Z_{a'} Z_b Z_{b'} \mathrm{e}^{\mathrm{i}(\omega_{ab}-\omega_{a'b'})t}\mathrm{e}^{\mathrm{i}\omega_{aa'}\tau} \times \left(G(0,0) + n_0 \int \mathrm{d}\omega\, \frac{J(\omega)(1\pm N(\omega))}{(\omega-\omega_{a'})(\omega-\omega_{b'})} + \left(1\pm n_0 + \int \mathrm{d}\omega\, \frac{J(\omega)(1\pm N(\omega))}{(\omega-\omega_{a'})(\omega-\omega_{b'})}\right) \times \int \mathrm{d}\omega\, \frac{J(\omega)N(\omega)}{(\omega-\omega_a)(\omega-\omega_{b'})}\right) \tag{4.31}$$

4.6 The wide-band limit: an example without bound states

In order to obtain explicit results, one has to specify the spectral density considered. As an illustrative example, we address here the simplest case where spectral densities are flat and span over the whole energy range, known as the wide-band limit. In this context, all spectral densities are constant: $J_\alpha(\omega) = \kappa_\alpha$. Note that the sophisticated machinery developed above is not necessary to derive the full solution of the system in this simplified situation [49]. The results obtained using direct calculation of course match with the general formulae given above.

We start by calculating the self-energy

$$\Sigma(x-\mathrm{i}\omega) = \sum_\alpha \kappa_\alpha \lim_{\omega_\mathrm{c}\to\infty} \int_{-\omega_\mathrm{c}}^{\omega_\mathrm{c}} \frac{\mathrm{d}\omega'}{\omega-\omega'+\mathrm{i}x} = -\mathrm{i}\pi\kappa\,\mathrm{sgn}(x) \tag{4.32}$$

with $\kappa = \sum_\alpha \kappa_\alpha$. Note that $\Sigma(z)$ exhibits a branch cut over the whole imaginary axis, illustrated by the factor $\mathrm{sgn}(x)$, as the spectral density is non-zero for all energies. It follows that the Laplace transform has no pole and there is hence no bound state.

The explicit calculation of $\varphi(t)$ is then straightforward,

$$\varphi(t) = \int_{-\infty}^{\infty} \mathrm{d}\omega\, \frac{\kappa \mathrm{e}^{-\mathrm{i}\omega t}}{(\omega-\omega_\mathrm{d})^2+\pi^2\kappa^2} = \mathrm{e}^{-\pi\kappa t}\mathrm{e}^{-\mathrm{i}\omega_\mathrm{d}t} \tag{4.33}$$

This yields

$$\psi(t,\omega) = -\mathrm{i}\int_0^t \mathrm{d}t'\,\varphi(t')\mathrm{e}^{-\mathrm{i}\omega(t-t')} = \frac{\mathrm{e}^{-\mathrm{i}\omega t} - \mathrm{e}^{-\pi\kappa t}\mathrm{e}^{-\mathrm{i}\omega_\mathrm{d}t}}{\omega-\omega_\mathrm{d}+\mathrm{i}\pi\kappa} \tag{4.34}$$

and

$$\chi(t,\omega,\omega') = -\mathrm{i}\int_0^t \mathrm{d}t'\,\psi(t',\omega')\mathrm{e}^{-\mathrm{i}\omega(t-t')} \tag{4.35}$$
$$= \frac{1}{\omega-\omega'}\left(\frac{\mathrm{e}^{-\mathrm{i}\omega t}}{\omega-\omega_\mathrm{d}+\mathrm{i}\pi\kappa} - \frac{\mathrm{e}^{-\mathrm{i}\omega' t}}{\omega'-\omega_\mathrm{d}+\mathrm{i}\pi\kappa}\right) + \frac{\mathrm{e}^{-\pi\kappa t}\mathrm{e}^{-\mathrm{i}\omega_\mathrm{d} t}}{(\omega-\omega_\mathrm{d}+\mathrm{i}\pi\kappa)(\omega'-\omega_\mathrm{d}+\mathrm{i}\pi\kappa)}$$

In this simplified framework, the long-time limit is straightforwardly read and the system approaches a steady state. The long-time occupation is given by

$$n(t\to\infty) = \sum_\alpha \int_{-\infty}^{\infty} \mathrm{d}\omega\,\frac{\kappa_\alpha n_\alpha(\omega)}{(\omega-\omega_\mathrm{d})^2+\pi^2\kappa^2} \tag{4.36}$$

which we see is independent of the initial occupation as expected in the absence of bound states.

Similarly, we find the long-time currents

$$j_\alpha(t\to\infty) = \frac{1}{2\pi}\sum_{\alpha'}\int_{-\infty}^{\infty}\mathrm{d}\omega\,\frac{4\pi^2\kappa_\alpha\kappa_{\alpha'}}{(\omega-\omega_\mathrm{d})^2+\pi^2\kappa^2}(n_\alpha(\omega)-n_{\alpha'}(\omega)) \tag{4.37}$$

These contain no oscillatory terms as expected in the absence of bound states and coincide exactly with the scattering theory for a single-level quantum dot (see section 4.7.2)

4.7 Comparison with approximate schemes

4.7.1 Master equation approach

Now that we have derived the full solution of the system, it is interesting to compare these exact results with the ones obtained with the approximate methods described earlier. We start with the master equation approach. For simplicity, we focus here on the fermionic version of the Fano-Anderson model. This is because the discrete level only has two states for fermions, it is then straightforward to draw a link between occupation and currents and the dynamics of the density matrix given by the master equation in this case. On the contrary, one has to consider infinitely-many possible states for the discrete level when bosons are involved.

The coupling Hamiltonian in the Fano-Anderson model (1.16) is given by

$$\hat{V} = \hbar\sum_{\alpha,k}\left(g_{\alpha k}\hat{d}^\dagger\hat{c}_{\alpha k} + g^*_{\alpha k}\hat{c}^\dagger_{\alpha k}\hat{d}\right) \tag{4.38}$$

We start from fatorized initial conditions as described by equation (3.53). In this context, we can define two correlation functions,

$$G_+(\tau) = \hbar^2 \sum_{\alpha,k} \sum_{\alpha',k'} g^*_{\alpha k} g_{\alpha' k'} \left\langle \hat{c}^{(\mathrm{int})}_{\alpha k}(\tau)^\dagger \hat{c}_{\alpha' k'} \right\rangle_{\mathrm{res}} \tag{4.39a}$$

$$G_-(\tau) = \hbar^2 \sum_{\alpha,k} \sum_{\alpha',k'} g_{\alpha k} g^*_{\alpha' k'} \left\langle \hat{c}^{(\mathrm{int})}_{\alpha k}(\tau) \hat{c}^\dagger_{\alpha' k'} \right\rangle_{\mathrm{res}} \tag{4.39b}$$

These can be dramatically simplified as the interaction-picture field operators are simply given by

$$\hat{c}^{(\mathrm{int})}_{rk}(\tau) = \mathrm{e}^{-\mathrm{i}\omega_{\alpha k}\tau} \hat{c}_{\alpha k} \tag{4.40}$$

This yields

$$G_+(\tau) = \hbar^2 \sum_{\alpha,k} |g_{\alpha k}|^2 n_{\alpha k} \mathrm{e}^{\mathrm{i}\omega_{\alpha k}\tau} = \hbar^2 \int \mathrm{d}\omega \, J(\omega) N(\omega) \mathrm{e}^{\mathrm{i}\omega\tau} \tag{4.41a}$$

$$G_-(\tau) = \hbar^2 \sum_{\alpha,k} |g_{\alpha k}|^2 (1 - n_{\alpha k}) \mathrm{e}^{-\mathrm{i}\omega_{\alpha k}\tau} = \hbar^2 \int \mathrm{d}\omega \, J(\omega)(1 - N(\omega)) \mathrm{e}^{-\mathrm{i}\omega\tau} \tag{4.41b}$$

This gives rise to the following transition rates for adding or removing a particle from the discrete level

$$\Gamma_+ = 2\pi J(\omega_{\mathrm{d}}) N(\omega_{\mathrm{d}}) \tag{4.42a}$$

$$\Gamma_- = 2\pi J(\omega_{\mathrm{d}})(1 - N(\omega)) \tag{4.42b}$$

The occupation of the discrete level, which identifies to the probability for this level to be occupied, then obeys the following master equation

$$\frac{\mathrm{d}n}{\mathrm{d}t} = \Gamma_+(1 - n) + \Gamma_- n \implies \frac{\mathrm{d}n}{\mathrm{d}t} + \Gamma n = \Gamma_+ \tag{4.43}$$

where we have defined

$$\Gamma = \Gamma_+ + \Gamma_- = 2\pi J(\omega_{\mathrm{d}}) \tag{4.44}$$

It is now necessary to identify the different time scales of the system in order to justify the Born-Markov approximations that yield the master equation (4.43). First, we have to infer the correlation time τ_{corr} which is the typical decay time of correlations. The typical width of the correlation functions (4.41) in time domain is the inverse of the width of its Fourier transform in frequency domain. Here the Fourier transforms can be straightforwardly read: $G_+(\tau) \to J(\omega)N(\omega)$ and $G_-(\tau) \to J(\omega)(1 - N(\omega))$. We then realize that the width of the Fourier transforms is essentially given by the width of the spectral density $J(\omega)$ which we denote by ω_{c}. As such, $\tau_{\mathrm{corr}} \sim 1/\omega_{\mathrm{c}}$.

We now have to estimate the damping time τ_{damp} of the system. We see from the master equation (4.43) that the occupation typically decays with the rate Γ

given in equation (4.44). This means that we can approximate the damping time of the occupation by $1/\Gamma$. Denoting by K the typical value of $J(\omega)$, we then take $\tau_{\mathrm{damp}} \sim 1/K$. The Born-Markov approximations are justified if $\tau_{\mathrm{corr}} \ll \tau_{\mathrm{damp}}$, which here boils down to $K \ll \omega_{\mathrm{c}}$. In other words, the master equation (4.43) holds if the spectral density is much wider than it is high.

It is straightforward to solve the master equation (4.43) for the time-dependent occupation,

$$n(t) = N(\omega_{\mathrm{d}}) + (n_0 - N(\omega_{\mathrm{d}}))\mathrm{e}^{-\Gamma t} \tag{4.45}$$

We then see that the discrete level occupation reaches a steady state with $n(t \to \infty) = N(\omega_{\mathrm{d}})$. It is interesting to note that this corresponds to the wide-band result (4.36) in the limit of vanishingly small coupling.

Given $n(t)$, we can calculate the currents from reservoir α via [19, 81]

$$j_\alpha(t) = \Gamma_+^{(\alpha)}(1 - n(t)) - \Gamma_-^{(\alpha)} n(t) \tag{4.46}$$

where

$$\Gamma_+^{(\alpha)} = 2\pi J_\alpha(\omega_{\mathrm{d}}) n_\alpha(\omega_{\mathrm{d}}) \tag{4.47a}$$

$$\Gamma_-^{(\alpha)} = 2\pi J_\alpha(\omega_{\mathrm{d}})(1 - n_\alpha(\omega_{\mathrm{d}})) \tag{4.47b}$$

The formula for the energy currents are the same with an extra prefactor of ω_{d}. This approximation thus considers transport only at the energy of the discrete level ω_{d}, so it takes into account neither the broadening nor the Lamb shift of the level.

More sophisticated weak-coupling approximations have gone beyond lowest order in the coupling. As an example we mention the diagrammatic techniques developed by Schoeller and Schön [82–85] in the 1990s. Neglecting certain classes of diagram, they have been able to resum a perturbation series to all orders in coupling. Their results account for level broadening but these methods have typically only been applied to the wide-band limit where there is no Lamb shift and then no bound states.

4.7.2 Scattering theory

The Fano-Anderson model can also be treated using the Landauer-Büttiker formalism. In this scope, we study transport between two electronic reservoirs via a single-level quantum dot. The scattering matrix of the dot is given by [19, 86]

$$\mathcal{S} = \begin{pmatrix} 1 & 0 \\ 0 & 1 \end{pmatrix} - \frac{2\mathrm{i}\pi}{\omega - \omega_{\mathrm{d}} + \mathrm{i}\pi(|g_{\mathrm{L}}|^2 + |g_{\mathrm{R}}|^2)} \begin{pmatrix} |g_{\mathrm{L}}|^2 & g_{\mathrm{L}}^* g_{\mathrm{R}} \\ g_{\mathrm{R}}^* g_{\mathrm{L}} & |g_{\mathrm{R}}|^2 \end{pmatrix} \tag{4.48}$$

where g_α represents the coupling amplitude between the discrete level and lead α. With $\kappa_\alpha = |g_\alpha|^2$, this leads to the transmission function

$$\mathcal{T}(\omega) = \frac{4\pi^2 \kappa_{\mathrm{L}} \kappa_{\mathrm{R}}}{(\omega - \omega_{\mathrm{d}})^2 + \pi^2(\kappa_{\mathrm{L}} + \kappa_{\mathrm{R}})^2} \tag{4.49}$$

We exactly retrieve the wide-band limit transmission of equation (4.37). This proves that, even though the Landauer-Büttiker formalism does not assume weak coupling, it completely fails to describe some important aspects of the model. Crucially, the effects of the Lamb shift are completely neglected which means that the transmission function features a resonance at the dot energy for any value of the coupling. We shall see later (sections 6.1.3 and 7.4.1) that it is not possible to fully understand the exact transport properties of the model if the Lamb shift is not taken into account.

Chapter 5

Mimicking the adiabatic turning on of level-reservoir coupling

The methods developed in the previous chapters are suited to the case of quench, a situation in which we consider the discrete level and reservoirs to be uncoupled before the coupling is suddenly turned on. This is not always possible in realistic set-ups, so we describe a procedure that mimics the adiabatic turning on of the level-reservoir coupling. Adding a vanishingly small constant to the spectral density, we ensure that all states thermalize in the long-time limit. This suppresses all memory of the initial preparation, and thus long-time oscillations of the occupation and currents, even in the presence of bound states. However, we show that the existence of bound states still gives rise to infinite-lifetime correlations in the discrete level occupation.

5.1 General description of the procedure

The formalism developed above heavily relies on the assumption that the coupling between the discrete level and the reservoirs is turned on at $t = 0$ and remains constant hereafter. This is why the discrete level still retains features of its initial preparation at long times. Indeed, as the coupling is turned on at $t = 0$, bound states may suddenly appear outside the continuum. These are by definition not coupled to any reservoir state and thus cannot thermalize. We can then intuitively understand that a particle initially in a bound state will remain trapped forever; conversely, if the bound state is initially empty, there is no possibility for a particle to occupy it. Whether a bound state is initially occupied or not depends on the overlap between this state and the discrete level given by Z_b and the initial occupation of the discrete level n_0. Even if this is a quite naive picture, it provides a rather accurate interpretation of the contribution from bound states in equations (4.20) and (4.21).

However, it can be difficult to perform a coupling quench in a realistic experiment

and an opposite situation where level-reservoir coupling is adiabatically turned on is then often considered. In this case, the coupling is increased at a pace slower than any other time scale in the problem such that the system is assumed to be in a steady state at any time. Hence, every state has infinite time to relax and reach thermal occupation. In principle, this type of preparation cannot be studied with the formalism developed in this study. However, we will show that one can actually reproduce the effects of adiabatic preparation in the case of a quench.

As explained above, a state thermalizes only if it is coupled to a reservoir state in the framework used in this thesis. Thus, we imagine that some underlying mechanism yields an additional coupling between the discrete level and reservoir modes at all energies. This will mimic the adiabatic preparation of the system provided that this additional dissipation process does not introduce a new structure in the spectral density. We thus model this new contribution by adding a constant term proportional to a small parameter η in the spectral densities,[1]

$$\tilde{J}_\alpha(\omega) = J_\alpha(\omega) + \eta\kappa_\alpha \tag{5.1}$$

In the following, we will perform all the calculations with the spectral densities $\tilde{J}_\alpha(\omega)$ and eventually take the limit $\eta \to 0$, thus going back to a situation where the spectral densities are $J_\alpha(\omega)$. We typically imagine that the advent of this new term in the spectral densities accounts for the inevitable inelastic effects occurring in a realistic set-up. These could be taking place "deep" in the reservoirs or in the environment of the level-reservoir system. However, the details of such phenomena are not crucial for the following calculation.

The addition of a small constant to the spectral density prevent it from vanishing. As such, infinite-lifetime bound states do not exist in the framework described above. This is a crucial point as it hints at the fact that persistent oscillations of the occupation or currents may never be observed in a real experiment due to the inelastic effects that any measurement induces (this is addressed with more details in section 7.3.1.2).

This framework described here was developed by Dhar and Sen [44] upon realizing that the dependence on initial occupation and persistent oscillations brought by bound states in the long-time occupation (4.20) remains in equilibrium set-ups. Their goal was thus to cancel these features by ensuring that bound states thermalize the same way continuum states do. To do so, they introduced auxiliary reservoirs which have the same temperatures and chemical potentials as the original reservoirs, but whose band structure is described by a wide-band-limit spectral density. This is equivalent to considering the modified spectral densities $\tilde{J}_\alpha(\omega)$ in equation (5.1). This approach yields convincing results at equilibrium, but, in non-equilibrium situations, we find that the long-time occupation depends on the

[1] In the following, we indicate by a tilde quantities for which spectral densities $\tilde{J}_\alpha(\omega)$ are used.

details of the equilibration process, that is on the κ_α, as shown in equation (5.6) below.

To overcome this issue, Stefanucci [45] advocated using another method, the partition-free approach. In this framework, first introduced by Cini [80], it is assumed that the discrete level and reservoirs are at equilibrium at a single temperature and chemical potential before an external electric is applied at $t = 0$ resulting in a voltage bias between the reservoirs. Consequently, the density matrix at time $t = 0$ cannot be written in the factorized form of equation (2.22). At equilibrium, the partition-free approach yields the expected results at equilibrium and unambiguous results out of equilibrium; it is to note that the occupation and currents can still exhibit persistent oscillations in this last case though. In the following, we will not use the partition-free approach because it fails to describe situations with reservoirs at different temperatures and is thus useless for the analysis of thermoelectric transport.

5.2 Adiabatic occupation

We start with the derivation of the new self-energy $\tilde{\Sigma}(z)$. It is obtained adding the wide-band-limit self-energy given in equation (4.32) to the original self-energy $\Sigma(z)$,

$$\tilde{\Sigma}(x - \mathrm{i}\omega) = \Sigma(x - \mathrm{i}\omega) - \mathrm{i}\pi\eta\kappa\,\mathrm{sgn}(x) \tag{5.2}$$

It is important to note that, as the additional term in the self-energy is purely imaginary, we have $\tilde{\Lambda}(\omega) = \Lambda(\omega)$. Using equation (4.20), it is then straightforward to obtain the long-time occupation,

$$\tilde{n}(t \to \infty) = \int_{-\infty}^{\infty} \mathrm{d}\omega\, \tilde{S}(\omega)\tilde{N}(\omega) \tag{5.3}$$

with

$$\tilde{S}(\omega) = \frac{\tilde{J}(\omega)}{(\omega - \omega_\mathrm{d} - \Lambda(\omega))^2 + \pi^2\tilde{J}(\omega)^2} \tag{5.4}$$

and

$$\tilde{N}(\omega) = \frac{1}{\tilde{J}(\omega)} \sum_\alpha \tilde{J}_\alpha(\omega) n_\alpha(\omega) \tag{5.5}$$

As explained earlier, we will now study this expression in the situation where the additional term in the spectral density becomes vanishingly small. For ω in the continuum, that is $J(\omega) \neq 0$, the limits of $\tilde{N}(\omega)$ and $\tilde{S}(\omega)$ as $\eta \to 0$ are defined unambiguously: we find the usual functions $N(\omega)$ and $S(\omega)$. The case $J(\omega) = 0$ is somewhat subtler. The limit of $\tilde{N}(\omega)$ depends on the details of each individual spectral density through the κ_α [44],

$$N(\omega) = \lim_{\eta\to 0} \tilde{N}(\omega) = \frac{1}{\kappa} \sum_\alpha \kappa_\alpha n_\alpha(\omega) \tag{5.6}$$

As for the local density of states $\tilde{S}(\omega)$, we use the following representation of the Dirac delta function

$$\delta(x) = \frac{1}{\pi} \lim_{\eta \to 0} \frac{\eta}{x^2 + \eta^2} \tag{5.7}$$

such that

$$\lim_{\eta \to 0} \tilde{S}(\omega) = \lim_{\eta \to 0} \frac{\eta}{(\omega - \omega_\mathrm{d} - \Lambda(\omega))^2 + \pi^2 \eta^2} = \delta(\omega - \omega_\mathrm{d} - \Lambda(\omega)) = \sum_b Z_b \delta(\omega - \omega_b) \tag{5.8}$$

Therefore, we obtain the adiabatic occupation

$$n_\mathrm{ad} = \lim_{\eta \to 0} \tilde{n}(t \to \infty) = \int \mathrm{d}\omega \, S(\omega) N(\omega) + \sum_b Z_b N(\omega_b) \tag{5.9}$$

This result is independent of the initial preparation even in a situation with bound states. Furthermore, these seem to have reached thermal equilibrium.

5.3 Adiabatic currents

Similarly to the occupation, we use equation (4.21) to obtain

$$\tilde{j}_\alpha(t \to \infty) = \frac{1}{2\pi} \sum_{\alpha'} \int \mathrm{d}\omega \, \tilde{\mathcal{T}}_{\alpha\alpha'}(\omega)(n_\alpha(\omega) - n_{\alpha'}(\omega)) \tag{5.10}$$

As before, the only subtlety in taking the limit $\eta \to 0$ comes from energies in a band gap. In this case, we have

$$\lim_{\eta \to 0} \tilde{\mathcal{T}}_{\alpha\alpha'}(\omega) = \lim_{\eta \to 0} \frac{4\pi^2 \eta^2 \kappa_\alpha \kappa_{\alpha'}}{(\omega - \omega_\mathrm{d} - \Lambda(\omega))^2 + \pi^2 \eta^2 \kappa^2} = \begin{cases} \dfrac{4\kappa_\alpha \kappa_{\alpha'}}{\kappa^2} & \text{if } \omega = \omega_b \\ 0 & \text{if } \omega \neq \omega_b \end{cases} \tag{5.11}$$

Hence, the transmission vanishes for all energies in the band gaps with the exceptions of the bound state energies ω_b. However, these special points do not contribute to the current. Indeed, the transmission peaks at bound state energies are infinitely narrow and have a finite height, their contributions to the integral in equation (5.10) thus vanish. Conversely, the local density states in equation (5.3) exhibited peaks of infinite height at these points.

In conclusion, the adiabatic currents reduce to the dc part of the long-time currents in equation (4.21),

$$j_\alpha^{(\mathrm{ad})} = \lim_{\eta \to 0} \tilde{j}_\alpha(t \to \infty) = \frac{1}{2\pi} \sum_{\alpha'} \int \mathrm{d}\omega \, \mathcal{T}_{\alpha\alpha'}(\omega)(n_\alpha(\omega) - n_{\alpha'}(\omega)) = j_\alpha^{(\mathrm{dc})} \tag{5.12}$$

5.4 Adiabatic correlations in the discrete level occupation

The framework used here is convenient to study correlations as we start with a situation where there is no bound state. Most of the terms in the general expression (4.30) for the long-time correlation function then vanish and we obtain similar results for bosons (plus sign) and fermions (minus sign),

$$\tilde{G}(\tau) = \int \mathrm{d}\omega\, \tilde{S}(\omega)\tilde{N}(\omega)\mathrm{e}^{\mathrm{i}\omega\tau} \int \mathrm{d}\omega'\, \tilde{S}(\omega')(1 \pm \tilde{N}(\omega'))\mathrm{e}^{-\mathrm{i}\omega'\tau} \tag{5.13}$$

Taking the limit $\eta \to 0$ in the above equation yields

$$\begin{aligned} G_{\mathrm{ad}}(\tau) = \lim_{\eta\to 0} \tilde{G}(\tau) = &\left(\int \mathrm{d}\omega\, S(\omega)N(\omega)\mathrm{e}^{\mathrm{i}\omega\tau} + \sum_b Z_b N(\omega_b)\mathrm{e}^{\mathrm{i}\omega_b\tau} \right) \\ &\times \left(\int \mathrm{d}\omega\, S(\omega)(1 - N(\omega))\mathrm{e}^{-\mathrm{i}\omega\tau} + \sum_b Z_b(1 \pm N(\omega_b))\mathrm{e}^{-\mathrm{i}\omega_b\tau} \right) \end{aligned} \tag{5.14}$$

If we now take the limit of large τ, we find again that the contribution of the continuum eventually vanishes,

$$G_{\mathrm{ad}}(\tau \to \infty) = \sum_{b,b'} Z_b Z_{b'} N(\omega_b)(1 \pm N(\omega_{b'}))\mathrm{e}^{\mathrm{i}\omega_{bb'}\tau} \tag{5.15}$$

Again, we find that all memory of the initial state is lost in the adiabatic case.

Chapter 6

Electron transport close to the band edge of a semiconductor

In this chapter, we consider a single-level quantum dot coupled to two semiconducting electron reservoirs with the same band structure. The dot level is assumed to be close to a band edge in the reservoirs whose spectral density is then phenomenologially described by a power law. In this situation, we show that a bound state exists only if the coupling exceeds a critical value. We analyze the effects of the appearance of this bound state on the properties of system. We particularly focus on transport properties and show that the band-edge transmission exhibits singular behaviour at the critical point. This affects the transport coefficients of the dot: the electrical and thermal conductances are maximal when the coupling is close to its critical value while the Seebeck coefficient abruptly drops at this point. Finally, we show that the critical point defines a sweet spot if the dot operates as a heat engine: One can get much larger power output without a significant decrease in efficiency close to this point.

6.1 General results

6.1.1 The spectrum

Using the general formulae derived in the previous chapter, a wide variety of situations can be studied depending on the density of states of the reservoirs. We will study here the case of a semi-infinite band, and thus a semi-infinite gap. We imagine a set-up where a single-level quantum dot is coupled to two semiconducting electron reservoirs with the dot level close to a band edge. The spectral density is phenomenologically assumed to go like a power law close to the band edge and is regularized with an exponential cut-off at high energies. Introducing the coupling

parameter K, the cut-off frequency ω_c and the spectral exponent s, we then write

$$J(\omega) = K\left(\frac{\omega}{\omega_c}\right)^s \mathrm{e}^{-\omega/\omega_c} \tag{6.1}$$

Without loss of generality, the zero of energy is set at the bottom of the band. This type of band structure can be observed in semiconductors, for example the local density of states at the surface of GaAs corresponds to a spectral of the type of equation (6.1) with $s = 1$ [87]. Similarly shaped density of states also arise in two-dimensional materials such as MoS_2 [88].

The details of the spectral density for each individual density are important only when studying transport properties. Here we will mainly focus on the case of symmetric coupling, namely, the situation where the two reservoirs have the same spectral density. This assumption is justified if the reservoirs are made of the same material and voltages are small. Indeed, electroneutrality imposes that each reservoir's band structure is shifted in energy proportionally to its bias; the assumption of symmetric coupling therefore requires this effect to be negligible, as in the linear response regime for example. Denoting the two reservoirs by L and R, the spectral densities corresponding to symmetric coupling are then given by

$$J_L(\omega) = J_R(\omega) = \frac{K}{2}\left(\frac{\omega}{\omega_c}\right)^s \mathrm{e}^{-\omega/\omega_c} \tag{6.2}$$

The first step of the calculation is the derivation of the self-energy. The integral giving $\Sigma(z)$ in equation (3.15) diverges if $s \leq -1$ which indicates that such spectral densities are unphysical. For $s > -1$, we find

$$\Sigma(z) = -K\Gamma(1+s)\left(-\frac{\mathrm{i}z}{\omega_c}\right)^s \Gamma\left(-s, -\frac{\mathrm{i}z}{\omega_c}\right)\mathrm{e}^{-\mathrm{i}z/\omega_c} \tag{6.3}$$

where $\Gamma(\zeta)$ and $\Gamma(\zeta, w)$ respectively denote the complete and incomplete gamma functions,

$$\Gamma(\zeta) = \int_0^\infty \mathrm{d}x\, x^{\zeta-1}\mathrm{e}^{-x} \tag{6.4}$$

$$\Gamma(\zeta, w) = \int_w^\infty \mathrm{d}x\, x^{\zeta-1}\mathrm{e}^{-x} \tag{6.5}$$

We then obtain the following Lamb shift

$$\Lambda(\omega) = \begin{cases} -K\left(\frac{\omega}{\omega_c}\right)^s \left((-1)^s\Gamma(1+s)\Gamma\left(-s, -\frac{\omega}{\omega_c}\right) + \mathrm{i}\pi\right)\mathrm{e}^{-\omega/\omega_c} & \text{if } \omega > 0 \text{ (band)} \\ -K\Gamma(1+s)\left(-\frac{\omega}{\omega_c}\right)^s \Gamma\left(-s, -\frac{\omega}{\omega_c}\right)\mathrm{e}^{-\omega/\omega_c} & \text{if } \omega < 0 \text{ (gap)} \end{cases} \tag{6.6}$$

We now turn to the study of bound states. These are defined through the solutions of equation (3.23), $\Omega(\omega_b) = 0$ with ω_b in a band gap. As already stated, equation (3.24) shows that there can be at most one bound state per band gap because $\Omega(\omega)$ is a strictly increasing function of ω. Consequently, there is only one potential bound state in the situation at stake here. It exists if $\Omega(\omega \to -\infty) < 0$ and $\Omega(\omega \to 0^-) > 0$. We always have $\Omega(\omega \to -\infty) = -\infty$, so the first criterion is then always fulfilled. On the other hand, equation (6.6) yields

$$\Omega(\omega \to 0^-) = \begin{cases} K\Gamma(s) - \omega_\mathrm{d} & \text{if } s > 0 \\ \infty & \text{if } s \leq 0 \end{cases} \tag{6.7}$$

If ω_d is negative there is always a bound state, but this is obvious because ω_d is in the band gap, so the dot state is energetically forbidden to decay into the reservoirs. We will not consider negative ω_d further hereafter. For positive ω_d, there always exists a bound state in cases where the spectral density diverges ($-1 < s < 0$) or is constant ($s = 0$) at the band edge. Conversely, if the spectral density vanishes at the band edge ($s > 0$), the bound state appears only if the dot-reservoir coupling is strong enough, namely $K > \omega_\mathrm{d}/\Gamma(s)$. In other words, the bound state exists only if the coupling parameter K exceeds the critical value K_b given by [53, 56, 89]

$$K_b = \begin{cases} \dfrac{\omega_\mathrm{d}}{\Gamma(s)} & \text{if } s > 0 \\ 0 & \text{if } -1 < s \leq 0 \end{cases} \tag{6.8}$$

This is shown in figure 6.1.

6.1.2 Steady-state occupation

We start by studying the properties of the dot density matrix in the steady state. It is formally independent of the details of each reservoir's spectral density. As such, it is not crucial to analyze an out-of-equilibrium set-up where reservoirs have different temperatures and voltages. Furthermore, the occupation will not exhibit any oscillation at long times as there is at most one bound state in the situation studied here.

In the case of a quench, the steady-state occupation of the quantum dot is given by [89]

$$n_\mathrm{quench} = \int \mathrm{d}\omega \, \frac{J(\omega)N(\omega)}{(\omega - \omega_\mathrm{d} - \Lambda(\omega))^2 + \pi^2 J(\omega)^2} + Z_b^2 \left(n_0 + \int \mathrm{d}\omega \, \frac{J(\omega)N(\omega)}{(\omega - \omega_b)^2} \right) \tag{6.9}$$

As for adiabatic preparation, we find [89]

$$n_\mathrm{ad} = \int \mathrm{d}\omega \, \frac{J(\omega)N(\omega)}{(\omega - \omega_\mathrm{d} - \Lambda(\omega))^2 + \pi^2 J(\omega)^2} + Z_b N(\omega_b) \tag{6.10}$$

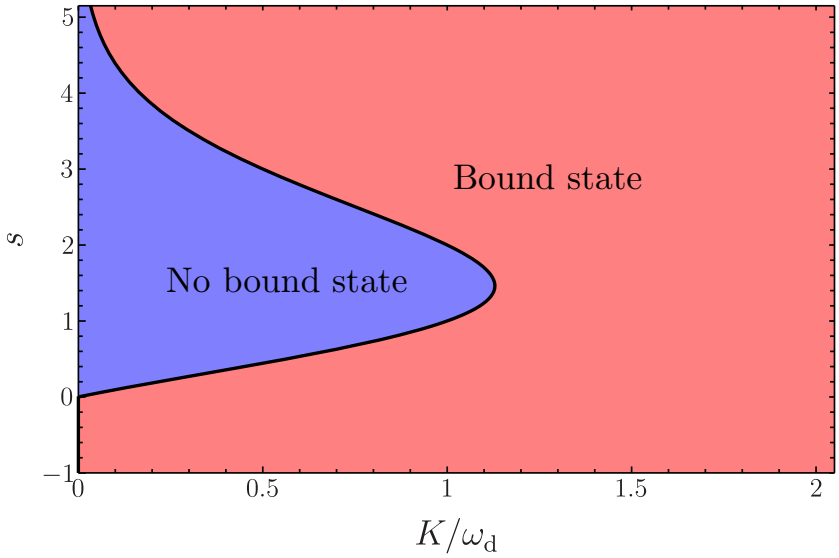

Figure 6.1 – Diagram showing the two possible regimes for a system with a power-law spectral density. For a given spectral exponent s, a bound state appears when the coupling parameter exceeds a critical value K_b (black line).

We see in figure 6.2 that the steady-state occupation is highly influenced by the presence of the bound state in the case of a quench as we can clearly identify two different regimes for $K < K_b$ and $K > K_b$, with a cusp at $K = K_b$. The dependence on the initial occupation for $K > K_b$ is clear. On the contrary, the adiabatic occupation is continuous at critical coupling and independent of the initial preparation.

6.1.3 Current and transmission

As previously stated, the fact that there is at most one bound state in the situation at stake here will prevent any persistent oscillation at long times. Hence, the currents do not depend on the initial preparation and are fully determined by the transmission function given by equation (4.22). Here we study a situation where the quantum dot is coupled to two electron reservoirs, current conservation along with the absence of long-time oscillations then yields

$$j = j_{\mathrm{L}} = -j_{\mathrm{R}} = \frac{1}{2\pi} \int \mathrm{d}\omega \, \mathcal{T}(\omega)(n_{\mathrm{L}}(\omega) - n_{\mathrm{R}}(\omega)) \tag{6.11}$$

As we assume that the dot is symmetrically coupled to the reservoirs, the transmission function is given by

$$\mathcal{T}(\omega) = \frac{\pi^2 J(\omega)^2}{(\omega - \omega_{\mathrm{d}} - \Lambda(\omega))^2 + \pi^2 J(\omega)^2} \tag{6.12}$$

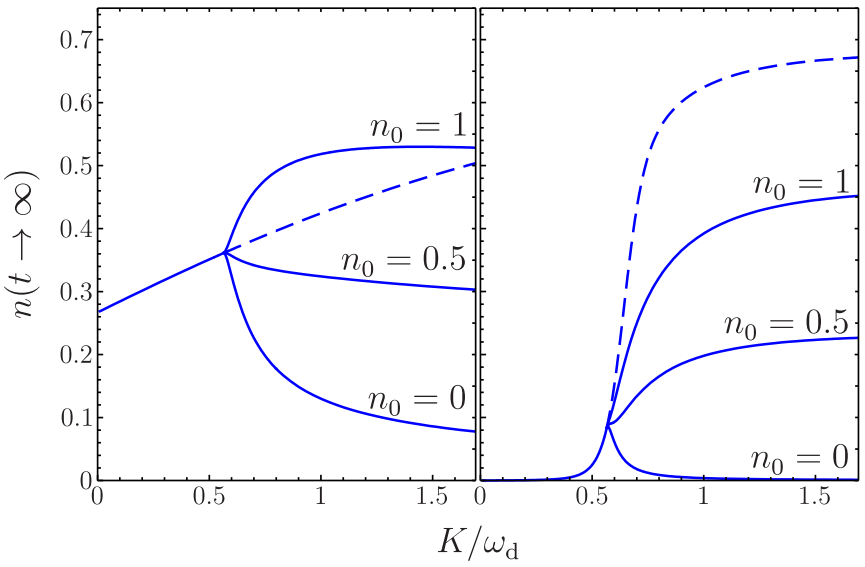

Figure 6.2 – Long-time dot occupation versus the dot-reservoir coupling K. This plot corresponds to the situation where the dot is coupled to the reservoirs with a power-law spectral density with $s = 1/2$ and $\omega_c = 10\omega_d$. The reservoirs have the same temperature, $k_B T = \omega_d$ on the left and $k_B T = 0.03\omega_d$ on the right, and chemical potential, $\mu = -0.01\omega_d$ for both plots. The solid lines representing the long-time occupation after a quench exhibit a clear change of behaviour for $K = K_b \simeq 0.564\omega_d$. For $K > K_b$, the long-time occupation depends on the initial occupation of the dot n_0. The dashed lines correspond to the adiabatic occupation and do not show the transition.

where $J(\omega)$ is the power-law spectral density (6.1).

Contrary to the steady-state occupation given in equations (6.9) and (6.10), the steady-state current in (6.11) does not depend explicitly on the existence of the bound state. However, we show that, due to the Lamb shift $\Lambda(\omega)$, the appearance of the bound state has a strong influence on the transmission [89]. Indeed, in the case of symmetric coupling, one can reach perfect transmission, that is $\mathcal{T}(\omega) = 1$, when $\omega - \omega_d - \Lambda(\omega) = 0$. At very weak coupling this is achieved for $\omega \simeq \omega_d$ since $\Lambda(\omega)$ is proportional to K. We clearly see that in figures 6.3 and 6.4 where the weak-coupling transmission (dark blue lines) exhibits a seemingly Lorentzian behaviour with a peak close to the bare dot energy ω_d. As the coupling increases the peak starts to lose its shape and drifts due to level repulsion.

This effect is encapsulated in $\Lambda(\omega)$ which describes the renormalization of the dot level due to the coupling to the reservoirs. Roughly speaking, if there are more reservoir modes above the dot level than below, the latter will tend to drift towards the band edge with the possibility of leaving the continuum when the coupling is

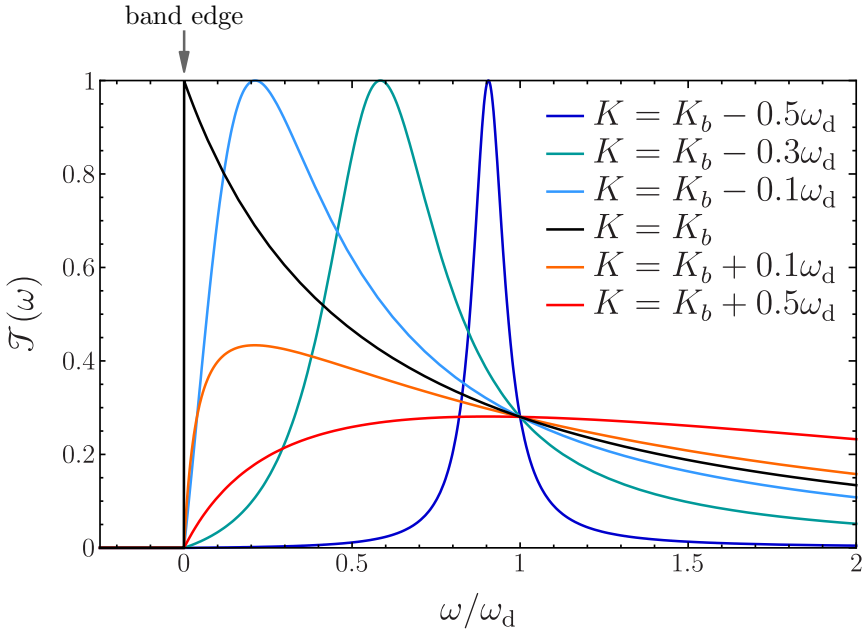

Figure 6.3 – Transmission as a function of energy for various values of the coupling parameter K when the spectal density vanishes at the band edge; it is given by a power law with $s = 1/2$ and $\omega_{\rm c} = 10\omega_{\rm d}$. For K much less than K_b (blue lines), the transmission function is a Lorentzian at the dot level. It then loses its shape and drifts towards the origin as the coupling increases up to its critical value (black line). When K exceeds K_b (orange lines), the transmission function becomes much flatter.

strong enough. This leads to the appearance of a bound state. This is basically what is shown in figure 6.3 where the spectral density has been chosen such that its maximum is above the dot energy level. The perfectly transmitting state, initially very close to the dot level, goes towards the band edge as the coupling is increased. At critical coupling, the peak is lying precisely on the band edge. Then, if the coupling exceeds its critical value, the transmission function is much flatter as the resonance in the continuum has become a bound state outside the continuum. On the contrary, if there are more reservoir modes below the dot level than above, the latter will be pushed towards the depth of the continuum. Consequently, a transmission peak exists for all values of the coupling parameter. This is what we can see in figure 6.4 where we have chosen a spectral density with a singularity at the band edge.

However, not all the properties of the system can be described solely by the influence of the Lamb shift. For example, the transmission function in figure 6.4 features a peak at the band edge for all values of the coupling parameter. We

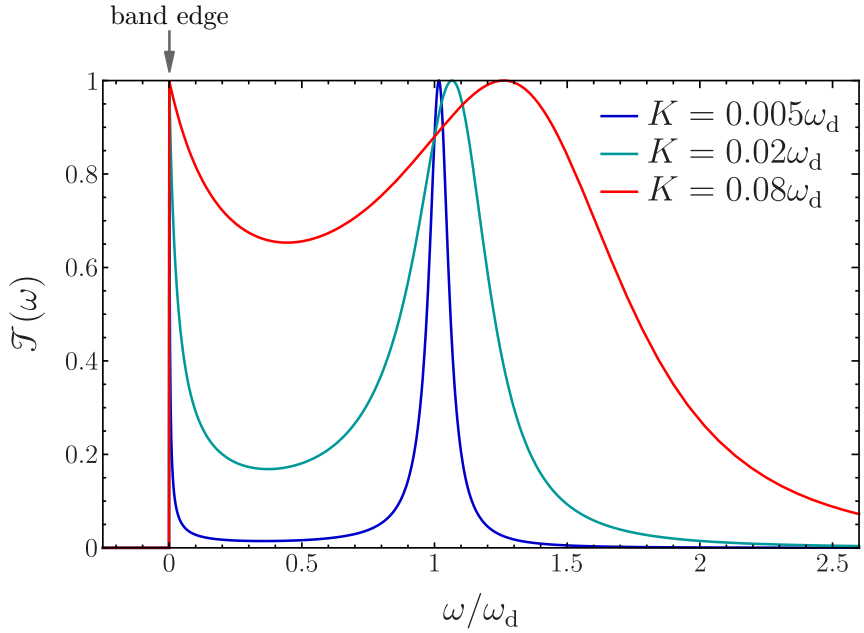

Figure 6.4 – Transmission as a function of energy for various values of the coupling parameter K when the spectral density diverges at the band edge; it is given by a power law with $s = -1/2$ and $\omega_c = 10\omega_d$. The divergence of the spectral density at the band edge gives rise to a peak at the band edge irrespective of the value of the coupling. At weak coupling, the transmission looks like a Lorentzian at the dot level, with an additional peak at the band edge.

will show later (see section 6.2.3) that this peak is not linked to a resonance of the renormalized dot level. It is instead due to the fact that both the numerator and the denominator in equation (6.12) vanish at the band edge. The competition between these two terms yields a peak of finite transmission at the band edge irrespective of the value of the coupling parameter. Moreover, we have shown that there is a bound state at arbitrarily weak coupling in the case of a diverging spectral density. Contrary to the case of figure 6.3, we cannot really interpret it as a resonance pushed outside the continuum. It rather seems to be linked to the divergence of the spectral density similarly to the transmission peak at the band edge [60].

This shows that the intuitive picture based on the displacement of the dot level due to the Lamb shift does not usually suffice to account accurately for the properties of the system. In the case of figure 6.4, such description fails because of a divergence in the spectral density but various situations can give rise to a strongly nonlinear Lamb shift causing such breakdown. One may for example think of a situation with several band gaps possibly giving rise to multiple bound states. How a single dot level may split into several bound states cannot be explained with the naive

arguments given above (see chapter 7).

6.2 Scaling close to the critical point

In order to precisely understand the change of behaviour of the system when the coupling reaches its critical value, we will now study in details some properties of the system close to the critical point.

6.2.1 Bound state energy

We first examine the bound state energy ω_b in the limit $K \to K_b^+$. First, we consider the case of a spectral density vanishing at the band edge, that is $s > 0$. Using equation (6.7), we find $\Omega(\omega \to 0^-) = 0$ at $K = K_b$. As ω_b is defined as the unique solution to $\Omega(\omega) = 0$, we deduce that $\omega_b \to 0^-$ when $K \to K_b^+$.

This last result also holds in the case of a non-vanishing spectral density. We prove this by contradiction (reductio ad absurdum). Hence, we assume that ω_b takes a finite (negative) value as K approaches K_b. For $s \leq 0$, $K_b = 0$, therefore, $\Lambda(\omega_b)$ vanishes in the limit $K \to K_b^+$ because $\Lambda(\omega)$ is proportional to K. We consequently find $\Omega(\omega) \simeq \omega - \omega_\mathrm{d}$, that is $\omega_b \simeq \omega_\mathrm{d}$ for $K \to K_b^+$. As we consider the situation where $\omega_\mathrm{d} > 0$, this is in contradiction with the fact that ω_b should be negative.

We thus conclude that the bound state energy always vanishes when the coupling parameter approaches its critical value, $\omega_b \to 0$ for $K \to K_b^+$. Hence, in order to obtain an estimate of ω_b close to the critical point $K = K_b$, we solve the equation $\Omega(\omega_b) = 0$ using an approximate expression of $\Omega(\omega)$ for $\omega \to 0^-$.

For $\omega < 0$, equation (6.6) yields

$$\Omega(\omega) = \omega - \omega_\mathrm{d} - \Lambda(\omega) = \omega - \omega_\mathrm{d} + K\Gamma(1+s)\left(-\frac{\omega}{\omega_\mathrm{c}}\right)^s \Gamma\left(-s, -\frac{\omega}{\omega_\mathrm{c}}\right)\mathrm{e}^{-\omega/\omega_\mathrm{c}} \quad (6.13)$$

We then see that the main difficulty in order to infer the leading behaviour of $\Omega(\omega \to 0^-)$ is the study of $\Gamma(-s, w)$ for $w \to 0^+$. We have

$$w^s\Gamma(-s,w) = \begin{cases} w^s\Gamma(-s) + \displaystyle\sum_{k=0}^{\infty} \frac{(-w)^k}{k!(s-k)} & \text{if } s \notin \mathbb{N} \\ \dfrac{(-w)^s}{\Gamma(1+s)}(h_s - \gamma - \ln w) + \displaystyle\sum_{\substack{k=0 \\ k\neq s}}^{\infty} \frac{(-w)^k}{k!\,(s-k)} & \text{if } s \in \mathbb{N} \end{cases} \quad (6.14)$$

where the case of integer s features the Euler constant γ and the s-th hamonic number

$$h_s = \sum_{k=1}^{s} \frac{1}{k} \quad (6.15)$$

From equation (6.14), we see that the leading-order terms of $w^s\Gamma(-s,w)$ for $w \to 0^+$ differ for $s < 1$ and $s > 1$ depending on whether or not w^s dominates over w. For completeness, it is also important to treat the cases $s = 0$ and $s = 1$ separately.

- **Bound state energy for** $0 < |s| < 1$

  If $0 < |s| < 1$, w^s dominates over w, and equation (6.14) gives

$$w^s\Gamma(-s,w) \underset{w\to 0^+}{\simeq} \frac{1}{s} + w^s\Gamma(-s) \tag{6.16}$$

Expanding all the other terms in $\Omega(\omega)$ to order s then yields

$$\Omega(\omega) \underset{\omega\to 0^-}{\simeq} -\omega_\mathrm{d} + K\Gamma(s) - \frac{\pi K}{\sin(\pi s)}\left(-\frac{\omega}{\omega_\mathrm{c}}\right)^s \tag{6.17}$$

We now solve $\Omega(\omega_b) = 0$ using the above approximation to obtain

$$\omega_b \underset{K\to K_b^+}{\simeq} -\omega_\mathrm{c}\left(\frac{\sin(\pi s)}{\pi K}(K\Gamma(s) - \omega_\mathrm{d})\right)^{1/s} = -\omega_\mathrm{c}\left(\frac{\Gamma(s)\sin(\pi s)}{\pi K}\right)^{1/s}(K - K_b)^{1/s} \tag{6.18}$$

- **Bound state energy for** $s > 1$

  If $s > 1$, the w dominates over w^s, and equation (6.14) gives[1]

$$w^s\Gamma(-s,w) \underset{w\to 0^+}{\simeq} \frac{1}{s} - \frac{w}{s-1} \tag{6.19}$$

We then expand $\Omega(\omega)$ keeping all terms of order ω to find

$$\Omega(\omega) \underset{\omega\to 0^-}{\simeq} \omega - \omega_\mathrm{d} + K\Gamma(s) + K\Gamma(s-1)\frac{\omega}{\omega_\mathrm{c}} \tag{6.20}$$

We then find

$$\omega_b \underset{K\to K_b^+}{\simeq} -\frac{\omega_\mathrm{c}(K\Gamma(s) - \omega_\mathrm{d})}{\omega_\mathrm{c} + K\Gamma(1-s)} = -\frac{\omega_\mathrm{c}\Gamma(s)(K - K_b)}{\omega_\mathrm{c} + K\Gamma(1-s)} \tag{6.21}$$

- **Bound state energy for** $s = 0$

For completeness, we have to address some peculiar cases where s is integer. We start with $s = 0$. Equation (6.14) here yields

$$w^s\Gamma(-s,w) \underset{w\to 0^+}{\simeq} -\gamma - \ln w \tag{6.22}$$

[1]The cases $s \notin \mathbb{N}$ and $s \in \mathbb{N}$ give the same result if we stick to next-to-leading order terms.

$\Omega(\omega)$ is then approximated as follows

$$\Omega(\omega) \underset{\omega\to 0^-}{\simeq} -\omega_\mathrm{d} - \gamma K - K\ln\left(-\frac{\omega}{\omega_\mathrm{c}}\right) \tag{6.23}$$

We consequently obtain

$$\omega_b \underset{K\to K_b^+}{\simeq} -\omega_\mathrm{c}\mathrm{e}^{-\left(\gamma+\frac{\omega_\mathrm{d}}{K}\right)} \tag{6.24}$$

- **Bound state energy for $s = 1$**

  The last case to treat is $s = 1$. Using equation (6.14) we find

$$w^s\Gamma(-s,w) \underset{w\to 0^+}{\simeq} 1 - w(1-\gamma-\ln w) \tag{6.25}$$

The expansion of $\Omega(\omega)$ then reads

$$\Omega(\omega) \underset{\omega\to 0^-}{\simeq} \omega - \omega_\mathrm{d} + K + K\left(1-\gamma-\ln\left(-\frac{\omega}{\omega_\mathrm{c}}\right)\right)\frac{\omega}{\omega_\mathrm{c}} \tag{6.26}$$

Solving $\Omega(\omega_b) = 0$ is not straightforward here. One eventually finds

$$\omega_b \underset{K\to K_b^+}{\simeq} -\omega_\mathrm{c}\left(\frac{\omega_\mathrm{d}}{K}-1\right)\Big/W\left(\left(\frac{\omega_\mathrm{d}}{K}-1\right)\mathrm{e}^{\gamma-\frac{\omega_\mathrm{c}}{K}}\right) \tag{6.27}$$

where $W(w)$ denotes the lower branch of the Lambert function.

6.2.2 Overlap of the bound state with the dot level

Now that the behaviour of the bound state energy close to the critical point is known, we estimate the overlap Z_b between the bound state and the bare dot level. This is of fundamental importance as this quantity appears explicitly influences the steady-state dot occupation. It is defined in equation (3.26),

$$Z_b = \frac{1}{1-\Lambda'(\omega_b)} \tag{6.28}$$

The derivative of $\Lambda(\omega)$ for $\omega < 0$ is deduced from equation (6.6),

$$\Lambda'(\omega) = \frac{K\Gamma(1+s)}{\omega}\left(1+\left(\frac{\omega}{\omega_\mathrm{c}}-s\right)\left(-\frac{\omega}{\omega_\mathrm{c}}\right)^s\Gamma\left(-s,-\frac{\omega}{\omega_\mathrm{c}}\right)\mathrm{e}^{-\omega/\omega_\mathrm{c}}\right) \tag{6.29}$$

As $\omega_b \to 0^-$ for $K \to K_b^+$, we have to estimate $\Lambda'(\omega \to 0^-)$ in order to find the behaviour of Z_b close to the critical point. As before, we obtain different results depending on the value of the spectral exponent s.

- **Dot overlap for** $0 < |s| < 1$

  For $0 < |s| < 1$, we find

$$\Lambda'(\omega) \underset{\omega\to 0^-}{\simeq} -\frac{\pi s K}{\omega_c \sin(\pi s)}\left(-\frac{\omega}{\omega_c}\right)^{s-1} \tag{6.30}$$

$\Lambda'(\omega)$ thus behaves like ω^{s-1} for $\omega \to 0^-$. As $s < 1$, it means that $\Lambda'(\omega)$ diverges in this limit. Therefore, we can approximate Z_b as follows $Z_b \simeq -1/\Lambda'(\omega_b)$. Using the estimate of ω_b in equation (6.18), we obtain

$$Z_b \underset{K\to K_b^+}{\simeq} \begin{cases} \dfrac{\omega_c}{s}\left(\dfrac{\sin(\pi s)}{\pi K}\right)^{\frac{1}{s}} (K\Gamma(s) - \omega_d)^{\frac{1-s}{s}} & \text{if } 0 < s < 1 \\ -\dfrac{\omega_c}{s}\left(-\dfrac{\sin(\pi s)}{\pi K}\right)^{\frac{1}{s}} (\omega_d - K\Gamma(s))^{\frac{1-s}{s}} & \text{if } -1 < s < 0 \end{cases} \tag{6.31}$$

Here it has been necessary to distinguish between the cases with positive s and negative s as the above expression involves raising negative numbers to non-integer powers if s is negative.

- **Dot overlap for** $s > 1$

  If $s > 1$, $\Lambda'(\omega)$ takes a constant value for $\omega \to 0^-$,

$$\Lambda'(\omega) \underset{\omega\to 0^-}{\simeq} -\frac{K\Gamma(s-1)}{\omega_c} \tag{6.32}$$

This directly yields

$$Z_b \underset{K\to K_b^+}{\simeq} \left(1 + \frac{K\Gamma(s-1)}{\omega_c}\right)^{-1} = \frac{\omega_c}{\omega_c + K\Gamma(s-1)} \tag{6.33}$$

- **Dot overlap for** $s = 0$

As before, cases with s integer have be treated separately. We start with $s = 0$. We find

$$\Lambda'(\omega) \underset{\omega\to 0^-}{\simeq} \frac{K}{\omega} \tag{6.34}$$

Similarly to the case $0 < |s| < 1$, $\Lambda'(\omega)$ diverges for $\omega \to 0^-$. As such, Z_b reads $Z_b \simeq -1/\Lambda'(\omega_b)$. Using the approximate expression in (6.24), we then obtain

$$Z_b \underset{K\to K_b^+}{\simeq} \frac{\omega_c}{K} \mathrm{e}^{-\left(\gamma + \frac{\omega_d}{K}\right)} \tag{6.35}$$

- **Dot overlap for $s = 1$**

The final case is $s = 1$. We have

$$\Lambda'(\omega) \underset{\omega\to 0^-}{\simeq} \frac{K}{\omega_\mathrm{c}}\left(1+\gamma+\ln\left(-\frac{\omega}{\omega_\mathrm{c}}\right)\right) \tag{6.36}$$

Using equation (6.27), we eventually find

$$Z_b \underset{K\to K_b^+}{\simeq} \left(1-\frac{(1+\gamma)K}{\omega_\mathrm{c}}+\frac{K}{\omega_\mathrm{c}}\ln\left(\frac{W\left((\omega_\mathrm{d}/K-1)\mathrm{e}^{\gamma-\frac{\omega_\mathrm{c}}{K}}\right)}{\omega_\mathrm{d}/K-1}\right)\right)^{-1} \tag{6.37}$$

- **Value at critical coupling**

It is interesting to note that the expressions derived above enable us to infer the formal limit of Z_b for $K \to K_b^+$, that is the value of the overlap between the bound state and the dot level at the critical point. All in all, we find

$$\lim_{K\to K_b^+} Z_b = \begin{cases} 0 & \text{if } -1 < s \leq 1 \\ \left(1+\dfrac{\omega_\mathrm{d}}{(s-1)\omega_\mathrm{c}}\right)^{-1} & \text{if } s > 1 \end{cases} \tag{6.38}$$

Z_b takes a finite value at the critical point if $s > 1$ whereas it vanishes in any other case hinting at a much abrupter transition.

6.2.3 Transmission function

Even though the transmission function does not depend explicitly on the existence of the bound state here, its features at the band edge seem closely related to the latter as seen in figures 6.3 and 6.4. To have a better understanding of this connection, it is then necessary to thoroughly study the behaviour of $\mathcal{T}(\omega)$ for $\omega \to 0^+$. To do so, we write the transmission function as follows

$$\mathcal{T}(\omega) = \frac{\pi^2 J(\omega)^2}{(\omega-\omega_\mathrm{d}-\Lambda(\omega))^2+\pi^2 J(\omega)^2} = \frac{1}{1+t(\omega)^2} \tag{6.39}$$

with

$$t(\omega) = \frac{\omega-\omega_\mathrm{d}-\Lambda(\omega)}{\pi J(\omega)} = \frac{\omega-\omega_\mathrm{d}}{\pi K}\left(\frac{\omega}{\omega_\mathrm{c}}\right)^{-s}\mathrm{e}^{-\omega/\omega_\mathrm{c}} + \left(\frac{(-1)^s}{\pi}\Gamma(1+s)\Gamma\left(-s,-\frac{\omega}{\omega_\mathrm{c}}\right)+\mathrm{i}\right) \tag{6.40}$$

We can perform the expansion of $t(\omega)$ for $\omega \to 0^+$. As before, different cases have to be taken into account depending on whether or not s is integer.

- **Band-edge transmission for $s \notin \mathbb{N}$**

In the general case, $t(\omega)$ is expanded as follows

$$t(\omega) = \frac{K\Gamma(s) - \omega_\mathrm{d}}{\pi K}\left(\frac{\omega}{\omega_\mathrm{c}}\right)^{-s} - \cot(\pi s) + \frac{1}{\pi K}\sum_{k=1}^{\infty}\left(\frac{1}{k!}\left(\frac{K\Gamma(1+s)}{s-k} - \omega_\mathrm{d}\right) + \frac{\omega_\mathrm{c}}{(k-1)!}\right)\left(\frac{\omega}{\omega_\mathrm{c}}\right)^{k-s} \tag{6.41}$$

The leading-order term for $\omega \to 0^+$ is then easily read

$$t(\omega) \underset{\omega\to 0^+}{\simeq} \begin{cases} -\cot(\pi s) & \text{if } -1 < s < 0 \text{ and } s \neq -\dfrac{1}{2} \\ \dfrac{K - K_b}{\pi K\Gamma(s)}\left(\dfrac{\omega}{\omega_\mathrm{c}}\right)^{-s} & \text{if } s > 0 \text{ or } s = -\dfrac{1}{2} \end{cases} \tag{6.42}$$

In the case of a diverging spectral density ($s < 0$), we see from equation (6.42) that the transmission function takes a finite value at the band edge. We find

$$\mathcal{T}(\omega) \underset{\omega\to 0^+}{\simeq} \sin^2(\pi s) \tag{6.43}$$

Conversely, in the case of a vanishing spectral density ($s > 0$), equation (6.42) yields

$$\mathcal{T}(\omega) \underset{\omega\to 0^+}{\simeq} \frac{\pi^2 K^2 \Gamma(s)^2}{(K - K_b)^2}\left(\frac{\omega}{\omega_\mathrm{c}}\right)^{2s} \tag{6.44}$$

The above expression is not valid at critical coupling as the leading-order term of $t(\omega)$ given in equation (6.42) vanishes if $K\Gamma(s) = \omega_\mathrm{d}$, that is if $K = K_b$. We then have to consider the next-to-leading term in the expansion (6.41) of $t(\omega)$. Again, there are two different possibilities depending on the value of s,

$$t(\omega)\Big|_{K=K_b} \underset{\omega\to 0^+}{\simeq} \begin{cases} -\cot(\pi s) & \text{if } 0 < s < 1 \text{ and } s \neq \dfrac{1}{2} \\ \dfrac{\Gamma(s)}{\pi}\left(\dfrac{1}{s-1} + \dfrac{\omega_\mathrm{c}}{\omega_\mathrm{d}}\right)\left(\dfrac{\omega}{\omega_\mathrm{c}}\right)^{1-s} & \text{if } s > 1 \text{ or } s = \dfrac{1}{2} \end{cases} \tag{6.45}$$

This finally yields

$$\mathcal{T}(\omega)\Big|_{K=K_b} \underset{\omega\to 0^+}{\simeq} \begin{cases} \sin^2(\pi s) & \text{if } 0 < s < 1 \\ \dfrac{\pi^2\omega_\mathrm{d}^2}{\Gamma(s-1)^2(\omega_\mathrm{d} + (s-1)\omega_\mathrm{c})^2}\left(\dfrac{\omega}{\omega_\mathrm{c}}\right)^{2(s-1)} & \text{if } s > 1 \end{cases} \tag{6.46}$$

- **Band-edge transmission for $s \in \mathbb{N}$**

As before, the cases where s is integer have to be considered separately. Moreover, the case $s = 0$ also needs a special treatment here. Indeed, for $s \in \mathbb{N}$ but $s \neq 0$ we have

$$t(\omega) = \frac{K\Gamma(s) - \omega_\mathrm{d}}{\pi K}\left(\frac{\omega}{\omega_\mathrm{c}}\right)^{-s} - \frac{1}{\pi}\left(\gamma - h_s - \frac{s\omega_\mathrm{c} - \omega_\mathrm{d}}{K\Gamma(1+s)} + \ln\left(\frac{\omega}{\omega_\mathrm{c}}\right)\right) + \frac{1}{\pi K}\sum_{\substack{k=1 \\ k\neq s}}^{\infty}\left(\frac{1}{k!}\left(\frac{K\Gamma(1+s)}{s-k} - \omega_\mathrm{d}\right) + \frac{\omega_\mathrm{c}}{(k-1)!}\right)\left(\frac{\omega}{\omega_\mathrm{c}}\right)^{k-s} \tag{6.47}$$

Even if the above expansion differs from equation (6.41) in general, this difference does not lie in the leading-order term for $\omega \to 0^+$. As such, the behaviour of the transmission at the band edge is generally given by equation (6.44). This is no longer valid at the critical point. As before, the next-to-leading order term in expansion (6.47) has to be considered in this case. There is only one case where the discrepancies between equations (6.41) and (6.47) can be seen at next-to-leading order: $s = 1$. In this situation, we have

$$t(\omega)\Big|_{K=K_b} \underset{\omega\to 0^+}{\simeq} -\frac{1}{\pi}\left(\gamma - \frac{\omega_\mathrm{c}}{\omega_\mathrm{d}} + \ln\left(\frac{\omega}{\omega_\mathrm{c}}\right)\right) \tag{6.48}$$

This yields

$$\mathcal{T}(\omega)\Big|_{K=K_b} \underset{\omega\to 0^+}{\simeq} \left(1 + \frac{1}{\pi^2}\left(\gamma - \frac{\omega_\mathrm{c}}{\omega_\mathrm{d}} + \ln\left(\frac{\omega}{\omega_\mathrm{c}}\right)\right)^2\right)^{-1} \tag{6.49}$$

For completeness, we finally treat the case $s = 0$. We have

$$t(\omega) = -\frac{1}{\pi}\left(\gamma + \frac{\omega_\mathrm{d}}{K} + \ln\left(\frac{\omega}{\omega_\mathrm{c}}\right)\right) + \frac{1}{\pi K}\sum_{k=1}^{\infty}\left(\frac{\omega_\mathrm{c}}{(k-1)!} - \frac{1}{k!}\left(\omega_\mathrm{d} + \frac{K}{k}\right)\right)\left(\frac{\omega}{\omega_\mathrm{c}}\right)^{k} \tag{6.50}$$

The transmission function consequently reads

$$\mathcal{T}(\omega) \underset{\omega\to 0^+}{\simeq} \left(1 + \frac{1}{\pi^2}\left(\gamma + \frac{\omega_\mathrm{d}}{K} + \ln\left(\frac{\omega}{\omega_\mathrm{c}}\right)\right)^2\right)^{-1} \tag{6.51}$$

- **Summary of band-edge transmission**

To summarize, we have shown that the behaviour of the transmission function at the band edge strongly depends on the value of the spectral exponent s. In the

general case, we find

$$\mathcal{T}(\omega) \underset{\omega\to 0^+}{\simeq} \begin{cases} \sin^2(\pi s) & \text{if } -1 < s < 0 \\ \left(1 + \frac{1}{\pi^2}\left(\gamma + \frac{\omega_\mathrm{d}}{K} + \ln\left(\frac{\omega}{\omega_\mathrm{c}}\right)\right)^2\right)^{-1} & \text{if } s = 0 \\ \frac{\pi^2 K^2 \Gamma(s)^2}{(K-K_b)^2}\left(\frac{\omega}{\omega_\mathrm{c}}\right)^{2s} & \text{if } s > 0 \end{cases} \tag{6.52}$$

However, if $s > 0$, this estimate is not valid at the critical point. We instead have

$$\mathcal{T}(\omega)\Big|_{K=K_b} \underset{\omega\to 0^+}{\simeq} \begin{cases} \sin^2(\pi s) & \text{if } 0 < s < 1 \\ \left(1 + \frac{1}{\pi^2}\left(\gamma - \frac{\omega_\mathrm{c}}{\omega_\mathrm{d}} + \ln\left(\frac{\omega}{\omega_\mathrm{c}}\right)\right)^2\right)^{-1} & \text{if } s = 1 \\ \frac{\pi^2 \omega_\mathrm{d}^2}{\Gamma(s-1)^2(\omega_\mathrm{d} + (s-1)\omega_\mathrm{c})^2}\left(\frac{\omega}{\omega_\mathrm{c}}\right)^{2(s-1)} & \text{if } s > 1 \end{cases} \tag{6.53}$$

This shows that the behaviour at the band edge is completely different at critical coupling than at any other coupling. For example, for $s = 1/2$ we see that the transmission vanishes at the band edge for all coupling K except the critical coupling K_b; in contrast, we have perfect transmission at the band edge, $\mathcal{T}(\omega \to 0^+) = 1$, at exactly $K = K_b$. Such singular behaviour at critical coupling highlights the influence of the transition to the bound state on the transport properties of the system.

6.3 Transport properties

We have just seen that the appearance of the bound state in the gap is related to a change of behaviour of the transmission function close to the band edge. However, transmission is usually not an observable quantity. It is then necessary to understand how this change in the transmission will influence the transport properties of the system. To do so, we will infer the thermoelectric response of the system with the tools introduced in section 2.1.2 using the exact transmission function (6.12). We stick to the regime of linear response as the assumption of symmetric coupling is not consistent with a large bias voltage between the two leads. It is however compatible with the regime of linear response as one can show that there is no correction to the transmission function at first order in voltage.

We focus here on the case of $s = 1/2$ (shown in figure 6.3) to highlight the changes induced by the appearance of the bound state at the critical point [89]. Transport coefficients are deduced from the integrals ι_n given in equation (2.14). Roughly speaking, the function $\Phi(\omega)$ featuring in these integrals and defined in

equation (2.11) describes an energy filter centred on the chemical potential μ and of width $k_{\mathrm{B}}T$. Hence, as we intend to study the changes in the transmission at the band edge, we analyze cases where the chemical potential lies in the band gap with the temperature chosen accordingly: we take $\mu < 0$ and $T \simeq -\mu/k_{\mathrm{B}}$.

The electrical and thermal conductances are given in figures 6.5 and 6.6 respectively. We clearly see that these conductances exhibit abrupt peaks close to the critical point. The electrical conductance being simply proportional to ι_0, we can then relate this peak to the "accumulation" of the transmission at the band edge as the coupling approaches its critical value. However, the connection between the properties of the transmission and the behaviour of transport coefficients is not always automatic. For example, we observe a peak close to the critical point in the thermal conductance whose precise origin is not clear as various factors compete with each other here. Conversely, such competition leads to different features for the Seebeck coefficient displayed in figure 6.7 which exhibits a sharp drop at the critical point.

These transport coefficients then enable us to study the thermodynamic properties of the device as explained in section 1.3.2. In figure 6.8, we see that the power factor GS^2 also features a peak close to the critical point. Hence, contrary to what one could naively think, strong coupling does not always mean larger power output. Here, it is useless to go above critical coupling if one hopes for high power generation. It is also interesting to note that the height and centre of the peaks in the power factor do not depend much on the value of the chemical potential.

As for the efficiency of the thermoelectric, the figure of merit ZT is displayed in figure 6.9. At low coupling, the figure of merit increases with coupling but then drops sharply at the critical point. At strong coupling, it does not exhibit any significant variation. Note that ZT goes to infinity at zero coupling but this divergence takes place on a very small coupling scale which makes it invisible in figure 6.9.

The thermodynamic behaviour of the device is summarized in figure 6.10. It displays the efficiency of the thermoelectric versus its power ouput for various values of the coupling parameter. In agreement with the results of figures 6.8 and 6.9, we see that the maximum efficiency does not vary much with coupling contrary to the maximum power output. The device can generate much more power close to the critical point without impacting its efficiency. This is a strong incentive to operate the device close the critical point rather than in the regime of strong coupling for optimal thermodynamic response.

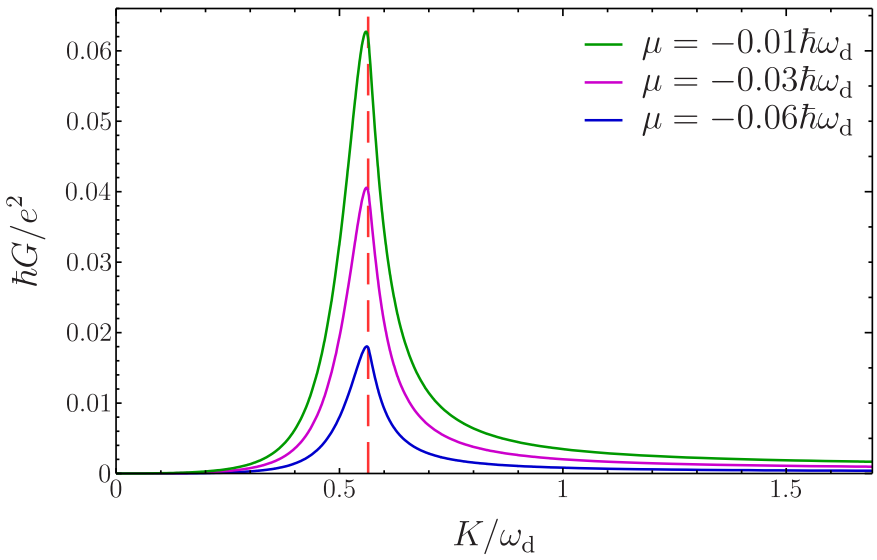

Figure 6.5 – Electrical conductance G (in dimensionless units) versus coupling K for different values of the chemical potential when the spectral density is a power law with $s = 1/2$. Other parameters are $\omega_\mathrm{c} = 10\omega_\mathrm{d}$ and $T = 0.03\omega_\mathrm{d}/k_\mathrm{B}$. The dashed vertical line indicates the critical coupling.

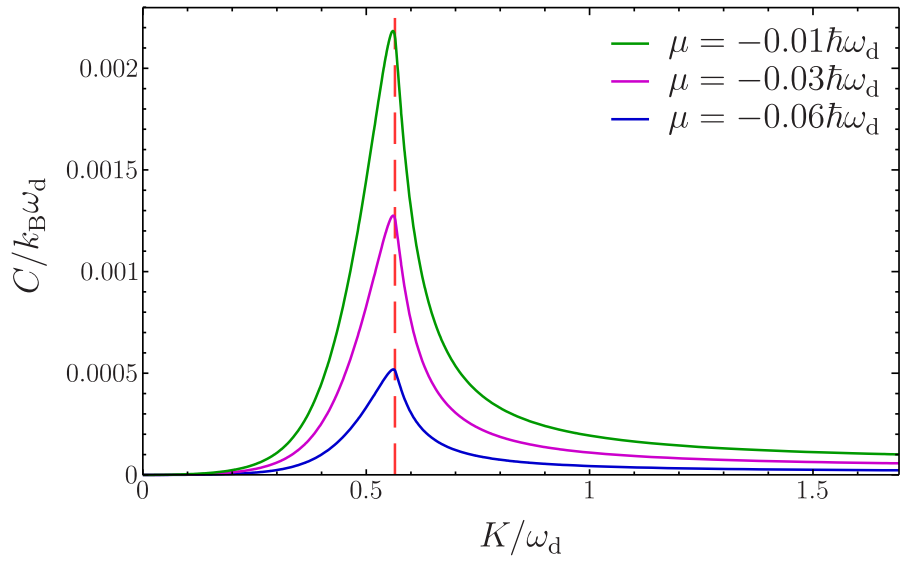

Figure 6.6 – Thermal conductance C (in dimensionless units) versus coupling K for different values of the chemical potential when the spectral density is a power law with $s = 1/2$. Other parameters are $\omega_\mathrm{c} = 10\omega_\mathrm{d}$ and $T = 0.03\omega_\mathrm{d}/k_\mathrm{B}$. The dashed vertical line indicates the critical coupling.

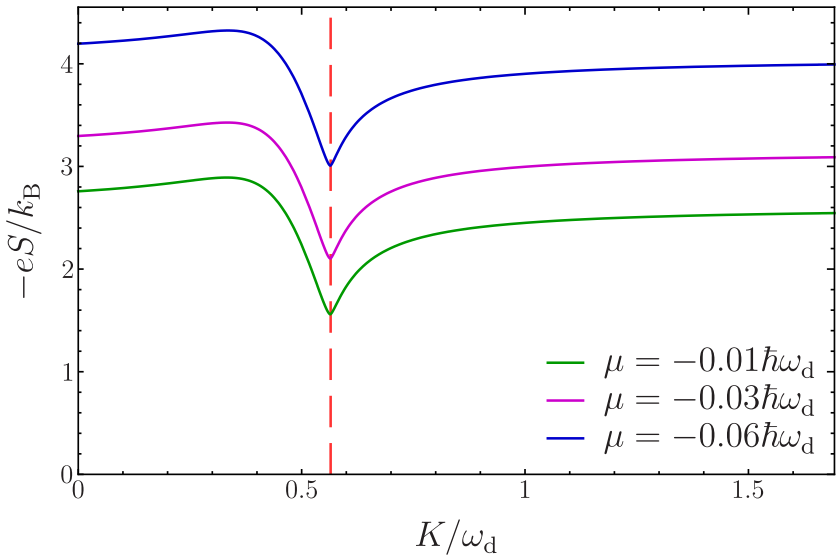

Figure 6.7 – Seebeck coefficient S (in dimensionless units) versus coupling K for different values of the chemical potential when the spectral density is a power law with $s = 1/2$. Other parameters are $\omega_c = 10\omega_d$ and $T = 0.03\omega_d/k_B$. The dashed vertical line indicates the critical coupling.

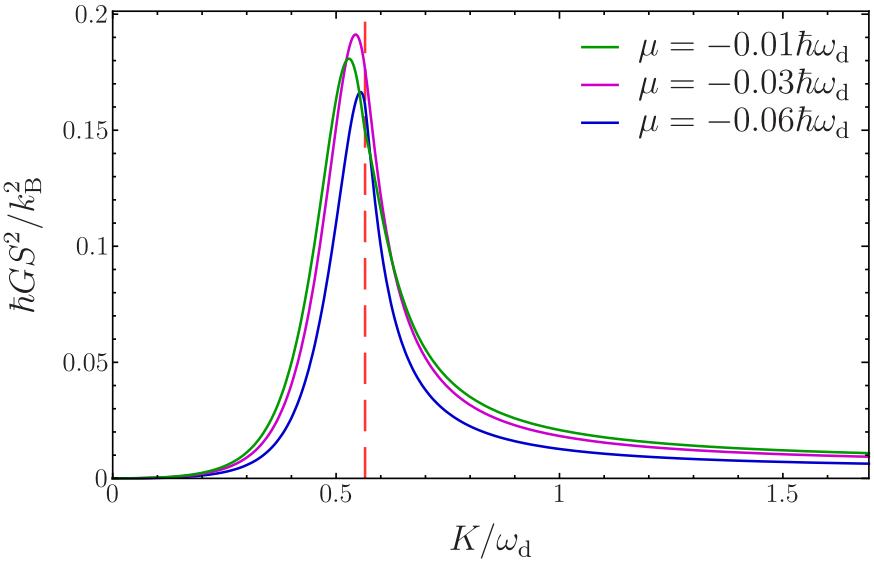

Figure 6.8 – Thermoelectric power factor GS^2 (in dimensionless units) versus coupling K for different values of the chemical potential when the spectral density is a power law with $s = 1/2$. Other parameters are $\omega_c = 10\omega_d$ and $T = 0.03\omega_d/k_B$. The dashed vertical line indicates the critical coupling.

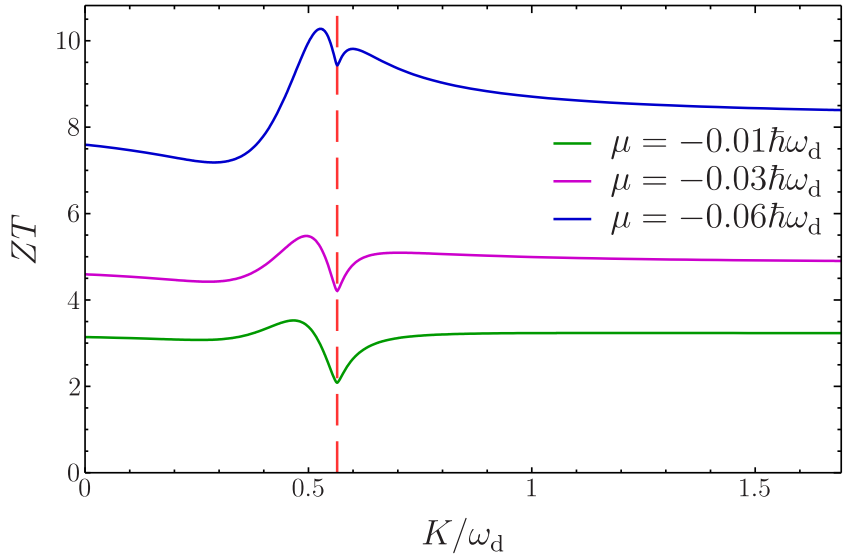

Figure 6.9 – Dimensionless figure of merit ZT versus coupling K for different values of the chemical potential when the spectral density is a power law with $s = 1/2$. Other parameters are $\omega_{\mathrm{c}} = 10\omega_{\mathrm{d}}$ and $T = 0.03\omega_{\mathrm{d}}/k_{\mathrm{B}}$. The dashed vertical line indicates the critical coupling.

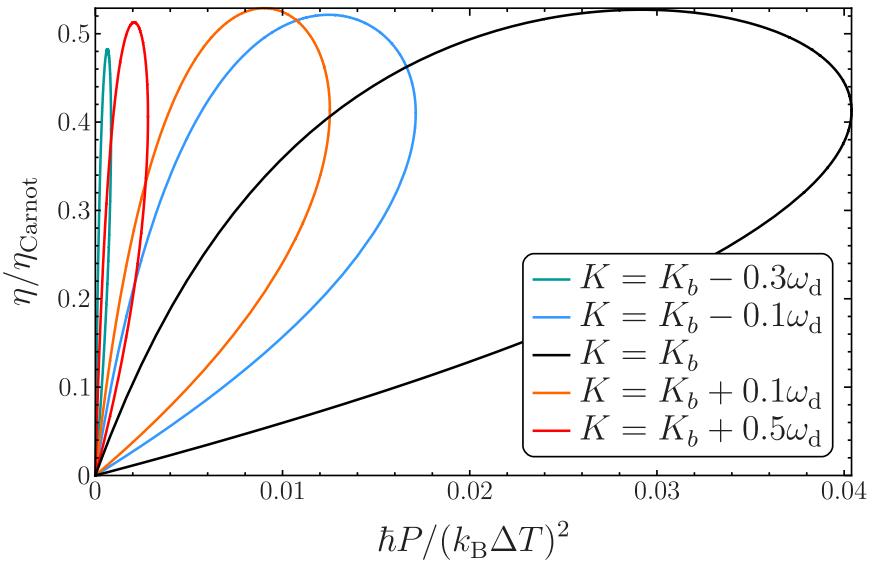

Figure 6.10 – Plot of the curves of efficiency versus power output; each curve is generated by varying the bias voltage across the dot. The spectral density is a power law with $s = 1/2$, other parameters are $\omega_{\mathrm{c}} = 10\omega_{\mathrm{d}}$, $T = 0.03\omega_{\mathrm{d}}/k_{\mathrm{B}}$ and $\mu = 0.06\hbar\omega_{\mathrm{d}}$. We clearly see that one can get much larger power output without a noticeable reduction in efficiency at critical coupling.

Chapter 7

Multiple perfectly transmitting states for tight-binding models

In this chapter, we study various set-ups where the discrete level is coupled to reservoirs described by a tight-binding Hamiltonian exhibiting narrow bands. We consider three different situations: coupling to the extremity of a one-dimensional chain, coupling to the middle of such chain and coupling to the middle of a two-dimensional square lattice. Each of these cases give rise to a different spectral density with its own features. We are mainly interested in the effects of the strongly nonlinear Lamb shifts arising in such situations. We analyze resonances which correspond to perfectly transmitting states when occurring in the band. Counter-intuitively, we show that a single discrete level can give rise to multiple perfectly transmitting states yielding a transmission function resembling that of a multi-level system. We also show that perfectly transmitting states can appear even when the discrete level is outside the reservoirs' energy bands. Finally, we try study the connection between this rich physics and the features of the local density of states.

7.1 Spectral density for tight-binding models

7.1.1 Density of states for tight-binding models

Nonlinear Lamb shifts commonly arise in cases where the spectral density exhibits rapid variations. It is thus convenient to consider situations giving rise to narrow energy bands to ensure that the typical scale of variation of the spectral density is smaller than the bandwidth. One of the simplest situations in which one encounters bands of finite range in energy is the case of hyperrectangular lattices described by a tight-binding Hamiltonian. If we only consider nearest-neighbour

hopping, this gives rise to a dispersion relation of the following kind [90]

$$\omega(\vec{k}) = -\sum_{j=1}^{d} \gamma_j \cos\Big(k_j a_j\Big) \tag{7.1}$$

The wave vector $\vec{k}$ takes values in the first Brillouin zone. a_j denotes the lattice spacing in the j direction of space and γ_j is the corresponding hopping integral. Note that we have defined the zero of energy as the middle of the band here. The dispersion relation (7.1) then gives rise to an energy band extending from $-\omega_\mathrm{c}$ to ω_c, with $\omega_\mathrm{c} = \sum_j \gamma_j$.

The density of states for such model reads

$$\nu(\omega) = \sum_{\vec{k}\in\mathrm{BZ}} \delta\Big(\omega - \omega(\vec{k})\Big) = \mathscr{D}\left(\prod_{j=1}^{d} \int_{-\pi/a_j}^{\pi/a_j} \mathrm{d}k_j\right) \delta\Big(\omega - \omega(\vec{k})\Big) \tag{7.2}$$

where $\mathscr{D}$ is a constant proportional to the volume of the system. Rewriting the delta function above with its Fourier components and upon a simple change of variables, we obtain

$$\nu(\omega) = \frac{\mathscr{D}}{2\pi} \int_{-\infty}^{\infty} \mathrm{d}\tau\, \mathrm{e}^{\mathrm{i}\omega\tau} \prod_{j=1}^{d} \frac{1}{a_j} \int_{-\pi}^{\pi} \mathrm{d}\theta_j\, \mathrm{e}^{-\mathrm{i}\gamma_j\tau\cos\theta_j} \tag{7.3}$$

Introducing the Bessel function [78]

$$J_0(z) = J_0(-z) = \frac{1}{2\pi} \int_{-\pi}^{\pi} \mathrm{d}\theta\, \mathrm{e}^{-\mathrm{i}z\cos(\theta)} \tag{7.4}$$

we find that the density of states reads

$$\nu(\omega) = D \int_0^{\infty} \mathrm{d}\tau \cos(\omega\tau) \prod_{j=1}^{d} J_0(\gamma_j\tau) \tag{7.5}$$

where we have introduced a new constant D.

We will focus on the case of hypercubic lattices in the following. As such, we take all the γ_j to be equal which yields a compacter form for the density of states,

$$\nu(\omega) = D \int_0^{\infty} \mathrm{d}\tau \cos(\omega\tau) J_0\Big(\frac{\omega_\mathrm{c}\tau}{d}\Big)^d \tag{7.6}$$

7.1.2 One-dimensional chain

In one dimension, it can be shown that equation (7.6) yields

$$\nu(\omega) = \frac{D}{\sqrt{\omega_\mathrm{c}^2 - \omega^2}} \tag{7.7}$$

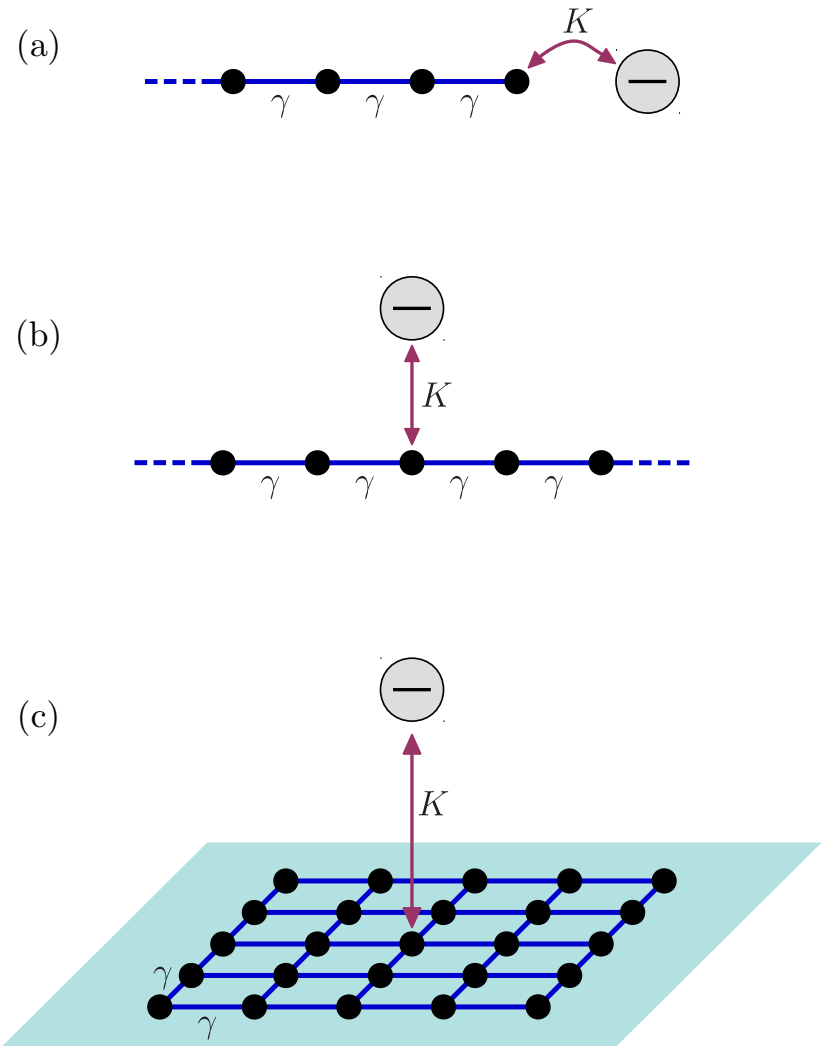

Figure 7.1 – The different situations studied in this chapter. In (a), the discrete level is coupled to the extremity of a one-dimensional chain while in (b) it is coupled to the middle of such chain. In (c), the discrete level is coupled to a site deep in the middle of a two-dimensional square lattice.

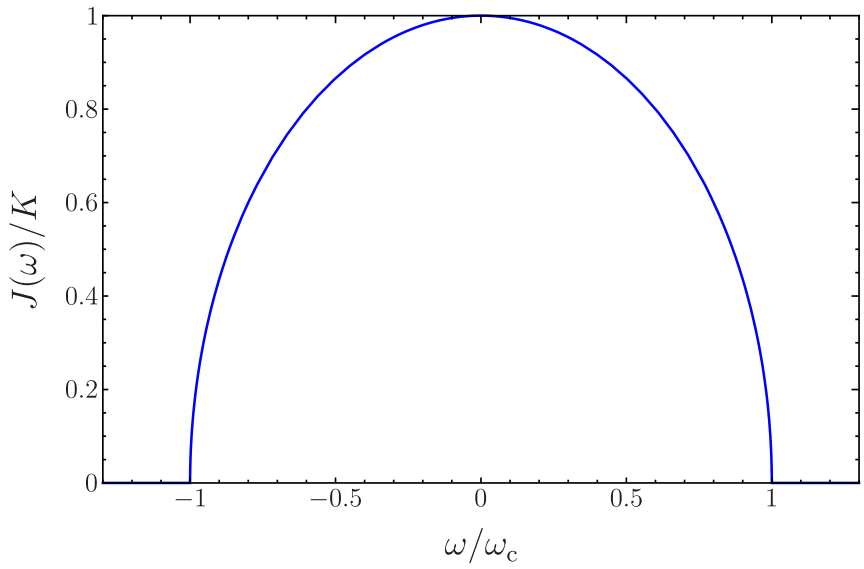

Figure 7.2 – Spectral density for a discrete level coupled to the extremity of one-dimensional chain ($s = 1/2$).

However, the results derived in this work do not depend on the density of states per se but on the spectral density. Besides the density of states it is then also necessary to take into account the coupling to the the discrete level. We consider cases where the discrete level is coupled to a single site of the chain. In order to retrieve a Hamiltonian of the form (1.16), one then has to understand how the coupling to a single site of the chain spreads within the many eigenmodes of the tight-binding Hamiltonian. To do so, one has to consider the overlap between the eigenmodes of the chain and the wavefunction associated to a single site in this chain. This can lead to very different spectral densities depending on the position of the site in the chain [51, 91]. Here, we focus on two possible situations.

First, we consider the case where the discrete level is coupled to an extremity of the chain (see figure 7.1a). The overlap between an eigenstate of energy ω with the first site of the chain is proportional to $\sqrt{\omega_c^2 - \omega^2}$. For the calculation of the spectral density, one takes the square modulus of the coupling of the discrete level to the eigenstates of the reservoir. In combination with the density of states (7.7), this then yields

$$J(\omega) = K\sqrt{1 - \frac{\omega^2}{\omega_c^2}} \tag{7.8}$$

where all constants have been absorbed into K. This spectral density is shown in figure 7.2.

Next, we consider the case where the discrete level is coupled to a site in the middle of the chain (see figure 7.1b). In the thermodynamic limit, periodic and open

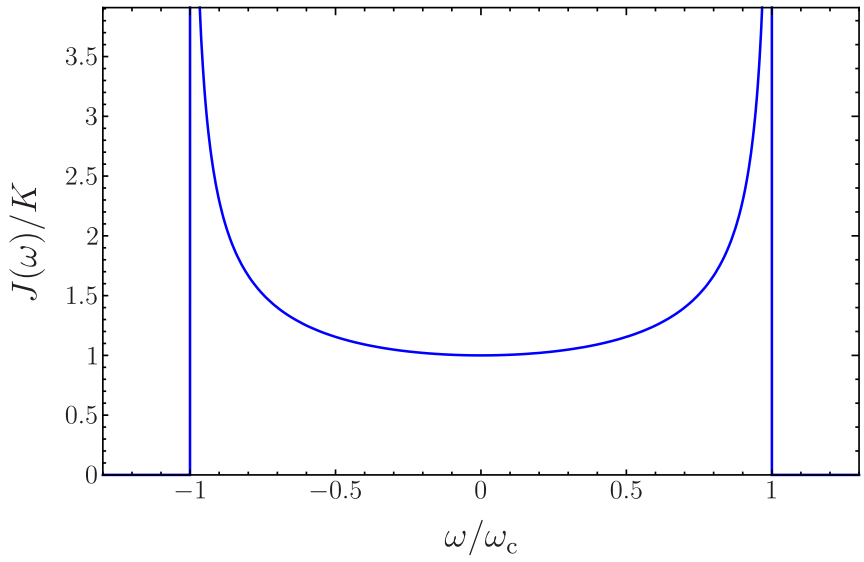

Figure 7.3 – Spectral density for a discrete level coupled to the middle of one-dimensional chain ($s = -1/2$). It features square root divergences (Van Hove singularities) at each band edge.

boundary conditions give equivalent results. For periodic boundary conditions, the eigenstates of the tight-binding Hamiltonian are plane waves; taking the square modulus, we realize that each of these is coupled with the same intensity to the discrete level. The case of open boundary conditions is subtler: One finds that the discrete level can only interact with only half of the modes at a given energy but, due to different definitions of the wave vectors and the Brillouin zone, there are twice as many modes at this energy. All in all, we find that the spectral density is simply proportional to the density of states (7.7) such that we can write

$$J(\omega) = \frac{K}{\sqrt{1-\omega^2/\omega_c^2}} \tag{7.9}$$

where all constants have been absorbed into K. This spectral density is shown in figure 7.3.

In the following, it will be convenient to write the spectral density with the general form

$$J(\omega) = K\left(1-\frac{\omega^2}{\omega_c^2}\right)^s \tag{7.10}$$

where $s = 1/2$ if the discrete level is at the extremity of the chain and $s = -1/2$ if it is in the middle.

7.1.3 Two-dimensional square lattice

In the case of a two-dimensional square lattice, equation (7.6) yields the following density of states

$$\nu(\omega) = DE\left(1 - \frac{\omega^2}{\omega_c^2}\right) \tag{7.11}$$

where $E(w)$ denotes the elliptic integral

$$E(w) = \int_0^{\pi/2} \frac{\mathrm{d}\theta}{\sqrt{1 - w\sin^2\theta}} \tag{7.12}$$

We can see that the density of states (7.11) takes a constant value at the band edges and exhibits a logarithmic divergence at the centre of the band. However, its general behaviour is not easy to study analytically. It will then often be convenient to consider an approximate density of states reproducing the same behaviour, namely

$$\nu_{\text{approx}}(\omega) = D\left(\frac{\pi}{2} - \ln\left|\frac{\omega}{\omega_c}\right|\right) \tag{7.13}$$

Similarly to the one-dimensional case, the way the discrete level is coupled to the tight-binding reservoir has a strong influence on the spectral density. In the case of a two-dimensional lattice, one can imagine a wide-range of possibilities for which the spectral density may be very challenging to determine: coupling to a site on a corner, on the side or in the middle of the lattice for example. Here, we will only consider the case where the discrete level is coupled to a site in the middle a two-dimensional lattice (see figure 7.1c). Then, the spectral density is proportional to the density of states (7.11),

$$J(\omega) = KE\left(1 - \frac{\omega^2}{\omega_c^2}\right) \tag{7.14}$$

where all constants have been absorbed into K. Similarly, the spectral density corresponding to the approximate density of states (7.13) is given by

$$J_{\text{approx}}(\omega) = K\left(\frac{\pi}{2} - \ln\left|\frac{\omega}{\omega_c}\right|\right) \tag{7.15}$$

These spectral densities are shown in figure 7.4.

7.2 Nonlinear Lamb shifts

The Lamb shift has a fundamental importance in order to understand the response of the discrete level to the coupling to the reservoirs. It is mainly the behaviour of the Lamb shift which characterizes the various resonances giving rise to bound states in gaps or peaks of transmission in bands.

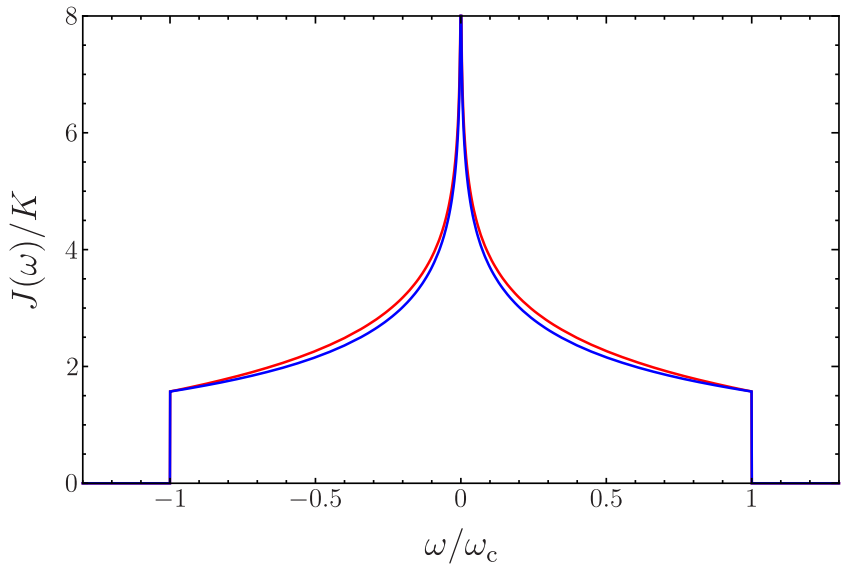

Figure 7.4 – Spectral density for a discrete level coupled to a site in the middle of two-dimensional square lattice. The blue line corresponds to the exact result while the red line is an approximation for which analytical calculations are possible. Both feature a logarithmic divergence at the centre of the band

7.2.1 One-dimensional chain

In the case of the one-dimensional chain, the spectral densities (7.10) are simple enough so that the Lamb shift can be calculated analytically. However, we cannot find a formula giving the Lamb shift for any value of the exponent s so we treat the cases $s = 1/2$ and $s = -1/2$ separately.

- **Lamb shift for** $s = 1/2$

If the discrete level is coupled to a site at the end of the chain, we find

$$\Lambda(\omega) = \begin{cases} \dfrac{\pi K \omega}{\omega_c} & \text{if } |\omega| < \omega_c \text{ (band)} \\ \dfrac{\pi K}{\omega_c}\left(\omega - \operatorname{sgn}(\omega)\sqrt{\omega^2 - \omega_c^2}\right) & \text{if } |\omega| > \omega_c \text{ (gaps)} \end{cases} \tag{7.16}$$

Here the Lamb shift is continuous and takes a finite value at the band edges (see figure 7.5). Moreover, while the Lamb shift is always a decreasing function of ω outside the band, it is here increasing inside the band. It is this feature of the in-band Lamb shift that enables the existence of several resonances. In more mathematical terms, the equation $\omega - \omega_d - \Lambda(\omega) = 0$ cannot have several solutions if $\Lambda(\omega)$ decreases with ω in the whole energy range.

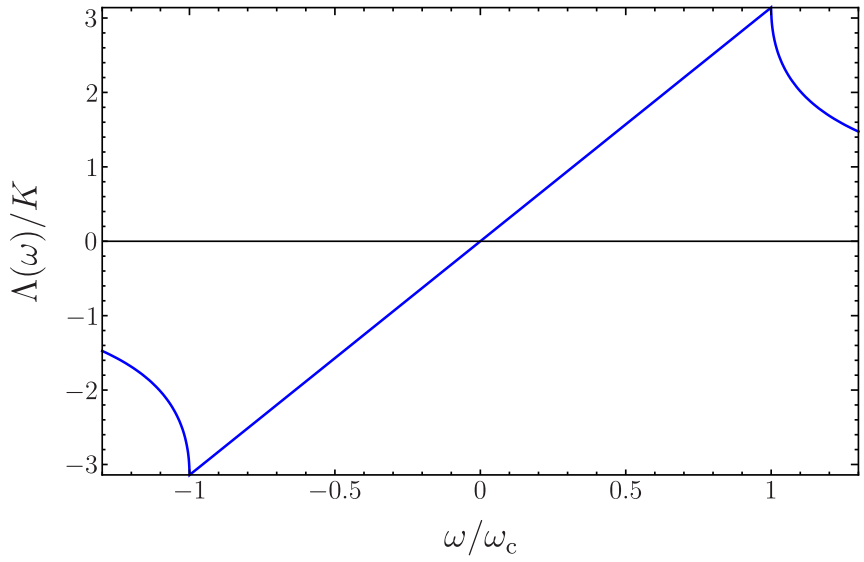

Figure 7.5 – Lamb shift for a discrete level coupled to the extremity of one-dimensional chain ($s = 1/2$).

- **Lamb shift for** $s = -1/2$

  In the case where the discrete level is coupled to the middle of the chain, we have

$$\Lambda(\omega) = \begin{cases} 0 & \text{if } |\omega| < \omega_c \text{ (band)} \\ \dfrac{\pi K \omega_c \operatorname{sgn}(\omega)}{\sqrt{\omega^2 - \omega_c^2}} & \text{if } |\omega| > \omega_c \text{ (gaps)} \end{cases} \tag{7.17}$$

Contrary to the case $s = 1/2$, the Lamb shift is not continuous at the band edges but diverges at these points (see figure 7.6). Strangely, the Lamb shift exactly vanishes for all energies inside the band. This means that the energy of the discrete level will remain unaffected by the coupling to the reservoir whatever its strength.

7.2.2 Two-dimensional square lattice

In the two-dimensional case, we cannot find an analytical formula for the Lamb shift arising from the exact spectral density given in equation (7.14). However, this

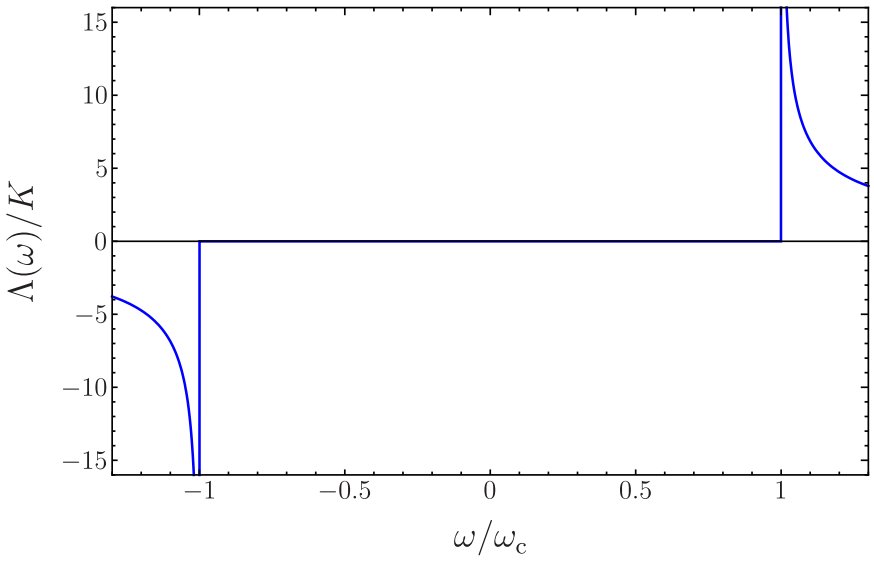

Figure 7.6 – Lamb shift for a discrete level coupled to the middle of one-dimensional chain ($s = -1/2$). Surprisingly, the value of the Lamb shift inside the band is identically zero.

is possible in the case of the approximate expression (7.15) and we find

$$\Lambda_{\text{approx}}(\omega) = \begin{cases} K\left(L\left(\frac{\omega_c}{\omega}\right) - L\left(-\frac{\omega_c}{\omega}\right)\right. & \text{if } |\omega| < \omega_c \text{ (band)} \\ \qquad \left. + \frac{\pi}{2}\ln\left(\frac{\omega_c+\omega}{\omega_c-\omega}\right) - \mathrm{i}\pi\,\mathrm{sgn}(\omega)\ln\left|\frac{\omega}{\omega_c}\right|\right) & \\ K\left(L\left(\frac{\omega_c}{\omega}\right) - L\left(-\frac{\omega_c}{\omega}\right) + \frac{\pi}{2}\ln\left(\frac{\omega+\omega_c}{\omega-\omega_c}\right)\right) & \text{if } |\omega| > \omega_c \text{ (gaps)} \end{cases} \tag{7.18}$$

where $L(w)$ denotes the dilogarithmic function,

$$L(w) = -\int_0^w \mathrm{d}x\,\frac{\ln(1-x)}{x} \tag{7.19}$$

Similarly to the case $s = -1/2$, the Lamb shift diverges at the band edges (see figure 7.7). However, the in-band structure of the Lamb shift is much more subtler here. Namely, we observe a discontinuity of $\Lambda(\omega)$ in the middle of the band stemming from the logarithmic divergence of the spectral density at this point. More precisely, we find

$$\Lambda_{\text{approx}}(\omega \to 0^+) - \Lambda_{\text{approx}}(\omega \to 0^-) = \pi^2 K \tag{7.20}$$

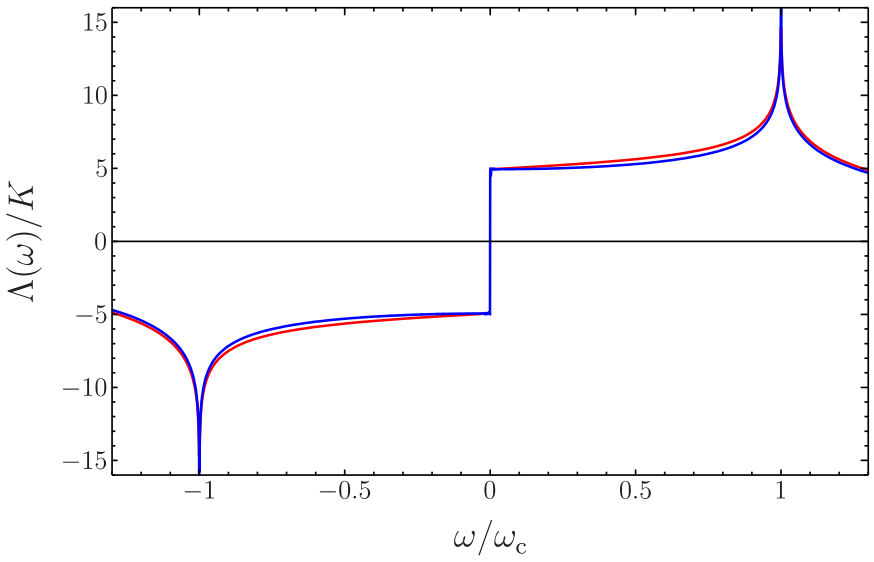

Figure 7.7 – Lamb shift for a discrete level coupled to the site in the middle of two-dimensional square lattice. The blue line corresponds to the exact result which is obtained numerically; the red line corresponds to an approximation for which analytical calculations are possible. The logarithmic divergence at the centre of the band in the spectral density yields a discontinuity of the Lamb shift.

7.3 Experimental considerations

7.3.1 Thermoelectric experiments

7.3.1.1 Transmission measured using low-temperature conductance

In thermoelectric transport experiments, one typically measures the thermoelectric response of a device in order to infer its transport coefficients. As explained in section 2.1.2, these coefficients can be completely determined from the transmission function of the thermoelectric device but the transmission itself cannot be measured directly in general. Transport coefficients are indeed given by the integrals ι_n which are essentially convolutions of the transmission function $\mathcal{T}(\omega)$ with the function $\Phi(\omega)$ defined in equation (2.11). The latter essentially acts as an energy filter centred at the average chemical potential μ whose typical width is given by the average temperature T. Hence, if T is very small with respect to the typical scale of variation of $\mathcal{T}(\omega)$, the convolution of the latter with $\Phi(\omega)$ will give the value of the transmission at μ [19,24,66]. In other words, $\Phi(\omega)$ becomes a delta function in the limit of low temperature. This allows for dramatic simplifications of the transmission-dependence of transport coefficients. In particular, the electrical

conductance takes the following simple form

$$G = \frac{e^2}{h}\mathcal{T}\left(\frac{\mu}{\hbar}\right) \tag{7.21}$$

The transmission function of a single-level quantum dot can then be measured through the electrical conductance when one connects two reservoirs via the dot introducing a small voltage bias and keeping the set-up at low temperature. We consider here the case were both reservoirs have the same chemical composition such that the assumption (6.2) of symmetric coupling holds. We recall that perfect transparency of the dot can only be achieved in the case of symmetric coupling.

In order to probe the in-band structure of the transmission, it is then necessary to vary the chemical potentials of both reservoirs simultaneously which has been done using a back gate for one- and two-dimensional samples [92–95]. With this technique one can electrostatically dope the system in order to change the position of the chemical potential with respect to the band structure. This permits to perform all measurements with a single sample instead of fabricating many with different doping factors.

7.3.1.2 Probing the local density of states through scanning tunneling spectroscopy

The local density of states can be measured using scanning tunneling spectroscopy, a technique which permits to probe the local electronic structure of a sample [96]. This technique is based on the measurement of the tunneling current between the sample of interest and the tip of a scanning tunneling microscope. Here, we imagine the case where the tip of a microscope is weakly coupled to a quantum dot itself coupled to a reservoir. We measure the current resulting from an applied bias voltage between the tip and the reservoir. The assumption of weak coupling between the microscope and the dot is crucial here: First, this enables us to neglect the internal electronic structure of the tip which we simply describe in the wide-band limit, $J_{\mathrm{tip}}(\omega) = \kappa$. Furthermore, weak dot-tip coupling means that the influence of the bias applied to the tip on the dot level is negligible.

In this framework, the electric current entering the tip can be obtained using equation (4.21),

$$I = \frac{e}{2\pi}\int \mathrm{d}\omega\, \mathcal{T}(\omega)(n_{\mathrm{tip}}(\omega) - n_{\mathrm{res}}(\omega)) \tag{7.22}$$

where the transmission function is given by

$$\mathcal{T}(\omega) = \frac{4\pi^2\kappa J_{\mathrm{res}}(\omega)}{(\omega - \omega_{\mathrm{d}} - \Lambda_{\mathrm{res}}(\omega))^2 + \pi^2(J_{\mathrm{res}}(\omega) + \kappa)^2} \tag{7.23}$$

We recall that a reservoir in the wide-band limit does not induce any Lamb shift which is why only $\Lambda_{\mathrm{res}}(\omega)$ appears in the expression above. Due to the assumption of

weak dot-tip coupling, the second term in the denominator above can be simplified neglecting the contribution of the tip to the total spectral density,

$$\mathcal{T}(\omega) \simeq \frac{4\pi^2\kappa J_{\rm res}(\omega)}{(\omega-\omega_{\rm d}-\Lambda_{\rm res}(\omega))^2+\pi^2 J_{\rm res}(\omega)^2} = 4\pi^2\kappa S_{\rm res}(\omega) \tag{7.24}$$

where $S_{\rm res}(\omega)$ denotes the local density of states in the situation where the dot is only coupled to the reservoir. It is then clear that the current entering the tip enables a measure of the local density of states on the dot.

The tip and reservoir are assumed to be at the same temperature but a voltage bias V is applied to the tip such that $n_{\rm tip}(\omega) = n_{\rm res}(\omega + eV/\hbar)$. Hence, the only term depending on the bias voltage in the current in equation (7.22) is the Fermi factor for the tip. If we then consider the derivative of the current with respect to the voltage bias, we find

$$\frac{{\rm d}I}{{\rm d}V} = -2\pi e^2\kappa \int {\rm d}\omega\, S_{\rm res}(\omega)\Phi\Big(\omega+\frac{eV}{\hbar}\Big) \tag{7.25}$$

where $\Phi(\omega)$ is defined in equation (2.11). In the limit of low temperature, the variations of the transmission function can be neglected and we obtain

$$\frac{{\rm d}I}{{\rm d}V} = -\frac{2\pi e^2\kappa}{\hbar} S_{\rm res}\Big(\frac{\mu-eV}{\hbar}\Big) \tag{7.26}$$

where μ denotes the chemical potential of the reservoir. Hence, measuring the current entering the tip while changing the bias voltage applied to the tip permits to measure the variations of local density of states for the dot as it is simply proportional to the slope of the current-voltage characteristic of the system.

It is important to note that contributions from the bound states have not been considered here. This is because their lifetime is not infinite in the set-up studied here due to the influence of the tip of the microscope. This situation is similar to the framework used in chapter 5 to simulate adiabatic turning on of the dot-reservoir couplings. The very weak coupling to the tip gives a very long but finite lifetime to the bound states which will then eventually decay. In other words, the resonances appearing as delta functions in the local density of states (3.49) become Lorentzian functions with finite width. This suggests that the persistent oscillations in the occupation and currents seen in equations (4.20) and (4.21) cannot be observed experimentally as any measurement apparatus would destroy them by granting a finite lifetime to bound states.

7.3.2 Microwave tight-binding experiments

The tight-binding lattices giving rise to the nonlinear Lamb shifts described in section 7.2 can be artificially engineered with microwave experiments. It has

been shown experimentally that the tight-binding regime can be reproduced using dielectric discs with high refractive index sandwiched between two metallic plates [97–99]. The discs are designed such that they support a single microwave mode whose precise frequency is determined by the size of the disc. The electromagnetic field is mostly confined within the discs but evanescent waves in the empty space between two discs give rise to a coupling between these. This highly versatile experimental set-up mimics the physics of tight-binding lattices and various spectral densities can then be easily generated by changing the spatial arrangement of discs as explained in section 7.1. A crucial feature of these tight-binding microwave experiments is that the intensity of the coupling between two discs can be tuned by changing the distance between these discs [97–99]. An experiment corresponding to the Fano-Anderson model can then be engineered with two lattices comprising a large number of discs, acting as reservoirs, both coupled to a disc of different size, playing the role of the discrete level. The coupling parameter K in this experiment can be varied by changing the distance between the different-sized disc and the reservoir discs to which it is coupled.

One should note that our solution of the Fano-Anderson Hamiltonian is independent of the statistics of the particles involved and can thus be applied to these microwave experiments. Furthermore, measurements of transport properties and local densities of states in these set-ups is also possible. The transmission function of the discrete level is directly observable by injecting a monochromatic beam at frequency Ω in reservoir L, such that $n_{\mathrm{L}}(\omega)$ is sharply peaked around $\omega = \Omega$ while $n_{\mathrm{R}}(\omega) = 0$. The local density of states at a specific disc can be measured using a technique similar as that described in section 7.3.1.2; the tip of the microscope is here replaced by an antenna [97–99].

7.4 Theoretical results

7.4.1 Resonances and transmission properties

As already pointed in section 6.1.3, the Lamb shift plays a crucial role in the behaviour of the transmission. We are particularly interested in resonances, that is energies satisfying $\omega - \omega_{\mathrm{d}} - \Lambda(\omega) = 0$. When outside a band, they correspond to infinite-lifetime bound states; within a band, they yield perfectly transmitting states satisfying $\mathcal{T}(\omega) = 1$ if one assumes symmetric coupling. One could intuitively think that perfect transmission can only be reached close to the energy of the discrete level but this is only true in cases where the Lamb shift can be ignored as in the wide-band limit. We have already seen that level repulsion could push a perfectly transmitting state outside the continuum consequently giving rise to a bound state. However, this is not the full picture and we will see here that nonlinear Lamb shifts can have various counter-intuitive effects. For example, it can give rise to multiple

perfectly transmitting states meaning that the single level in the strong coupling regime behaves like a multi-level system would behave in the weak coupling regime.

In order to understand the various effects of nonlinear Lamb shifts, it is convenient to represent the number of perfectly transmitting states and infinite-lifetime bound states on a "phase diagram" for the coupling parameter K and the discrete level energy ω_{d}.

- **Resonances and transmission for $s = 1/2$**

The Lamb shift is here simple enough that resonances can be calculated exactly. For ω in the band, the equation $\omega - \omega_{\mathrm{d}} - \Lambda(\omega) = 0$ can only have one solution,

$$\omega_* = \frac{\omega_{\mathrm{d}}\omega_{\mathrm{c}}}{\omega_{\mathrm{c}} - \pi K} \tag{7.27}$$

It is however necessary to ensure that ω_* is in the band, that is $|\omega_*| < \omega_{\mathrm{c}}$. There are two possibilities for this condition to be satisfied,

$$K < K_< = \frac{\omega_{\mathrm{c}} - |\omega_{\mathrm{d}}|}{\pi} \tag{7.28}$$

or

$$K > K_> = \frac{\omega_{\mathrm{c}} + |\omega_{\mathrm{d}}|}{\pi} \tag{7.29}$$

These two values of the coupling allow us to define three different regimes depicted in the phase diagram of figure 7.8. In each regime, the transmission function exhibits different features as shown in figure 7.9. Assuming the discrete level is inside the band, we have a perfectly transmitting state close to the discrete level at weak coupling. As the coupling is increased, this resonance is pushed towards the band edge closest to the discrete level. It reaches the band edge when $K = K_<$ and then becomes a bound state outside the band. The value of the transmission inside the band then drops until a new resonance appears at the opposite band edge for $K = K_>$. Surprisingly, a perfectly transmitting state and a bound state appear simultaneously at this point. This contrasts with the usual handwaving arguments identifying bound states as perfectly transmitting states pushed out of the band by level repulsion. In the strong coupling regime, the remaining peak gets broader and moves towards the centre of the band.

We point out that there is an interesting special case where the discrete is transparent to all electrons of the band. Indeed, if $\omega_{\mathrm{d}} = 0$ and $K = K_< = K_> = \omega_{\mathrm{c}}/\pi$, we have $\omega - \omega_{\mathrm{d}} - \Lambda(\omega) = 0$ for all energies in the band. We have an infinite number of resonances which means that the transmission function is identically equal to one in the whole band. This corresponds to the case where the discrete level is identical to the sites in the chains.

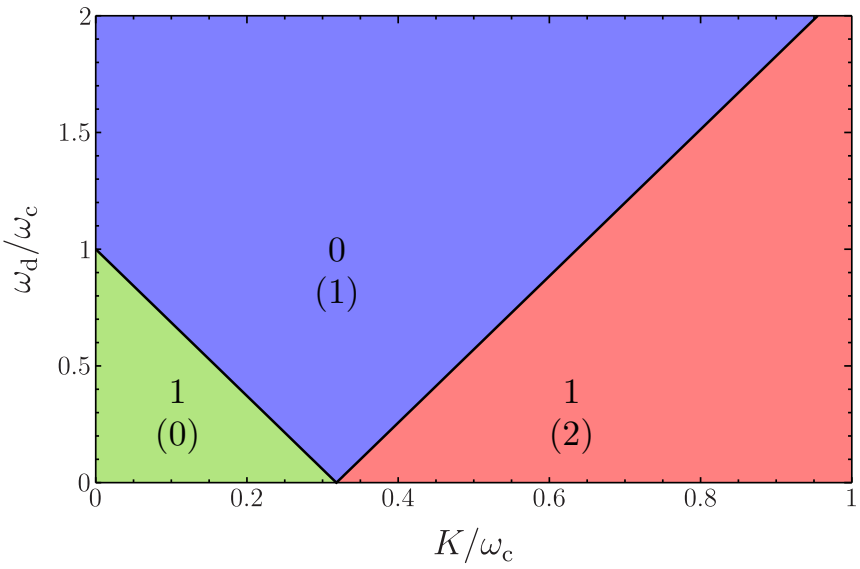

Figure 7.8 – Phase diagram for a discrete level coupled to the extremity of one-dimensional chain ($s = 1/2$). The number of in-band resonances for each region is displayed; the number in parentheses is the number of bound states.

The case where the discrete level is outside the band is especially interesting here as we see from figure 7.8 that there is always a perfectly transmitting state at strong coupling whatever the value of the discrete energy level ω_d. One could have expected residual transmission through the discrete level due to the level-broadening induced by the coupling, but the Lamb shift is usually thought of as accounting for the level repulsion phenomenon that tends to push the discrete level away from the band. It is thus very surprising to observe here that the Lamb shift gives rise to a perfectly transmitting state in the strong coupling regime. The transmission function of the discrete level when its energy is outside the reservoirs' band is shown in figure 7.10. At weak coupling, there is only one resonance corresponding to a bound state that almost completely coincides with the discrete level. Such bound state does not participate in dc transport and the transmission function then only consists of the minute contribution of continuum states. As the coupling is increased, we can see a transmission peak forming at the band edge opposite to the discrete level and a resonance appears at this edge for $K = K_>$. It then immediately splits into an additional bound state and a perfectly transmitting state which moves towards the centre of the band.

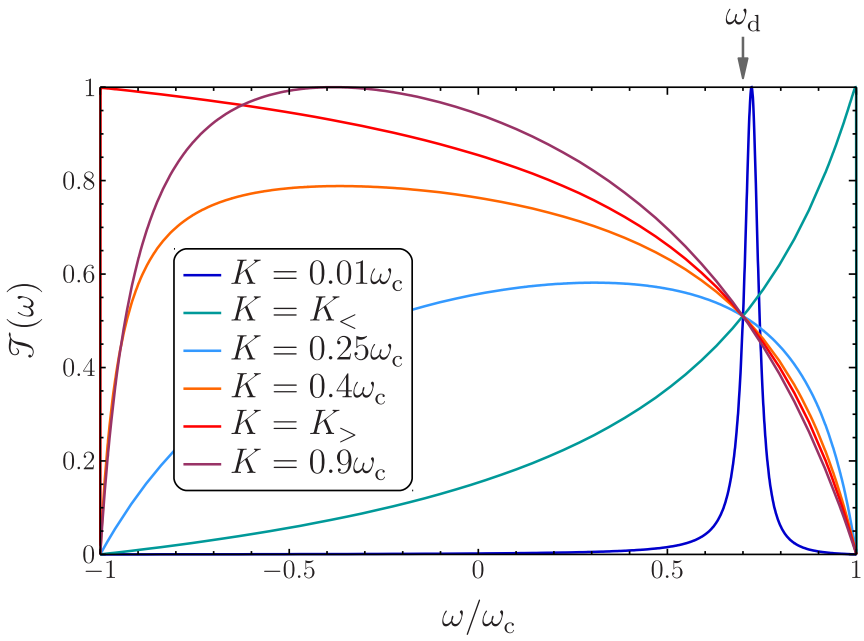

Figure 7.9 – Transmission versus energy for various values of the coupling parameter K for a discrete level coupled to the extremity of one-dimensional chain ($s = 1/2$). The discrete energy level is inside the reservoirs' band ($\omega_{\mathrm{d}} = 0.7\omega_{\mathrm{c}}$).

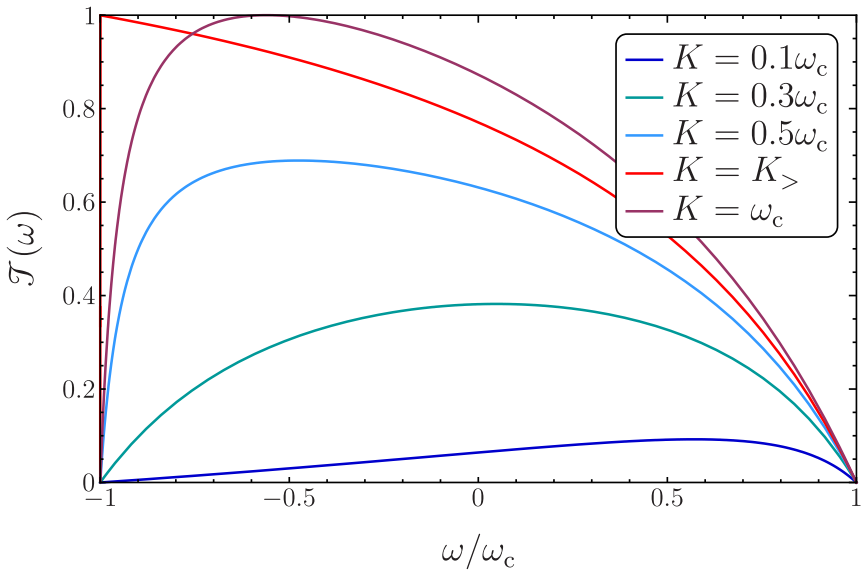

Figure 7.10 – Transmission versus energy for various values of the coupling parameter K for a discrete level coupled to the extremity of one-dimensional chain ($s = 1/2$). Even though the discrete energy level is outside the reservoirs' band ($\omega_{\mathrm{d}} = 1.2\omega_{\mathrm{c}}$), a perfectly transmitting state appears at strong coupling.

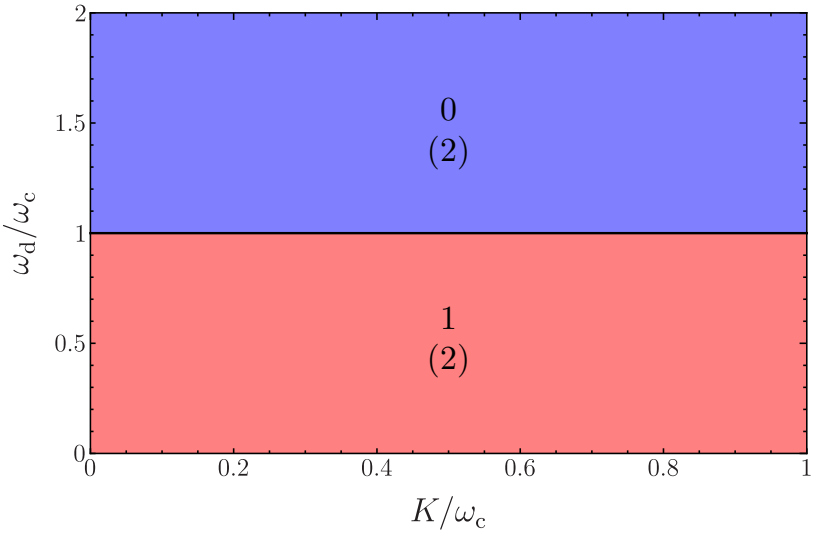

Figure 7.11 – Phase diagram for a discrete level coupled to the middle of one-dimensional chain ($s = -1/2$). The number of in-band resonances for each region is displayed; the number in parentheses is the number of bound states.

- **Resonances and transmission for $s = -1/2$**

This case is by far the simplest as the Lamb shift is identically zero in the band. This means that transmission is always perfect at the discrete level here, except if it is outside the band obviously. The phase diagram of this system is shown in figure 7.11. It is however important to point out that perfect transmission is also achieved at both band edges as shown in figure 7.12. These peaks of perfect transmission do not arise from resonances though; they are due to the divergence of the spectral density at the band edges. When the coupling is increased, all transmission peaks get broader. Furthermore, due to the divergence of the Lamb shift at the band edges outside the continuum, there always is one bound state in each gap.

- **Resonances and transmission for a square lattice**

This case is by far the most complicated to describe due to the very nonlinear structure of the Lamb shift. We distinguish four different types of in-band resonances which are displayed in figure 7.13. First, we have the usual bare resonance; it is close to the discrete level for weak coupling and is then shifted towards the nearest band edge due to level repulsion. Moreover, the divergence of the Lamb shift at the band edges give rise two edge resonances. One should also note that the Lamb shift diverges on both sides of each band edge which means that this system exhibits a bound state in each band gap for all values of the coupling. Finally, an additional

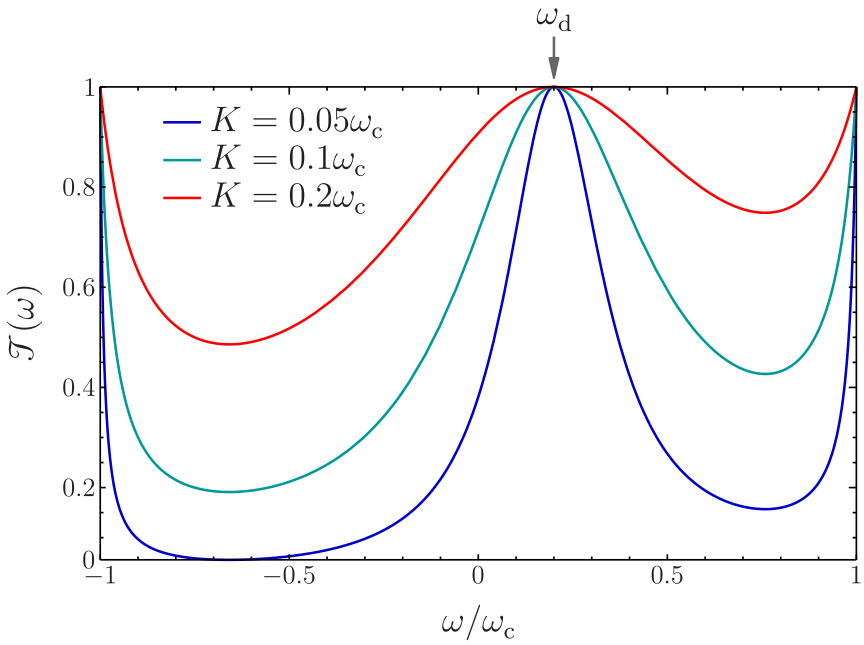

Figure 7.12 – Transmission versus energy for various values of the coupling parameter K for a discrete level coupled to the middle of one-dimensional chain ($s = -1/2$).

resonance appears at the opposite of the discrete level when $K = 2\omega_d/\pi^2$ due to the discontinuity of the Lamb shift at the centre of the band. Besides all the resonances described above, there is an additional peak of perfect transmission at the centre of the band. This peak exists for all values of the coupling and it does not correspond to a resonance but actually results from the divergence of the spectral density at the centre of the band.

The phase diagram for this system is shown in figure 7.14 while figure 7.15 displays the rich structure of the transmission function in this system. At weak coupling and if the discrete level is inside the band, one finds three resonances, the bare resonance and the two edge resonances. If the discrete level is outside the band, only one edge resonance appears. As the coupling is increased, the bare resonance is shifted towards the nearest band edge and it eventually merges with the corresponding edge resonance; both of them then disappear. Concomitantly, the jump of the Lamb shift at the centre of the band increases with coupling which give rise to the appearance of the discontinuity resonance at $K = 2\omega_d/\pi^2$. Similarly to the bare resonance, the discontinuity resonance drifts towards the band edge and merges with the remaining edge resonance. Hence, no in-band resonance remains at strong coupling. We point out that depending on the position of the discrete level in the band, the phenomena described above may occur on different orders:

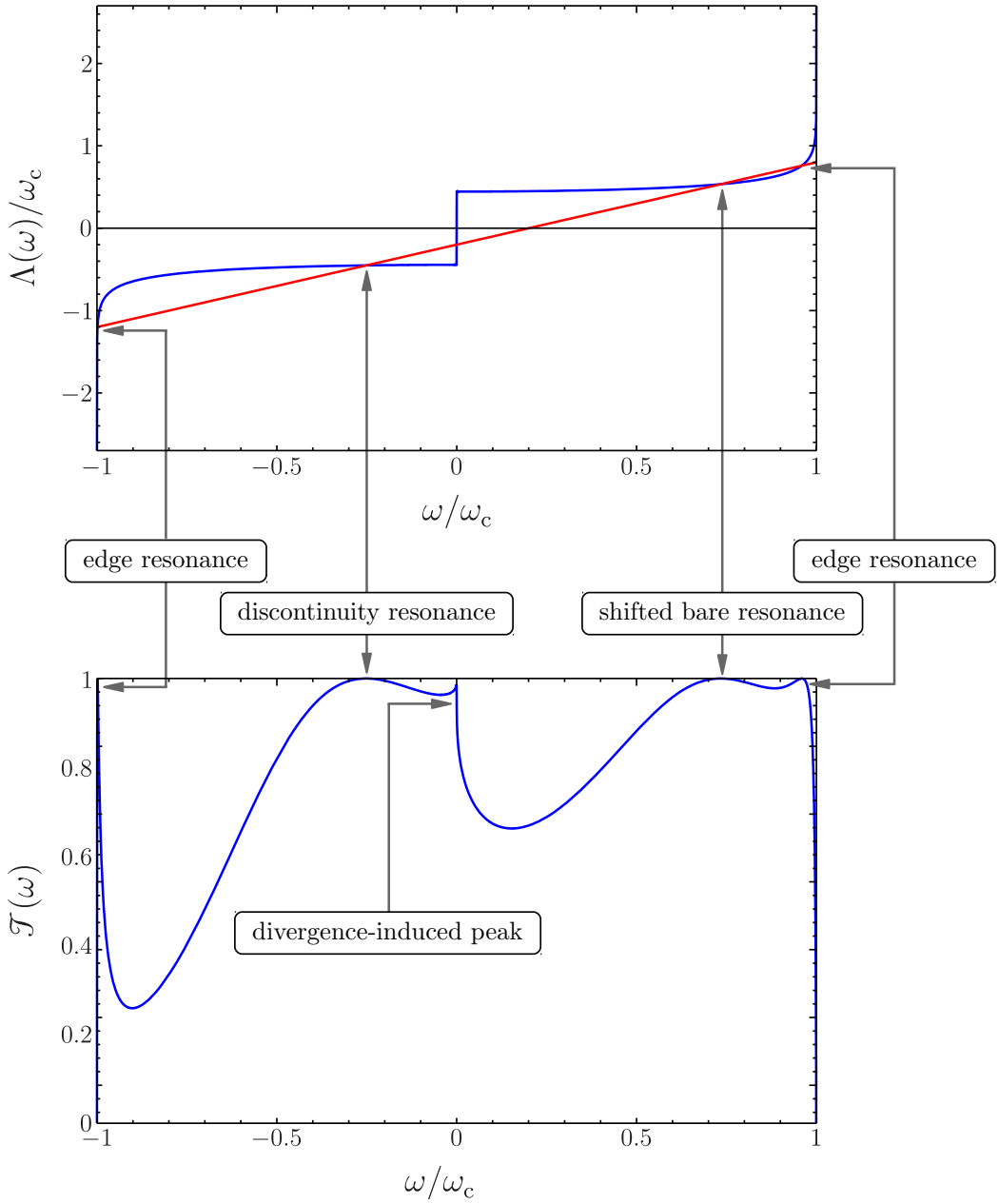

Figure 7.13 – Depiction of the different types of resonances for a discrete level coupled to a site in the middle of a two-dimensional square lattice. Each resonance corresponds to a perfectly transmitting state. An additional peak of perfect transmission appears at the centre of the band due to the divergence of the spectral density at this point.

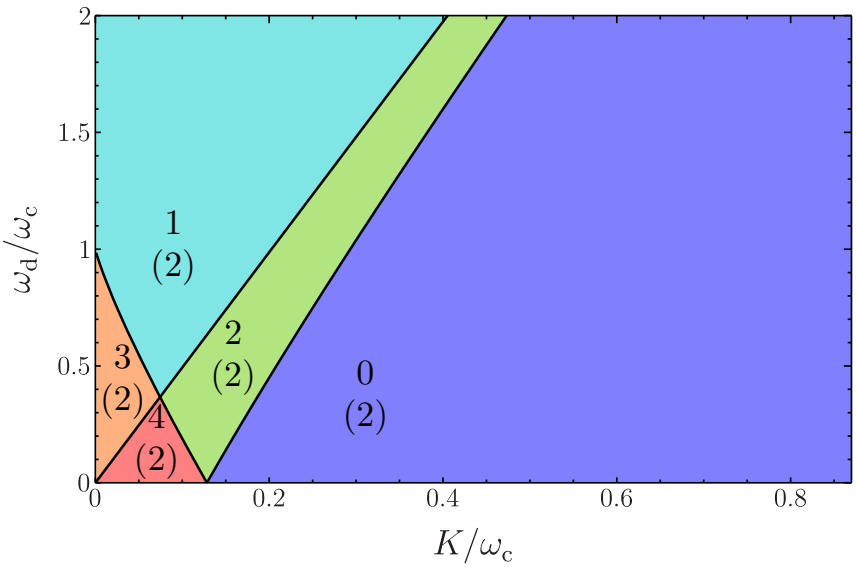

Figure 7.14 – Phase diagram for a discrete level coupled to a site in the middle of two-dimensional square lattice. The number of in-band resonances for each region is displayed; the number in parentheses is the number of bound states.

If ω_d is close to the centre of the band, the discontinuity resonance appears before the bare resonance dissapears and conversely if ω_d is closer to the band edge. One should finally note that the transmission function always vanishes at the band edges because the Lamb shift diverges at these points while the spectral density does not.

7.4.2 Local density of states

We now study the effects of the strong nonlinearity of the Lamb shift on the local density of states which essentially encodes the long-time state of the discrete level. In the weak coupling regime, the local density of states is typically a Lorentzian function centred at $\omega = \omega_d$ with a width given by the coupling parameter as in the wide-band result of equation (4.36). One could easily imagine introducing a shift of the discrete level or skewness in the Lorentzian function to account for the effects of stronger coupling phenomenologically. However, we will show here that this is largely insufficient to describe the rich structure of the local density of states in the cases studied here.

One could expect the local density of states to exhibit maxima at resonances, that is for ω such that $\omega - \omega_d - \Lambda(\omega) = 0$, similarly to the transmission function. This is true if the coupling is weak enough so that one neglects the variations of the spectral density because the denominator in the expression for $S(\omega)$ takes its minimal value at a resonance. This is not the case in general and it is often not

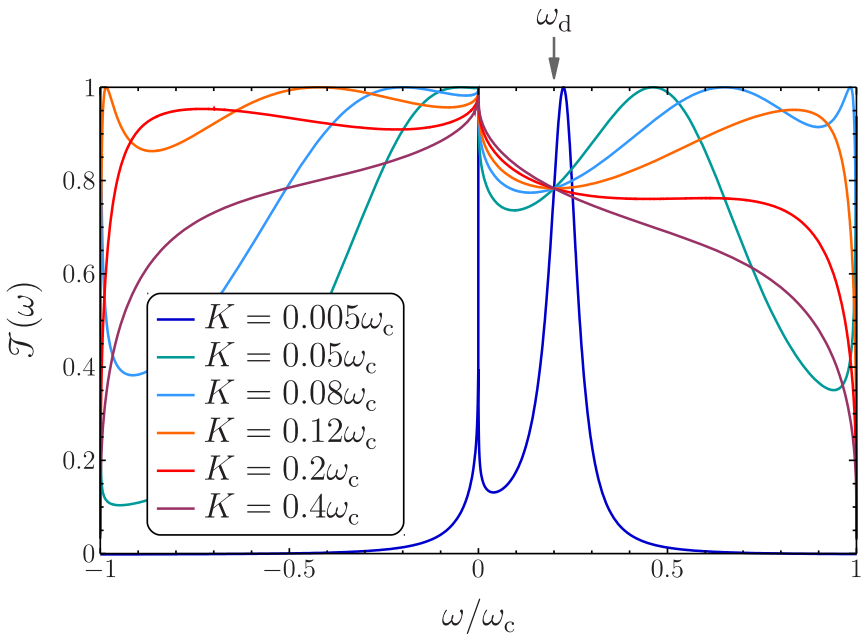

Figure 7.15 – Transmission versus energy for various values of the coupling parameter K for a discrete level coupled to a site in the middle of two-dimensional square lattice.

clear to draw a connection between the number of resonances and the structure of the local density of states in the situations studied here. However, it is still possible to see qualitative differences between the various coupling regimes.

- **Local density of states for** $s = 1/2$

Figure 7.16 shows the local density of states for a discrete level coupled to the extremity of a one-dimensional chain. At weak coupling, $S(\omega)$ is peaked around the resonance which moves towards the band edge closer to the band edge while getting narrower. Once it reaches the band edge at $K = K_<$, a bound state is created in the corresponding band gap and the value of the local density of states drops abruptly. A new peak appears at the other band edge when $K = K_>$. At this point, a resonance appears at the band edge. This resonance splits between the continuum and a second bound state. As the coupling increased, the resonance dilutes in the continuum with more weight going to the bound states.

- **Local density of states for** $s = -1/2$

The local density of states when the discrete level is coupled to the middle of a one-dimensional chain is shown in figure 7.17. In this case, $S(\omega)$ is always peaked

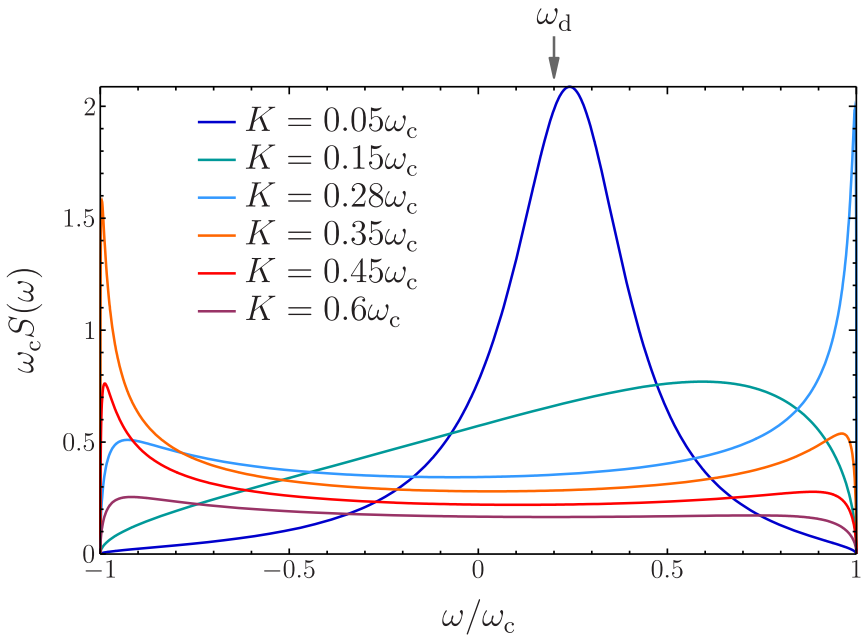

Figure 7.16 – In-band local density of states for a discrete level coupled to the extremity of one-dimensional chain ($s = 1/2$).

around ω_d as the vanishing Lamb shift does not induce any renormalization of the discrete level energy. As the coupling increases this peak gets wider and its height decreases dramatically as more weight goes to the bound states. The local density of states also features shoulders close to the band edges due to the divergences in the spectral density but it vanishes at both band edges.

- **Local density of states for a square lattice**

The local density of states for a discrete level coupled to a square lattice is shown in figure 7.18. Similarly to the transmission function, it exhibits a very rich structure. However, the connection between the behaviour of the local density of states and the phase diagram in figure 7.14 is rather involved. For example, the appearance of the discontinuity resonance does not seem to have a significative impact. On the contrary, edge resonances clearly give rise to peaks in the local density of states. We can also see the bare and discontinuity resonances slowly becoming shoulders before they merge with edge resonances. Similarly to the other cases discussed above, we clearly see that more weight goes to the bound states when the coupling is increased. Finally, we note that the local density of states vanishes at the centre of band for all values of the coupling. This is due to the divergence of the spectral density at this point which also gives rise to a peak of perfect transmission.

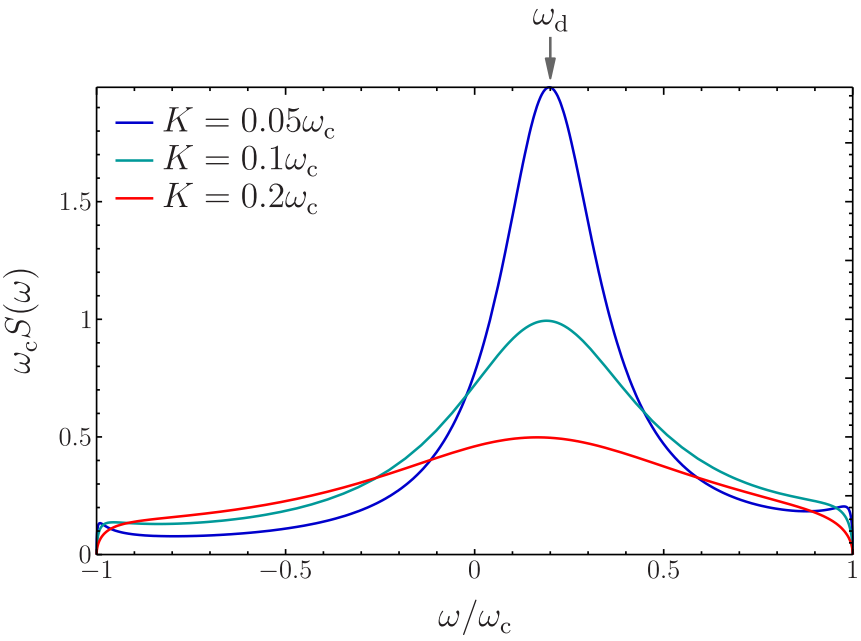

Figure 7.17 – In-band local density of states for a discrete level coupled to the middle of one-dimensional chain ($s = -1/2$).

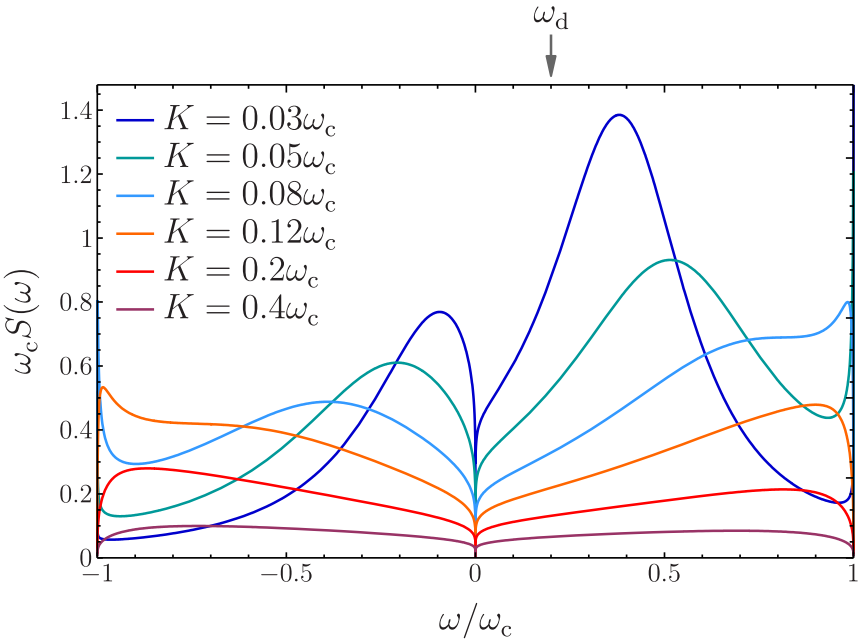

Figure 7.18 – In-band local density of states for a discrete level coupled to a site in the middle of two-dimensional square lattice.

Concluding remarks

This thesis studies the properties of a discrete quantum level coupled to macroscopic reservoirs. This system can be described by the exactly solvable Fano-Anderson model. The Hamiltonian being quadratic in terms of the creation and annihilation operators, the corresponding Heisenberg equations of motion constitute a set of first-order linear differential equations which is solved using a Laplace transform. In doing so, it is particularly important to take into account the contribution of bound states, eigenmodes of the full Hamiltonian whose energy lie in a band gap of the reservoirs. This solution formally gives one access to the time evolution of all the physical quantities of interest for this system, such as the occupation of the discrete level or the currents flowing out of each reservoir. However, the time-dependent formulae often turn out to be impossible to exploit analytically and we then decided to focus on the behaviour of the system at long times.

The long-time limit is carried out by extensive use of the Riemann-Lebesgue lemma and the results can be simplified considering the continuity equation which accounts for the conservation of the number of particles. This provides us with a fully analytical theory for thermoelectric transport through the discrete level: We find that the currents across the system satisfy a relation of the type of the Landauer formula, and the transmission function of the discrete level can be derived analytically. As expected, bound states do not participate in dc transport. Nevertheless, their contributions to the long-time state of the system turn out to be of primary importance and feature unexpected properties. First, they depend on the initial state of the discrete level expressing the fact that a particle in a bound state cannot escape to the continuum and thus remains trapped forever. Additionally, when there are two or more bound states, physical quantities do not reach a steady state but undergo persistent oscillations whose frequencies are given by the differences between bound state energies.

The aforementioned persistent oscillations at long times are a consequence of the initial preparation of the system. Our formalism is adapted to the case of a quench where, starting from a situation with decoupled discrete level and reservoirs, the coupling is abruptly turned on and remains constant afterwards. However, it is possible to mimic the opposite situation, where the coupling is turned on infinitely

slowly, by adding a vanishingly small constant to the spectral density. In this framework, all states, including the bound states, can thermalize which results in similar contributions for continuum states and bound states in the long-time limit. The influence of bound states can still be seen in the correlations of the occupation though.

Analyzing the transmission function of the discrete level, one can draw a connection between bound states and perfectly transmitting states, continuum states going from one reservoir to another without undergoing any reflection. The energies of these two types of states obey the same relation, but, contrary to bound states, perfectly transmitting states have energies lying within the continuum. The appearance of a bound state can then be interpreted as a perfectly transmitting state being Lamb shifted until it emerges out of the continuum when the coupling reaches a critical value. This transition dramatically impacts the organization of continuum states, and it is thus accompanied by significant changes for the thermoelectric transport properties of the discrete level. Namely, the electrical and thermal conductances are sharply peaked around the critical point while the Seebeck coefficient abruptly drops at critical coupling. Furthermore, we find that the critical point seems to define a sweet spot for thermoelectric transport across the discrete level: The power output can be much larger at this point without a noticeable decrease of efficiency.

Nevertheless, thorough analysis of situations with strongly nonlinear Lamb shifts shows that the physics of perfectly transmitting states is actually much richer than described above. Indeed, we show that the appearance of a bound state cannot always be interpreted as a perfectly transmitting state emerging out of the continuum. Such intricacies typically arise in situations where the continuum of reservoir states consists of narrow bands, as in the example of reservoirs described by tight-binding models considered here. We show that the nonlinear Lamb shift obtained in this type of set-ups can give rise to multiple perfectly transmitting states; the single discrete level hence seems to behave as a multi-level system. These peaks of perfect transmission even exist in situations where the energy of the discrete level is outside the energy range of the continuum. In the strong coupling regime, it is then possible to achieve perfect transmission at energies far-off from the bare discrete energy level.

Throughout this thesis, we have highlighted the rich physics embedded in the Fano-Anderson model. Even though this is one of the simplest open quantum systems one could think of, it exhibits many counter-intuitive features, especially in the regime of strong coupling to the reservoir. Essentially all of this rich physics is encoded in the Lamb shift; it is through this quantity that bound states and perfectly transmitting states are calculated. The Lamb shift fundamentally stems from the band structure of the reservoirs, and it vanishes in reservoirs described in the wide-band limit.

The usual derivation of the scattering matrix for a single-level quantum dot in the Landauer-Büttiker formalism ignores the band structure of the reservoirs. Hence, any result derived within this framework would completely overlook the influence of this band structure on the transmission properties of the scatterer. A worthwhile next step would be to generalize the results of this thesis to a system comprising an arbitrary number of discrete states. As such, the band structure of the reservoirs could be taken into account in the calculation of the scattering matrix of an arbitrary scatterer. However, finding the exact transport properties of the Fano-Anderson model has proven to be quite challenging, and there is no guarantee that it is possible to obtain simple formulae for a generic multi-level scatterer. A ready-to-use numerical code implementing the Lamb shift effects in this context would already be an important advance.

Furthermore, as electron-electron interactions are generally difficult to avoid in realistic experiments, it would be interesting to study how the Lamb shift physics is changed when Coulomb repulsion is considered. This is a very challenging problem and the tools developed in this thesis are not directly applicable to such situations. Indeed, electron-electron interactions add quartic terms to the Hamiltonian, and the Heisenberg equations of motion are then no longer linear. One way of proceeding would be to use a Hartree-Fock-type scheme where interaction terms in the Hamiltonian are simplified tracing out two operators out of four. The interacting Hamiltonian is then mapped on a non-interacting Hamiltonian with renormalized single-particle energy levels. However, this approximation is known to miss much of the physics of Coulomb blockade, and other more sophisticated approximations may need to be developed.

Finally, it is clear that strong coupling to a reservoir with a band structure not only affects the steady-state properties of the system but also its time evolution. A striking example of such influence is the possibility for persistent oscillations of the occupation of the discrete level in situations with two bound states or more. The problem of the decay time in this type of system is of significant interest for the design of quantum computers, that is computers in which classical bits are replaced by qubits. Indeed, one of the main current challenges in quantum computing is the control of the errors incurred by the instability of single qubits. To do so, subtle error correction schemes have been engineered making use of so-called ancilla qubits which are flipped whenever an error is detected. Fast and reliable algorithms thus require such qubits to be often reset to their ground state. Many proposed architectures would implement these ancilla qubits with photonic cavities which can be well-described by the Fano-Anderson model. Using tools from the weak-coupling theories of open quantum systems, one would argue that stronger coupling to the environment leads to faster decay. However, we have shown here that strong coupling can actually prevent the full decay of an excited state due to the existence of bound states. One then has to solve this trade-off problem to ensure fast and accurate

decay of the qubit to its ground state.

References

[1] S. Carnot. *Reflections on the motive power of fire and on machines fitted to develop that power*. Bachelier, 1824.

[2] L. Boltzmann. *Lectures on gas theory*, volume I. J. A. Barth, 1896.

[3] L. Boltzmann. *Lectures on gas theory*, volume II. J. A. Barth, 1898.

[4] S. W. Sheehan, H. Noh, G. W. Brudvig, H. Cao and C. A. Schmuttenmaer. *Plasmonic enhancement of dye-sensitized solar cells using core-shell-shell nanostructures*. The Journal of Physical Chemistry C, 117(2), 927–934, 2013. doi:10.1021/jp311881k.

[5] E. Johlin, A. Al-Obeidi, G. Nogay, M. Stuckelberger, T. Buonassisi and J. C. Grossman. *Nanohole structuring for improved performance of hydrogenated amorphous silicon photovoltaics*. ACS Applied Materials & Interfaces, 8(24), 15169–15176, 2016. doi:10.1021/acsami.6b00033.

[6] P. Reddy, S. Y. Jang, R. A. Segalman and A. Majumdar. *Thermoelectricity in molecular junctions*. Science, 315(5818), 1568–1571, 2007. doi:10.1126/science.1137149.

[7] J. Balachandran, P. Reddy, B. D. Dunietz and V. Gavini. *End-group-induced charge transfer in molecular junctions: effect on electronic-structure and thermopower*. The Journal of Physical Chemistry Letters, 3(15), 1962–1967, 2012. doi:10.1021/jz300668c.

[8] Y. Kim, W. Jeong, K. Kim, W. Lee and P. Reddy. *Electrostatic control of thermoelectricity in molecular junctions*. Nature Nanotechnology, 9(11), 881, 2014. doi:10.1038/nnano.2014.209.

[9] L. Cui, W. Jeong, S. Hur, M. Matt, J. C. Klöckner, F. Pauly, P. Nielaba, J. C. Cuevas, E. Meyhofer and P. Reddy. *Quantized thermal transport in single-atom junctions*. Science, 355(6330), 1192–1195, 2017. doi:10.1126/science.aam6622.

[10] L. Cui, R. Miao, K. Wang, D. Thompson, L. A. Zotti, J. C. Cuevas, E. Meyhofer and P. Reddy. *Peltier cooling in molecular junctions*. Nature Nanotechnology, 13(2), 122, 2018. doi:10.1038/s41565-017-0020-z.

[11] F. Hartmann, P. Pfeffer, S. Höfling, M. Kamp and L. Worschech. *Voltage fluctuation to current converter with Coulomb-coupled quantum dots*. Physical Review Letters, 114(14), 146805, 2015. doi:10.1103/PhysRevLett.114.146805.

[12] H. Thierschmann, R. Sánchez, B. Sothmann, F. Arnold, C. Heyn, W. Hansen, H. Buhmann and L. W. Molenkamp. *Three-terminal energy harvester with coupled quantum dots*. Nature Nanotechnology, 10(10), 854–858, 2015. doi:10.1038/nnano.2015.176.

[13] B. Roche, P. Roulleau, T. Jullien, Y. Jompol, I. Farrer, D. A. Ritchie and D. C. Glattli. *Harvesting dissipated energy with a mesoscopic ratchet*. Nature Communications, 6, 6738, 2015. doi:10.1038/ncomms7738.

[14] J. R. Prance, C. G. Smith, J. P. Griffiths, S. J. Chorley, D. Anderson, G. A. C. Jones, I. Farrer and D. A. Ritchie. *Electronic refrigeration of a two-dimensional electron gas*. Physical Review Letters, 102(14), 146602, 2009. doi:10.1103/PhysRevLett.102.146602.

[15] C.-W. Chang, D. Okawa, A. Majumdar and A. Zettl. *Solid-state thermal rectifier*. Science, 314(5802), 1121–1124, 2006. doi:10.1126/science.1132898.

[16] W. Kobayashi, Y. Teraoka and I. Terasaki. *An oxide thermal rectifier*. Applied Physics Letters, 95(17), 171905, 2009. doi:10.1063/1.3253712.

[17] D. M. T. van Zanten, F. Balestro, H. Courtois and C. B. Winkelmann. *Probing hybridization of a single energy level coupled to superconducting leads*. Physical Review B, 92(18), 184501, 2015. doi:10.1103/PhysRevB.92.184501.

[18] D. M. T. van Zanten, D. M. Basko, I. M. Khaymovich, J. P. Pekola, H. Courtois and C. B. Winkelmann. *Single quantum level electron turnstile*. Physical Review Letters, 116(16), 166801, 2016. doi:10.1103/PhysRevLett.116.166801.

[19] G. Benenti, G. Casati, K. Saito and R. S. Whitney. *Fundamental aspects of steady-state conversion of heat to work at the nanoscale*. Physics Reports, 694, 1–124, 2017. doi:10.1016/j.physrep.2017.05.008.

[20] L. D. Hicks and M. S. Dresselhaus. *Effect of quantum-well structures on the thermoelectric figure of merit*. Physical Review B, 47(19), 12727, 1993. doi:10.1103/PhysRevB.47.12727.

[21] R. Venkatasubramanian, E. Siivola, T. Colpitts and B. O'Quinn. *Thin-film thermoelectric devices with high room-temperature figures of merit.* Nature, 413(6856), 597, 2001. doi:10.1038/35098012.

[22] F. Giazotto, T. T. Heikkilä, A. Luukanen, A. M. Savin and J. P. Pekola. *Opportunities for mesoscopics in thermometry and refrigeration: Physics and applications.* Reviews of Modern Physics, 78(1), 217, 2006. doi:10.1103/RevModPhys.78.217.

[23] J. T. Muhonen, M. Meschke and J. P. Pekola. *Micrometre-scale refrigerators.* Reports on Progress in Physics, 75(4), 046501, 2012. doi:10.1088/0034-4885/75/4/046501.

[24] É. Akkermans and G. Montambaux. *Mesoscopic physics of electrons and photons.* EDP Sciences, 2004.

[25] W. M. Haynes. *CRC handbook of chemistry and physics.* CRC Press, 95$^{\text{th}}$ edition, 2014 (first published 1914).

[26] N. Pottier. *Nonequilibrium statistical physics: Linear irreversible processes.* EDP Sciences, 2007.

[27] C. Cohen-Tannoudji, B. Diu and F. Laloë. *Quantum mechanics.* EDP Sciences, 1973.

[28] J. J. Sakurai. *Modern quantum mechanics.* Addison-Wesley, 1985.

[29] J. Kondo. *Resistance minimum in dilute magnetic alloys.* Progress of Theoretical Physics, 32(1), 37–49, 1964. doi:10.1143/PTP.32.37.

[30] S. John and J. Wang. *Quantum electrodynamics near a photonic band gap: Photon bound states and dressed atoms.* Physical Review Letters, 64(20), 2418, 1990. doi:10.1103/PhysRevLett.64.2418.

[31] S. John and J. Wang. *Quantum optics of localized light in a photonic band gap.* Physical Review B, 43(16), 12772, 1991. doi:10.1103/PhysRevB.43.12772.

[32] S. John and T. Quang. *Spontaneous emission near the edge of a photonic band gap.* Physical Review A, 50(2), 1764, 1994. doi:10.1103/PhysRevA.50.1764.

[33] A. G. Kofman, G. Kurizki and B. Sherman. *Spontaneous and induced atomic decay in photonic band structures.* Journal of Modern Optics, 41(2), 353–384, 1994. doi:10.1080/09500349414550381.

[34] D. G. Angelakis, P. L. Knight and E. Paspalakis. *Photonic crystals and inhibition of spontaneous emission: an introduction*. Contemporary Physics, 45(4), 303–318, 2004. doi:10.1080/00107510410001676795.

[35] Y. Apertet, H. Ouerdane, C. Goupil and Ph. Lecoeur. *Irreversibilities and efficiency at maximum power of heat engines: The illustrative case of a thermoelectric generator*. Physical Review E, 85(3), 031116, 2012. doi:10.1103/PhysRevE.85.031116.

[36] G. Katz and R. Kosloff. *Quantum thermodynamics in strong coupling: Heat transport and refrigeration*. Entropy, 18(5), 186, 2016. doi:10.3390/e18050186.

[37] P. Strasberg and M. Esposito. *Stochastic thermodynamics in the strong coupling regime: An unambiguous approach based on coarse graining*. Physical Review E, 95(6), 062101, 2017. doi:10.1103/PhysRevE.95.062101.

[38] P. Strasberg, G. Schaller, T. L. Schmidt and M. Esposito. *Fermionic reaction coordinates and their application to an autonomous Maxwell demon in the strong-coupling regime*. Physical Review B, 97(20), 205405, 2018. doi:10.1103/PhysRevB.97.205405.

[39] W. Dou, M. A. Ochoa, A. Nitzan and J. E. Subotnik. *Universal approach to quantum thermodynamics in the strong coupling regime*. Physical Review B, 98(13), 134306, 2018. doi:10.1103/PhysRevB.98.134306.

[40] H. J. W Haug and A.-P. Jauho. *Quantum kinetics in transport and optics of semiconductors*. Springer, 2nd edition, 2008 (first published 1996).

[41] G. Stefanucci and R. van Leeuwen. *Nonequilibrium many-body theory of quantum systems*. Cambridge University Press, 2013.

[42] C. Caroli, R. Combescot, P. Nozières and D. Saint-James. *Direct calculation of the tunneling current*. Journal of Physics C: Solid State Physics, 4(8), 916, 1971. doi:10.1088/0022-3719/4/8/018.

[43] Y. Meir and N. S. Wingreen. *Landauer formula for the current through an interacting electron region*. Physical Review Letters, 68(16), 2512, 1992. doi:10.1103/PhysRevLett.68.2512.

[44] A. Dhar and D. Sen. *Nonequilibrium Green's function formalism and the problem of bound states*. Physical Review B, 73(8), 085119, 2006. doi:10.1103/PhysRevB.73.085119.

[45] G. Stefanucci. *Bound states in ab initio approaches to quantum transport: A time-dependent formulation.* Physical Review B, 75(19), 195115, 2007. doi:10.1103/PhysRevB.75.195115.

[46] U. Fano. *Effects of configuration interaction on intensities and phase shifts.* Physical Review, 124(6), 1866, 1961. doi:10.1103/PhysRev.124.1866.

[47] P. W. Anderson. *Localized magnetic states in metals.* Physical Review, 124(1), 41, 1961. doi:10.1103/PhysRev.124.41.

[48] J. Jin, M. W.-Y. Tu, W.-M. Zhang and Y. J. Yan. *Non-equilibrium quantum theory for nanodevices based on the Feynman-Vernon influence functional.* New Journal of Physics, 12(8), 083013, 2010. doi:10.1088/1367-2630/12/8/083013.

[49] G. Schaller. *Open quantum systems far from equilibrium.* Springer, 2014.

[50] G. E. Topp, T. Brandes and G. Schaller. *Steady-state thermodynamics of non-interacting transport beyond weak coupling.* EPL, 110(6), 67003, 2015. doi:10.1209/0295-5075/110/67003.

[51] C. U. Lei and W.-M. Zhang. *A quantum photonic dissipative transport theory.* Annals of Physics, 327(5), 1408–1433, 2012. doi:10.1016/j.aop.2012.02.005.

[52] Md. M. Ali, P.-Y. Lo, M. W.-Y. Tu and W.-M. Zhang. *Non-Markovianity measure using two-time correlation functions.* Physical Review A, 92(6), 062306, 2015. doi:10.1103/PhysRevA.92.062306.

[53] Y.-C. Lin, P.-Y. Yang and W.-M. Zhang. *Non-equilibrium quantum phase transition via entanglement decoherence dynamics.* Scientific reports, 6, 34804, 2016. doi:10.1038/srep34804.

[54] Md. M. Ali and W.-M. Zhang. *Nonequilibrium transient dynamics of photon statistics.* Physical Review A, 95(3), 033830, 2017. doi:10.1103/PhysRevA.95.033830.

[55] G. Engelhardt, G. Schaller and T. Brandes. *Bosonic Josephson effect in the Fano-Anderson model.* Physical Review A, 94(1), 013608, 2016. doi:10.1103/PhysRevA.94.013608.

[56] W.-M. Zhang, P.-Y. Lo, H.-N. Xiong, M. W.-Y. Tu and F. Nori. *General non-Markovian dynamics of open quantum systems.* Physical Review Letters, 109(17), 170402, 2012. doi:10.1103/PhysRevLett.109.170402.

[57] H.-N. Xiong, P.-Y. Lo, W.-M. Zhang and F. Nori. *Non-Markovian complexity in the quantum-to-classical transition.* Scientific Reports, 5, 13353, 2015. doi:10.1038/srep13353.

[58] R. S. Whitney, R. Sánchez and J. Splettstoesser. *Quantum thermodynamics of nanoscale thermoelectrics and electronic devices*. In *Thermodynamics in the quantum regime*, pages 175–206. Springer, 2018.

[59] H. Shiba. *A Hartree-Fock theory of transition-metal impurities in a superconductor*. Progress of Theoretical Physics, 50(1), 50–73, 1973. doi:10.1143/PTP.50.50.

[60] D. M. Basko. *Landau-Zener-Stueckelberg physics with a singular continuum of states*. Physical Review Letters, 118(1), 016805, 2017. doi:10.1103/PhysRevLett.118.016805.

[61] Y. Liu and A. A. Houck. *Quantum electrodynamics near a photonic bandgap*. Nature Physics, 13(1), 48, 2017. doi:10.1038/nphys3834.

[62] R. Landauer. *Spatial variation of currents and fields due to localized scatterers in metallic conduction*. IBM Journal of Research and Development, 1(3), 223–231, 1957. doi:10.1147/rd.13.0223.

[63] R. Landauer. *Electrical resistance of disordered one-dimensional lattices*. Philosophical Magazine, 21(172), 863–867, 1970. doi:10.1080/14786437008238472.

[64] M. Büttiker. *Four-terminal phase-coherent conductance*. Physical Review Letters, 57(14), 1761, 1986. doi:10.1103/PhysRevLett.57.1761.

[65] M. Büttiker. *Symmetry of electrical conduction*. IBM Journal of Research and Development, 32(3), 317–334, 1988. doi:10.1147/rd.323.0317.

[66] S. Datta. *Electronic transport in mesoscopic systems*. Cambridge University Press, 1997.

[67] S. Vinjanampathy and J. Anders. *Quantum thermodynamics*. Contemporary Physics, 57(4), 545–579, 2016. doi:10.1080/00107514.2016.1201896.

[68] H.-P. Breuer and F. Petruccione. *The theory of open quantum systems*. Oxford University Press, 2002.

[69] V. Gorini, A. Kossakowski and E. C. G. Sudarshan. *Completely positive dynamical semigroups of N-level systems*. Journal of Mathematical Physics, 17(5), 821–825, 1976. doi:10.1063/1.522979.

[70] G. Lindblad. *On the generators of quantum dynamical semigroups*. Communications in Mathematical Physics, 48(2), 119–130, 1976. doi:10.1007/BF01608499.

[71] C. Cohen-Tannoudji, J. Dupont-Roc and G. Grynberg. *Atom-photon interactions: Basic processes and applications*. EDP Sciences, 1988.

[72] K. Blum. *Density matrix theory and applications*. Springer, 3rd edition, 2012 (first published 1981).

[73] A. G. Redfield. *On the theory of relaxation processes*. IBM Journal of Research and Development, 1(1), 19–31, 1957. doi:10.1147/rd.11.0019.

[74] F. Bloch. *Generalized theory of relaxation*. Physical Review, 105(4), 1206, 1957. doi:10.1103/PhysRev.105.1206.

[75] A. Schiller and S. Hershfield. *Toulouse limit for the nonequilibrium kondo impurity: Currents, noise spectra, and magnetic properties*. Physical Review B, 58(22), 14978, 1998. doi:10.1103/PhysRevB.58.14978.

[76] J. Maciejko, J. Wang and H. Guo. *Time-dependent quantum transport far from equilibrium: An exact nonlinear response theory*. Physical Review B, 74(8), 085324, 2006. doi:10.1103/PhysRevB.74.085324.

[77] M. W.-Y. Tu, A. Aharony, O. Entin-Wohlman, A. Schiller and W.-M. Zhang. *Transient probing of the symmetry and the asymmetry of electron interference*. Physical Review B, 93(12), 125437, 2016. doi:10.1103/PhysRevB.93.125437.

[78] W. Appel. *Mathematics for physics and physicists*. H&K, 5th edition, 2017 (first published 2000).

[79] D. P. O'Leary and G. W. Stewart. *Computing the eigenvalues and eigenvectors of symmetric arrowhead matrices*. Journal of Computational Physics, 90(2), 497–505, 1990. doi:10.1016/0021-9991(90)90177-3.

[80] M. Cini. *Time-dependent approach to electron transport through junctions: General theory and simple applications*. Physical Review B, 22(12), 5887, 1980. doi:10.1103/PhysRevB.22.5887.

[81] D. Weinmann, W. Häusler and B. Kramer. *Transport properties of quantum dots*. Annalen der Physik, 508(8), 652–695, 1996. doi:10.1002/andp.2065080804.

[82] H. Schoeller and G. Schön. *Mesoscopic quantum transport: Resonant tunneling in the presence of a strong Coulomb interaction*. Physical Review B, 50(24), 18436, 1994. doi:10.1103/PhysRevB.50.18436.

[83] J. König, J. Schmid, H. Schoeller and G. Schön. *Resonant tunneling through ultrasmall quantum dots: Zero-bias anomalies, magnetic-field dependence, and boson-assisted transport*. Physical Review B, 54(23), 16820, 1996. doi:10.1103/PhysRevB.54.16820.

[84] J. König, H. Schoeller and G. Schön. *Cotunneling at resonance for the single-electron transistor*. Physical Review Letters, 78(23), 4482, 1997. doi:10.1103/PhysRevLett.78.4482.

[85] H. Schoeller. *Transport theory of interacting quantum dots* in *Mesoscopic electron transport*, pages 291–330. Springer, 1997. doi:10.1007/978-94-015-8839-3_8.

[86] Y. Alhassid. *The statistical theory of quantum dots*. Reviews of Modern Physics, 72(4), 895, 2000. doi:10.1103/RevModPhys.72.895.

[87] R. Timm, H. Eisele, A. Lenz, L. Ivanova, V. Vosseburger, T. Warming, D. Bimberg, I. Farrer, D. A. Ritchie and M. Dähne. *Confined states of individual type-II* GaSb/GaAs *quantum rings studied by cross-sectional scanning tunneling spectroscopy*. Nano Letters, 10(10), 3972–3977, 2010. doi:10.1021/nl101831n.

[88] A. Kerelsky, A. Nipane, D. Edelberg, D. Wang, X. Zhou, A. Motmaendadgar, H. Gao, S. Xie, K. Kang, J. Park, J. Teherani and A. Pasupathy. *Absence of a band gap at the interface of a metal and highly doped monolayer* MoS_2. Nano Letters, 17(10), 5962–5968, 2017. doi:10.1021/acs.nanolett.7b01986.

[89] É. Jussiau, M. Hasegawa and R. S. Whitney. *Signature of the transition to a bound state in thermoelectric quantum transport*. Physical Review B, 100(11), 115411, 2019. doi:10.1103/PhysRevB.100.115411.

[90] H. Alloul. *Introduction to the physics of electrons in solids*. Springer, 2010.

[91] H. J. W. M. Hoekstra. *On the tight-binding model for semi-infinite lattices*. Surface Science, 205(3), 523–548, 1988. doi:10.1016/0039-6028(88)90301-9.

[92] J. R. Williams, L. DiCarlo and C. M. Marcus. *Quantum Hall effect in a gate-controlled p-n junction of graphene*. Science, 317(5838), 638–641, 2007. doi:10.1126/science.1144657.

[93] J. Chen, H. J. Qin, F. Yang, J. Liu, T. Guan, F. M. Qu, G. H. Zhang, J. R. Shi, X. C. Xie, C. L. Yang, K. H. Wu, Y. Q. Li and L. Lu. *Gate-voltage control of chemical potential and weak antilocalization in* Bi_2Se_3. Physical Review Letters, 105(17), 176602, 2010. doi:10.1103/PhysRevLett.105.176602.

[94] M. C. Lemme, F. H. L. Koppens, A. L. Falk, M. S. Rudner, H. Park, L. S. Levitov and C. M. Marcus. *Gate-activated photoresponse in a graphene p–n junction*. Nano Letters, 11(10), 4134–4137, 2011. doi:10.1021/nl2019068.

[95] J. S. Lee, A. Richardella, D. R. Hickey, K. A. Mkhoyan and N. Samarth. *Mapping the chemical potential dependence of current-induced spin polarization in a topological insulator*. Physical Review B, 92(15), 155312, 2015. doi:10.1103/PhysRevB.92.155312.

[96] H. J. W. Zandvliet and A. van Houselt. *Scanning tunneling spectroscopy*. Annual Review of Analytical Chemistry, 2, 37–55, 2009. doi:10.1146/annurev-anchem-060908-155213.

[97] U. Kuhl, S. Barkhofen, T. Tudorovskiy, H.-J. Stöckmann, T. Hossain, L. de Forges de Parny and F. Mortessagne. *Dirac point and edge states in a microwave realization of tight-binding graphene-like structures*. Physical Review B, 82(9), 094308, 2010. doi:10.1103/PhysRevB.82.094308.

[98] S. Barkhofen, M. Bellec, U. Kuhl and F. Mortessagne. *Disordered graphene and boron nitride in a microwave tight-binding analog*. Physical Review B, 87(3), 035101, 2013. doi:10.1103/PhysRevB.87.035101.

[99] M. Bellec, U. Kuhl, G. Montambaux and F. Mortessagne. *Topological transition of Dirac points in a microwave experiment*. Physical Review Letters, 110(3), 033902, 2013. doi:10.1103/PhysRevLett.110.033902.